InP/ZnS nanocrystals for colour conversion in white light emitting diodes

Shirazi, Roza; Petersen, Paul Michael; Kardynal, Beata

Publication date:
2013

Document Version
Publisher's PDF, also known as Version of record

InP/ZnS nanocrystals for colour conversion in white light emitting diodes

Róża Shirazi

Supervised by: **Beata Kardynał**

Supervised by: **Paul Michael Petersen**

Diode Lasers and LED Systems

Department of Photonics Engineering

Technical University of Denmark

31-5-2013

"Choose a job you love, and you will never have to work a day in your life."

Confucius

Contents

Abstract

In this work a comprehensive study of a colloidal InP/ZnS nanocrystals (NC) as the colour conversion material for white light emitting diodes (WLED) is shown. Studied nanocrystals were synthesised by wet chemistry using one pot, hot injection method. A quantum efficiency (QE) of photoluminescence joined with a time resolved photoluminescence (TRPL) measurements of NCs covering the visible light spectrum range revealed a presence of a population of NCs that does not emit light upon photon absorption and it is significantly higher for a larger particles. By modifying local density of optical states, radiative and non-radiative recombination rates were determined and QE of 63% for the population of NCs that emit light was derived. A search for source of exciton losses in bright nanocrystals temperature resolved TRPL was studied and it revealed carrier trapping most likely at core-shell interface as well as at the surface and which competes with bright and dark exciton states. A presence of long-lived dark excitons and trapped charges lead to strong Auger recombination at high (relative to the trapping times) excitation. A colour conversion efficiency of the nanocrystals upon light absorption and in a process of resonant energy transfer varied from 0.03 to 0.05% and from 0.6 to 4.8 %, respectively. Finally, an analysis of luminous efficacy of radiation of hybrid WLEDs revealed that it is close to the theoretically predicted $\sim$ 300 lm/W for phosphor based WLED.

Acknowledgement

I would like to thank:

:: Beata Kardynal for giving me the opportunity of working with her, for the supervision and support she has given me through, nearly 4 years of my Ph.D. and for her patience;

:: Paul Michael for the supervision and support;

:: Alex and Claudia for support;

:: Martin, Henri and Jin for help in the lab;

:: Dennis and Carsten for help with experiments and helpful discussion on light quality;

:: Troels, Henri, Soren, Anders T for help with the matlab calculations;

:: Andras for TEM pictures;

:: Sara, Thor, Andrei, Troels for help, fun we had and for the motivation;

:: Michael for the golden housing and the bonding;

:: Peri, Junis, Chunyong and Pavlos from Southampton University for welcoming me in their group, helpful discussion and support;

:: Yura from Russian Institute of Science for helpful discussion and modelling of the RET as a function of carrier density. :: My family for great support and sacrificing they have done for this work to be completed.

It was pleasure working with you all, thank you!

Publications

1. **Journal publications**

   (a) "Temperature dependent recombination dynamics in InP/ZnS colloidal nanocrystals"; R. Shirazi, O. Kopylov, A. Kovacs, B. Kardynal, Applied Physics Letters 101, 9, 091910, 2012;

   (b) "Origin of Low Quantum Efficiency of Photoluminescence of InP/ZnS Nanocrystals." R. Shirazi, A. Kovacs, C. Gritti, D.D. Corell, A. Thorseth, C. Dam-Hansen, P. M. Petersen, B. Kardynal, Submitted ;

   (c) "Resonant energy transfer between InP/ZnS nanocrystals and InGaN QW as a function of carrier density." R. Shirazi, Y. Gladush, J.J. Rindermann, P. Andreakou, C. Li, P. Lagoudakis, B. Kardynal, To be submitted.

   (d) "High colour rendering index and high luminous efficacy of radiation of the nanocrystals based white light emitting diode." R. Shirazi, D.D. Corell, A. Thorseth, C. Dam-Hansen, P. M. Petersen, B. Kardynal, To be submitted.

2. **Refereed conference proceedings**

   (a) "Effect of GaN cap thickness on carrier dynamics in InGaN quantum wells" O. Kopylov, R. Shirazi,O. Svensk, S. Suihkonen, S.

Sintonen, M. Sopanen, B. Kardynal; Physica Status Solidi. C: Current Topics in Solid State Physics, 9, 3-4, 727-729, 2012;

(b) "MOCVD growth and characterization of near-surface InGaN/GaN single quantum wells for non-radiative coupling of optical excitations"; O. Svensk, S. Suihkonen, S. Sintonen, O. Kopylov, R. Shirazi, H. Lipsanen, M. Sopanen, B. Kardynal; Physica Status Solidi. C: Current Topics in Solid State Physics 9, 7, 1667-1669, 2012.

3. **Conference proceedings**

(a) "Design and geometry of hybrid white light-emitted diodes for efficient energy transfer from the quantum well to the nanocrystals"; O. Kopylov, A. Huck, R. Shirazi, K. Yvind, B. Kardynal; Proc. SPIE 8625, Gallium Nitride Materials and Devices VIII, 862524, 2013.

4. **Presentations**

(a) "Forster energy transfer in hybrid light emitting diode"; R. Shirazi, O. Kopylov, B. Kardynal, Winter Collage on Optics and Energy, Trieste, Italy, 2010;

(b) "Colloidal quantum dots enhanced white light emitting diode"; R.Shirazi,O. Kopylov, B. E. Kardynal, SPIE, San Francisco, USA, 2011;

(c) "Excitonic versus parasitic recombination in colloidal InP/ZnS nanocrystals" R.Shirazi,O. Kopylov, B. E. Kardynal, EXCON, Groningen, Netherlands 2012.

Chapter 1

Introduction

One of the major current challenges which the world is facing is reduction of energy consumption and the carbon footprint it have on the planet. As a result there is a pressure to find light sources which would combine high efficiency of the high pressure sodium vapour discharge lamp and the quality of light emitted by the incandescent lamp. The saving could be significant as lighting accounts for 17.5% of the world electricity consumption [1].

Semiconductor nanocrystals based white light emitting diodes are one of the technologies considered to be the future of white light generation because they combine advantages of electrical conductivity of the blue emitting diode and unique optical properties of the nanocrystals [2]. Semiconductor nanocrystals are particles with a crystalline structure consisting of no more than 10000 atoms which corresponds to their maximum size of 10 nm [3]. Their properties are significantly changed in comparison to bulk materials because of their finite size. In bulk semiconductors, energy band gap is a parameter which depends on the material itself and it doesn't change with the size of the sample. Tunability of quantum confinement and therefore of the electron wavefunction with the size, shape and structure of nanocrystals

allows modification of their absorption and emission [4] making design of the spectral properties of resulting white light easy [5]. The simple and cheap fabrication makes them particularly attractive.

As a results of the rising interest in the unique properties of nanocrystals [6], a synthesis of the semiconductor nanoparticles, also referred to as quantum dots to emphasize the small dimensions compared with electron wavefunctions, has seen a huge progress [7] during past three decades. A control of their size, shape and quality, which is prerequisite for all applications, has been achieved by separating two phases of the synthesis: nucleation and growth by rapid injection of precursors into a hot solution where the reaction takes place [8].

InP/ZnS core-shell nanocrystals can be fabricated using rapid one pot, one step synthesis [9, 10] and for experiments described below, they were synthesized using one pot, hot injection method [11]. All the InP/ZnS specimens were purchased from NN-Labs [12] and details of the synthesis described below are based on their publications [11]. InP cores were grown at 190^{o}C under constant evacuation and refilling with argon for water and oxygen free reaction. Nanocrystals of increasing sizes (and thus different emission wavelengths) were obtained by adjusting time of the reaction [4]. For the growth of the 0.3 nm thick ZnS shell, nanocrystals solution was kept at 220^{o}C for half an hour. Finally the nanocrystals were extracted from the reaction liquid by centrifuging, filtering, rinsing and octadecylamine has been added to passivate the surface of the nanocrystals as well as keep them apart from each other to avoid clustering. Schematic illustration of nanocrystals is shown in figure 1.1.

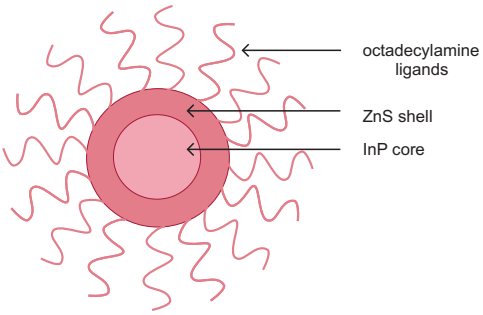

Figure 1.1: Schematic illustration of structure of InP/ZnS nanocrystal.

Important task in synthesis of nanocrystals is to achieve high external quantum efficiency for all sizes of nanocrystals for applications such as solid state lighting [13]. An excellence has already been demonstrated in the fabrication of Cd and Pb based core/shell nanocrystals, which have shown photoluminescence decaying as a single exponential function and a quantum yield of photoluminescence near unity [14, 15], however the toxicity of cadmium and lead based compounds limits their applications. On the other hand, a less-toxic III-V equivalent material, InP, requires further improvement of the nanocrystal synthesis [9, 11]. Core/shell InP/ZnS nanocrystals still do not have as high photoluminescence quantum yield as II-VI nanocrystals and exhibit wide size distribution giving rise to large full width half maximum.

InGaN/GaN blue emitting diode has been proposed [2] as the excitation source for nanocrystals as it is the only material system providing high enough energy of photons able to excite even the smallest nanocrystals (with absorption edge in the region of 450 nm) and because it emits in blue. Diode fabricated from this material show relatively high efficiency even though there are still several factors which limit their quality such as availability of lattice matched substrates on which GaN could be grown without the lattice strain. This results in a high density of treading dislocations [16, 17] bringing the internal quantum efficiency down. Additionally the diodes,

which are grown on c-plane sapphire substrates show piezoelectric polarization within the InGaN quantum well that causes the large build-in electric field complicating the recombination process. Some groups argue that the electric filed in the quantum wells, at room temperature, is much stronger than Coulomb forces, prohibiting electron - hole pairs to form excitons which brings the probability of photoluminescence down [18]. Another factor effecting the quality of the InGaN/GaN diodes is the indium inhomogeneities and indium segregation in the active region causing exciton localization [19]. This in opposite is believed to enhance the probability of photon emission by spatially confining wavefunctions of electrons and holes [19]. Even though InGaN/GaN diodes have such complicated basic optical properties and the extraction of light is challenging (caused by huge difference in refractive index of emitted photons (n=2.4) and air) the external quantum efficiency has reached 40% and is constantly improving [20].

Resonant energy transfer alongside optical absorption can be used to excite carriers in the nanocrystals. Resonant energy transfer (RET) is the process of non-radiative transmission of excitation energy from an excited state donor to the ground state acceptor. As this transfer relies on the Coulomb interactions, decay rate scales down with the distance between donor and acceptor and the dependence of the distance changes with the geometry of the device [21]. Another requirement for the efficient energy transfer is the large spectral overlap of the donor emission with acceptor absorption and parallel orientation of their dipoles.

Experimental realization of device consisting of electrically driven GaN diode with InGaN quantum wells in close proximity of the monolayer of CdSe nanocrystals has shown efficiency in the order of 13% from which 10% was assigned to RET [13]. It is significantly lower that theoretically pre-

dicted 55% [2] due to interplay between requirement of minimizing the distance between QW and nanocrystals and capping the quantum wells with thick barrier in order to minimize non-radiative losses. Etching through the InGaN quantum wells with thick barrier and filling the gaps with CdS nanocrystals was proposed [22] in order to resolve this issue. Efficiency of photoluminescence achieved in such device was 20% which was significantly higher than in the non-pattern device. Tunability of nanocrystals emission spectrum, gives the possibility of designing white light quality: by mixing few sizes of nanocrystals any correlated colour temperature with high rendering index can be achieved [23].

In this work, a concept of using InP/ZnS nanocrystals for white light emission from hybrid device consisting of layer of nanocrystals in close proximity of InGaN/GaN blue emitting diode is presented. Radiative (optical absorption) and non-radiative (RET) excitation methods are exploited to achieve colour conversion with possible simultaneous increase of device efficiency. Analysis of necessary conditions for colour conversion and methods of generating good light quality are described.

In the 2nd chapter necessary terms are introduced followed by the overview of existing technology of generation of white light from solid state devices. In chapter 3 the characterization methods of InP/ZnS nanocrystals are describing. In chapter 4 time-resolved photon counting technique is used alongside integrated photoluminescence measurements to determine InP/ZnS quantum efficiency and the low temperature time resolved photoluminescence is used to get insight into exciton dynamics. In the fifth chapter calculation of colour conversion efficiency of radiative and non-radiative excitation methods is shown followed by analytical determination of condition necessary for high quality of white light radiated from hybrid diode in chapter 6. Finally

conclusions are drawn from the work undertaken during the Ph.D period and described below.

Chapter 2

White Light Emitting Diodes

In this chapter definitions of terms in photometric and radiometric metrology systems relevant for the work in this thesis is provided followed by short description of ways of white light generation from solid state devices.

2.1 Theory

In Europe, the guidance on how to define and evaluate the quality of light and its generation efficiency is given by International Commission on Illumination, called also CIE from its French name Commission Internationale de l'Eclairage which also serves as international standardization body. Detailed guidelines on metrology and application in the field of light and lighting are described in CIE documents. They provide basic definitions of terms such as white light, black body radiator or chromaticity coordinates.

The human eye does not detect all the wavelengths equally; it is most sensitive in the green spectral region near 555 nm: the eye response function $V(\lambda)$, also called luminosity function, shown in figure 2.1, determines how effective, in stimulation of an eye, wavelengths in a visible range are. For

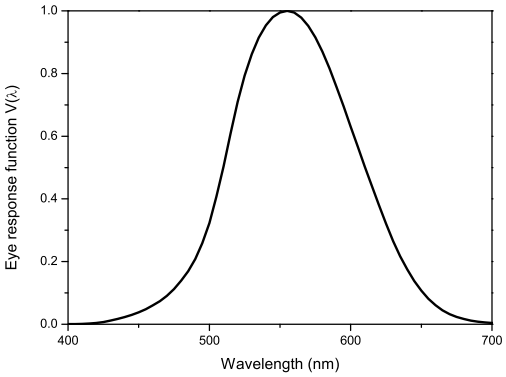

Figure 2.1: Eye response function for photopic vision defined by CIE 1924. The human eye is most sensitive in the region of 555 nm.

simplicity and clarity some of the values in this document will be given in radiometric system (as those are very often the measured ones), which differ from analogues photometry values by the value of eye response function. The change of the metrology system will be clearly stated.

White light can be understood as the continuous electromagnetic radiation in the wavelength range where the human eye shows sensitivity.

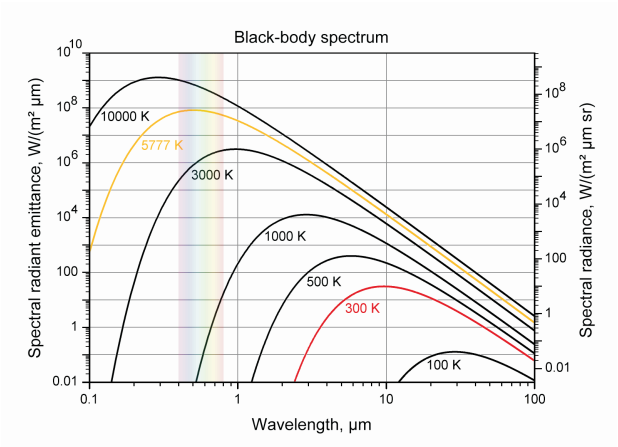

Figure 2.2: Spectrum of the black body radiator as a function of temperature. The spectral radiance increases with increasing black body's colour temperature.

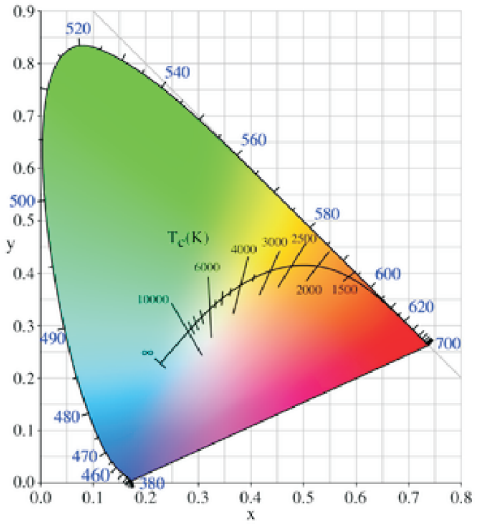

Figure 2.3: Planckian locus with lines of constant correlated colour temperatures and monochromatic emission wavelengths on the edge of the chromaticity space defined on CIE 1931 chromaticity diagram.

An ideal source of white light is the black body radiator, the spectrum of which depends only on body temperature (figure 2.2), which is called the Planck spectrum and which is described by Planck's law (equation 2.1)

$$L_\lambda(T) = \frac{2 \cdot h \cdot c^2}{\lambda^5} \cdot \frac{1}{e^{\frac{h \cdot c}{\lambda \cdot k_B \cdot T}} - 1}, \tag{2.1}$$

where L_λ is spectral radiance (in radiometry; luminance is analogues photometric unit), h is Planck constant, c is speed of light in vacuum, λ is wavelength of radiation, k_B is Boltzman constant and T is temperature.

In photometry, white light is mathematically defined by chromaticity coordinates from which first two are dimensions on chromaticity diagram and the third one is luminance or density of luminous intensity in given direction (cd/m^2). The black body radiator, is defined on the chromaticity diagram as a line called planckian locus, shown in figure 2.3. Its shape is specified by the changes of black body's colour temperature from deep red

at low temperatures to blue at high temperatures. The distance between coordinates of the given light source and the planckian locus is called coordinates distance (CD) and is used to define white light. The light with chromaticity coordinates spaced from the planckian locus not further that $5.4 \cdot 10^{-3}$ represent white light.

CIE identifies two values which describe light quality: colour rendering index (CRI) and correlated colour temperature (CCT). The colour rendering index gives information about the ability of a light source to faithfully reproduce colours of various objects in comparison with a natural light source for example daylight. If the light appearing white to eye, illuminates an objects of different colours and the colours of those objects appear different under this illumination than under the sun light it means that the light sources CRI is lower than the maximum possible value of 100 of a black body radiator (the theoretical minimum value of white light's CRI is 0). This comparison method, for 8 different test colour samples, is used to quantify CRI of any white light source. Motorway lighting often uses high discharge lamps filled with sodium vapours which produce yellow – orange light and is missing radiation in the rest of the spectrum. The CRI index of this sort of light is low and its value is around 20. CIE recommends the use of light sources with CRI not lower than 80, for most of the indoor applications.

The International Commission on Illumination gives the following definition of the CCT: the correlated colour temperature is the temperature of the planckian radiator whose perceived colour most closely resembles that of the given stimulus, at the same brightness and under specific viewing conditions [24]. CCT has only meaning for white light as it gives indication on its appearance – it is perceived warm for the values of CCT below 3300

K and cool when the light has a lot of blue radiation with CCT value above 5000 K, CCT between 3300 K and 5000 K is perceived as neutral. Correlated colour temperature is an important parameter for lighting designers, it helps to decide which light source is suitable for certain applications. For example, lamps generating warm light are used for domestic applications, neutral ones for office spaces and cold ones for hospitals. Up to date, light produced by commercially available solid state devices have relatively high efficiencies with good colour rendering indices for neutral and cool white light, however, the source for domestic applications is still missing.

The photometric value of luminous efficacy of radiation (η_R) is a measure of how efficiently the solid state device produces light in a visible range. It is the ratio of the amount of light generated by the light source - luminous flux Φ_{lum} to its power defined as the radiant flux Φ_{rad} of the sources output, and it is expressed in units of lumen per watts.

$$\eta_R = \frac{\Phi_{lum}}{\Phi_{rad}} \tag{2.2}$$

In an ideal situation, pure monochromatic green light with emission at single wavelength of 555 nm, where the human eye is most sensitive, reaches a luminous efficacy of 683 lm/W. For a continuum spectrum in visible range, the maximum theoretical value is considered to be anywhere between 260 - 300 lm/W if the luminous energy is evenly spread across the visible range [25]. Its value depends on the chosen range of the visible radiation.

The luminous efficacy of light source, as opposed to the luminous efficacy of radiation η_R, is a measure of how efficiently the visible light is produced from the input power, for example an electrical ($I \cdot V$) or a chemical power. Its unit is lm/W, the same as in the case of luminous efficacy of

Light source	η_R (lm/W)	η (%)	CCT (K)	CRI
Ideal 555 nm [26]	683	100	NA	NA
Black body [27]	54.7	8	4000	100
	82	12	5000	100
	95.9	14	6636.4	100
Theoretical phosphor based white LED [25]	260 - 300	38 - 44	4700	100
73 W white LED [28]	73	11	2700	82
30 W compact fluorescent [28]	65	10	2500	80
40 W tungsten incandescent [28]	10.4	1.5	2700	100
600 W high discharge sodium vapour [28]	150	22	2000	20

Table 2.1: Comparison of different light sources with theoretical predictions for white light emitting diodes. Values of luminous efficiency has been calculated on the assumption that its maximum value 100 % is for luminous efficacy of radiation of 683 lm/W.

radiation. For the diode, it is defined as the ratio of the luminous flux and the electrical power.

To avoid confusion, luminous flux is often replaced with radiant flux resulting in radiometric measure of light source efficiency. In this case it is represented as a percentage and called efficiency of a light source η:

$$\eta = \frac{\Phi_R}{I \cdot V} \tag{2.3}$$

In a table 2.1 luminous efficacy of radiation, efficiency of a light source, CRI and CCT of a few different sources are compared. Looking at the ideal source - black body radiator shown for different correlated colour tempera-

tures it is clear that high luminous efficacy of radiation can be achieved for higher values of CCT and it has to be sacrificed if lower temperatures are required. This is an effect which can be seen on the figure 2.2, where the black body for higher colour temperatures shows higher values of spectral radiance L_λ.

2.2 Overview of methods of white light generation from solid state devices

White light can be generated from solid state devices in several ways and, with time, new methods are being researched. Since the first light emitting diode has been developed [29], a huge progress has been achieved in terms of LEDs wavelength emission and the efficiency. However up to now light quality and efficiency of white light emitting diodes (WLED) haven't satisfied all conditions needed for the lighting applications. Below, a description of the currently used technologies in producing white light from solid state devices are presented, including comments on its performance.

Diode based WLEDs

The generation of white light from a nearly monochromatic solid state device can be achieved by adding the spectra of multiple diodes. Theoretically, to achieve white light, any two light sources can be used, provided they have the right power ratio and emit at the wavelengths which chromaticity coordinates connected by straight line, cross the planckian locus on the chromaticity diagram as shown by points (x_1, y_1) and (x_2, y_2) in fig-

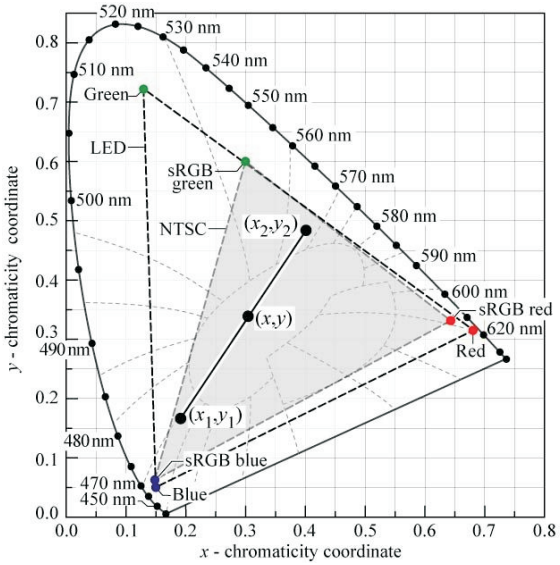

Figure 2.4: Illustration of principles of colour mixing based on two light sources with chromaticity coordinates x_i and y_i. The resulting white light source has the (x,y) coordinates. RGB triangle for mixing three colours is also shown. Image sourced from [30].

ure 2.4. If three or four spectra of diodes are mixed, the resulting white light has a chromaticity coordinates which are a linear combination of the individual chromaticity coordinates weighted by density of luminous intensity (also shown in figure 2.4 by sRGB blue, sRGB green and sRGB red points). It means that resulting light's coordinates are enclosed in the area which is formed by connecting the chromaticity coordinates of emission from individual diodes. For example, for diodes emitting in blue, red and green (RGB), schematically shown in figure 2.5, almost all colour temperatures of white light can be obtained.

For the dichromatic WLED, GaN with InGaN quantum wells of various indium content is used to produce purple-blue (380 nm) to green-blue (486 nm) light emission. Materials such as GaP, GaAsP or AlGaInP with emission in the yellow-green, orange to red region respectively, are being used as complimentary sources to blue light. Generation of white light with those

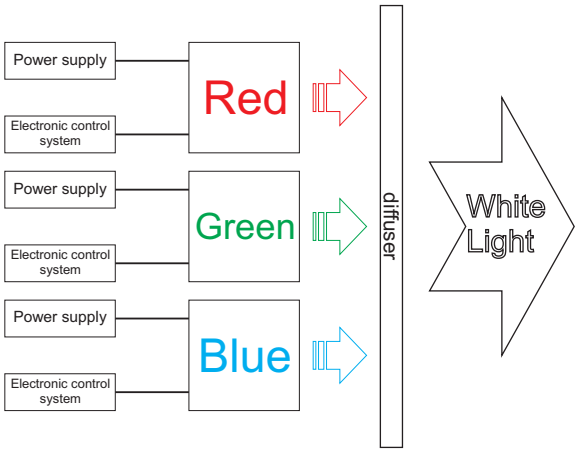

Figure 2.5: Schematic illustration of generation of white light based on multiple diodes emitting, for example, in red, green and blue.

materials can be realized as two separate diodes mounted next to each other in the diode housing, or in a single chip of semiconductor with two active regions emitting at different wavelengths. The later was demonstrated with a GaN based device which was designed to have two quantum wells from which first had an emission in blue (450 nm) and the second in yellow (520 nm) spectral region [31]. This type of devices, theoretically, can achieve very high luminous efficacy of radiation with the value of 440 lm/W [30], however their colour rendering index will be poor, as the spectrum contains only two nearly monochromatic peaks. This type of diode can find application in the areas where high illumination levels are required, however its quality is not important such as parking lots or street lighting.

For applications where the quality of light is crucial, the use of more than two diodes covering, with their emission, wider spectrum is necessary. The most common combination uses red, green and blue chips conveniently called RGB. Increasing the number of sources emitting at different wavelengths gives the flexibility of adjusting the correlated colour temperature and simultaneously improves the CRI value but decreases the luminous ef-

ficacy. It has been demonstrated that cool white light with 6500 K CCT and CRI value of 84 can be generated by the diodes emitting at 450, 540 and 610 nm with full width half maxima of their spectra (FWHM) of 23 nm, 44 nm and 19 nm respectively [32]. For luminous fluxes ratio adjusted to achieve CCT of 6500 K luminous efficacy of radiation as high as 319 lm/W can be realized. The resulting white light spectrum covering the wide part of the visible radiation with three peaks from which the widest had its maximum around the wavelength were the eye is most sensitive to light has contributed to the accomplished results.

The spectral properties of the diodes, such as the luminous flux, the maximum emission wavelength and the spectral width of emission, are very sensitive to changes of the temperature of the device which can rise with increased current supply or extended working time. The chromaticity coordinates of white light depend on all of these spectral properties, so even a small variation of one of them will change the appearance of white light. Each diode then needs to have its own electronic control system adjusting the value of the current supply and in result luminous flux (Φ_{lum}) of the diode so that the desired quality of white light remain unchanged. However this increases the currents needed to run the device and results in decreased efficiency of the WLED. The need for this current regulation system for each colour chip in a diode brings the overall production costs up causing restricted applicability of multicoloured WLEDs.

Colour conversion based WLEDs

In 1994, high brightness blue InGaN/AlGaN LED has been developed [33] and, since then, the idea of using it as a basis for the white light emit-

ter has been explored. The 2.7% value of external quantum efficiency for the emission of 450 nm with FWHM of 70 nm of a diode driven at 20 mA was the highest reported at the time. Even though it now seems very low, this power of emission was enough to excite the wavelength converting medium $Y_3Al_5O_{12}$:Ce, commonly called YAG or phosphors, and obtain white light [34].

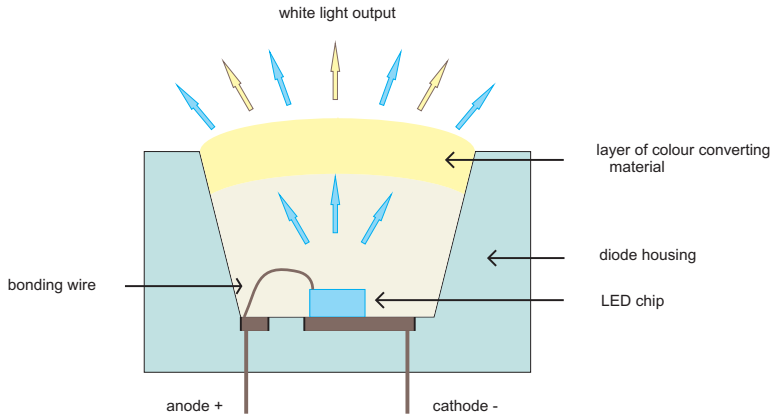

Figure 2.6: Schematic illustration of LED generating white light based on colour conversion method.

Light emitting diode generating white light based on the colour conversion method consists of GaN chip with InGaN quantum wells, emitting high energy photons, surrounded by a dome filled with material used to down-convert part of the emission spectrum of the chip suspended in silica (figure 2.6). Both spectra, blue and yellow, from colour converting medium, add up to provide the impression of white light. The spectrum of such white light emitting diode can achieve high values of luminous efficacy due to the fact that yellow peak is wide and covers most of the wavelength range under eye response function, shown in figure 2.7. As the spectrum contains only two peaks (even if the yellow one is wide) colour rendering index can be

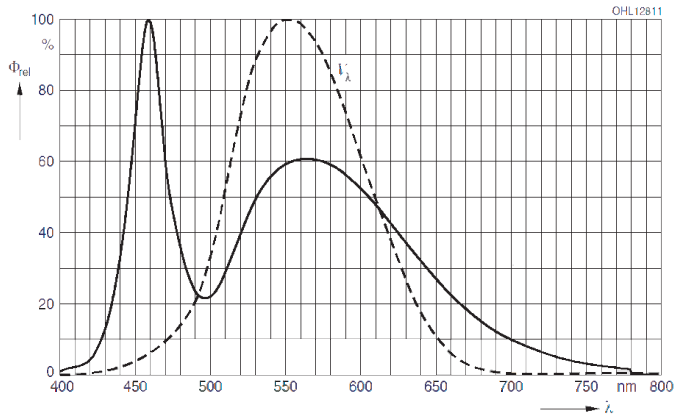

Figure 2.7: Typical spectrum of YAG based WLED (solid line) with eye response function (dashed line) [28]

improved by use of mixture of different down converting materials. Similar to generation of white light from multicolour diodes, mixing of phosphors emitting in blue, green and red was proposed to better approximate the spectrum of a black body radiator [35]. Device with RGB phosphors has improved rendering capabilities of the WLED with the CRI value above 90, however its efficiency dropped due to energy losses in the materials down-converting blue emission into red (Stoke's shift). It has been theoretically predicted that due to the Stoke's shift blue to red conversion efficiency can reach value 65% at most [30].

Phosphor based diodes has shown good quality white light with high luminous efficacies however the main disadvantage of this technique is the stability of chromaticity coordinates of white light. Phosphors tend to age and gradually loose their power of emission: this effect, in turn, causes colour changes in the resulting white light. There are several mechanisms which contribute towards the ageing of phosphors: one of them is heat, produced by diodes during their standard operations. If this heat is not driven away by the heat sink it will degrade the quality of the white light. Stability of

CCT of white light is also dependent on the variation of thickness of the phosphor(s) layers. Advanced deposition techniques need to be used for coating the semiconductor chip with phosphor to the highest precision to avoid colour differences between WLEDs of the same correlated colour temperature.

This method of generation of white light from solid state devices is the best available trade off between the light quality (CRI), luminous efficacy and production costs. It does not, however, satisfy requirement set for the optimal light source. To improve efficiency of phosphor based WLED and maintain the quality of light through the lifetime of the device new down-converting materials needs to be developed with reduced energy losses.

Organic materials such as polymers and dyes has been researched as down-converting media in white light emitting diodes. One of the advantages of using dyes as a wavelength converting medium is the small distance between absorption and emission peaks (Stoke's shift). Such devices can theoretically give higher luminous efficacy of radiation than those with phosphors, because less energy is lost due to Stokes shift as the form of heat. There is a vast range of dye materials emitting at almost any wavelength in the visible light range, including green and red, so dye based devices can generate light with high colour rendering index. Due to the need of suspending dyes in a matrix like substance, the production of such devices requires thermal deposition in vacuum, which is an expensive process. Advanced deposition brings also advantages: uniform and homogeneous films with well defined excitonic structures which contributes to the high efficiencies of the resulting WLEDs. The major drawback is the lifetime of dyes; these materials tend to become optically inactive after a considerably shorter time than that of phosphors or semiconductors.

Polymers, similarly to dyes, are produced in a vast range of emission wavelengths giving opportunity to optimize emission spectrum to match the one of the ideal. An additional advantage in using polymers or dyes in WLEDs is the possibility of excitation in alternative ways such as resonant energy transfer. Enhancement of 16.5% has been reported for the use of energy transfer alongside absorption re-emission process in polymer based WLED [36].

Chapter 3

Experimental methods

3.0.1 Integrated photoluminescence

Quantum efficiency of photoluminescence can be determined experimentally from the relation between absorbed and emitted light as described by equation:

$$QE = \frac{N_{em}}{N_{abs}}, \tag{3.1}$$

where N_{abs} is a number of absorbed photons and N_{em} is a number of emitted photons.

The most accurate way of measuring light emitted by nanocrystals is by placing the sample inside an integrating sphere. In this way the representative sample of total photoluminescence signal, emitted in all directions is measured [37]. The light absorbed by nanocrystals can then be calculated from a difference between the total incident excitation light beam signal measured in empty sphere (N_{empty}) and in the presence of the sample in the sphere (N_{sample}). This relation is shown by the equation:

$$N_{abs} = N_{empty} - N_{sample}, \tag{3.2}$$

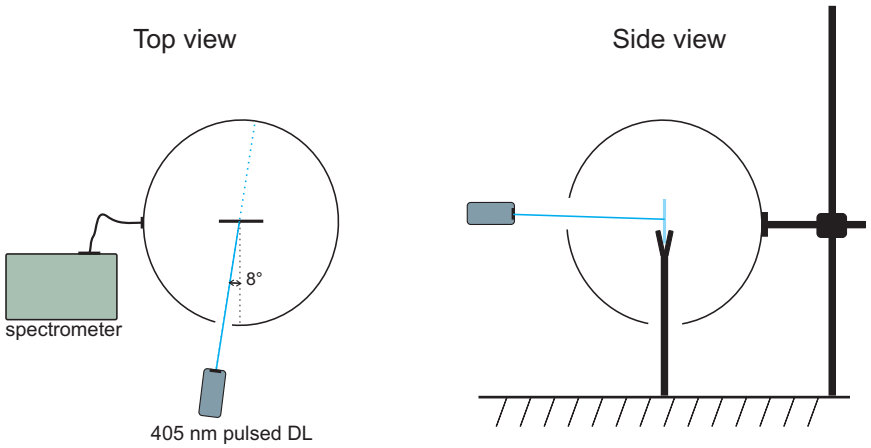

Figure 3.1: Nanocrystals quantum efficiency experiment setup.

In this experiment a set of InP/ZnS samples was measured. The samples were prepared by drop-casting of nanocrystal' solution on non-absorbing and non-emissive substrates of fused silica.

The corner of the sample's substrate was clamped in the sample holder (coated by the $BaSO_4$ paint used to cover the inside of the integrating sphere), and the 6 inch integrating sphere was lowered down onto a sample, into a fixed position so that the sample was exactly in the middle of the sphere and the sphere position for the following measurements was reproducible. Samples were optically excited by PicoQuant pulsed diode laser emitting at 405 nm through the one inch diameter port, 8 degrees from the perpendicular direction to the sample (as shown in figure 3.1) so that the excitation beam, reflected from the sample did not leave the sphere. The laser beam was aligned in such a way that the entire area covered with the nanocrystals was uniformly illuminated. The reflected and scattered laser light and the light emitted from the nanocrystals was sampled by coupling into an 1000 μm diameter optic fibre connected to the Andor spectrometer, which has spectral resolution of 0.55 nm. On the input port of the spectrometer 750 nm short pass filter was installed in order to eliminate second

harmonics signal from the laser. However, this filter does not influence measurements presented in this thesis as the visible part of the spectrum is of our interest.

The measurements were corrected for setup self - absorption losses, with an auxiliary lamp. In order to perform measurements for this correction, light from a 50 W incandescent light source was coupled into the sphere through the excitation port. Two measurements were recorded: with sample mounted inside the sphere ($A^{test}(\lambda)$) and without it ($A(\lambda)$). The values acquired were used in the calibration process described below.

The entire system was calibrated using a F976 spectral irradiance standard lamp with known spectral distribution of radiant power as a reference. Calibration was performed in a completely dark room with black walls, ceiling and floor, for the set up shown in figure 3.1. Neither the sample nor the sample holder were present inside the sphere during calibration. F976 spectral irradiance lamp was mounted 50 cm away from the middle of the sphere as recommended by CIE and its light was coupled into a sphere through the excitation port. The signal for test light source $S_{test}(\lambda)$ and reference light source $S_{ref}(\lambda)$ followed by background measurements $B_{test}(\lambda)$ and $B_{ref}(\lambda)$ for both of the light sources were recorded. The light sources for the background measurements were switched off. The results of the measurements were calculated with the use of the formula:

$$\Phi_R(\lambda) = \Phi_{ref}(\lambda) \cdot \frac{S_{test}(\lambda) - B_{test}(\lambda)}{S_{ref}(\lambda) - B_{ref}(\lambda)} \cdot \frac{\tau^{ref}}{\tau^{test}} \cdot \frac{A(\lambda)}{A^{test}(\lambda)} \tag{3.3}$$

where $\Phi_R(\lambda)$ and $\Phi_{ref}(\lambda)$ are radiant fluxes of test light source (nanocrystals) and reference light source, respectively, τ^{test} and τ^{ref} are exposure time of test and reference light source and their backgrounds, respectively

and $A^{test}(\lambda)$ and $A(\lambda)$ are signals from auxiliary lamp for the sphere with sample mounted inside and without it, respectively.

3.0.2 Time resolved photoluminescence

Time correlated single photon counting technique probes the changes of the carrier population after the illumination with a short pulse of light and thus can be used to study carrier's dynamics.

Experimental setup

For time resolved measurements samples were excited with a PicoQuant pulsed diode laser emitting at the wavelength of 405 nm, which is above the bandgap of InP core (1.34 eV) but below the bandgap of ZnS shell (3.54 eV). Samples for low temperature measurements were mounted inside a helium cooled cold finger cryostat. The laser excitation consisted of a train of 70 ps long light pulses, with the repetition rate of 2.5 MHz. Light emitted by the nanocrystals was focused on an input slit of a spectrometer; a 7 nm band of the spectrum centred at the selected wavelengths were isolated with an output slit and focused on a Si single photon avalanche photodiode (APD). Decay curves at these particular emission wavelengths were measured using time resolved single photon counting. The schematic illustration of the set up is shown in figure 3.2.

Time resolution of the system, determined by the laser diode pulse width and the response time of the APD, was 200 ps while the photoluminescence decay curves were recorded over one period of the laser signal, 400 ns. The period of the laser pulse train was sufficiently long (400 ns) to

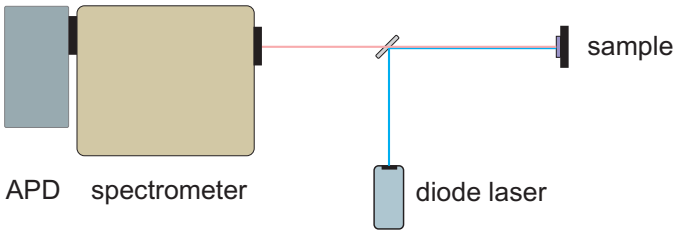

Figure 3.2: Time resolved photoluminescence set up.

allow the recombination of most excitons generated by one laser pulse before the arrival of the next one. It was confirmed by comparing the level of the signal before arrival of the excitation pulse and the signal at the end of the recorded period. As a result of low photon absorption probability, the laser frequency was sufficient to avoid multiple exciton generation, which would result in a very fast Auger recombination [38].

Data analysis

Unlike in the case of quantum dots in semiconductor bulk materials, environment of colloidal nanocrystals is complex and less controllable [10, 39, 40]. Even in the core-shell nanocrystals, photo-excited carriers can be transferred to the shell surfaces and more generally to defects or decay via coupling to ligands leading to complicated carrier dynamics [41]. As a result, photoluminescence (PL) decay curves from the nanocrystals measured following light pulse excitation are most often multi-exponential and difficult to interpret [42].

Several models have been suggested in order to qualitatively describe nanocrystals photoluminescence decay, such as multiexponential functions [43, 44], log-normal distribution of decay rates [45, 46] or stretched exponential model [47, 48, 49]. The evidence that the normalization of the stretched

exponential function for the emitters with quantum efficiency lower than 100% is incorrect has resulted in excluding this method in further analysis [45].

In the same publication statistical analysis of log-normal distribution of set of exponential functions is suggested as an alternative and superior to stretched exponential method. The fitting function has a form:

$$f(t) = \int_0^\infty \sigma(k_{tot}) \cdot e^{-t \cdot k_{tot}} dk_{tot} \tag{3.4}$$

where $\sigma(k_{tot})$ is the distribution of total decay rates k_{tot} and is equal to:

$$\sigma(k_{tot}) = A \cdot e^{-(\frac{ln(k_{tot}) - ln(k_{mf})}{\gamma})^2} \tag{3.5}$$

where A is the normalization constant, k_{mf} is most frequent decay rate and γ is related to width of the distribution of decay rates (Δk) at 1/e value in the following way:

$$\Delta k = 2 \cdot k_{mf} \cdot sinh(\gamma) \tag{3.6}$$

The example of fitting of a decay curve of InP/ZnS nanocrystals emitting at wavelength of 655 nm measured in the homogeneous environment of toluene is shown if figure 3.3. The fitting quality is confirmed by the $\chi^2 = 1.1$. This value is based on the residuals and show the discrepancy between observed values and the values expected under the model in question where value of 1 is the ideal. The decay times are much longer than the instrument response function thus the deconvolution of those functions is not necessary however as a result of this the residuals around 0 time are slightly higher. Fitting gives the values of $k_{mf} = 2.7 \cdot 10^7\ s^{-1}$ and $\Delta k = 4.4 \cdot 10^7\ s^{-1}$.

Multiexponential fitting with two [50, 51] or three [38, 43, 52, 53] com-

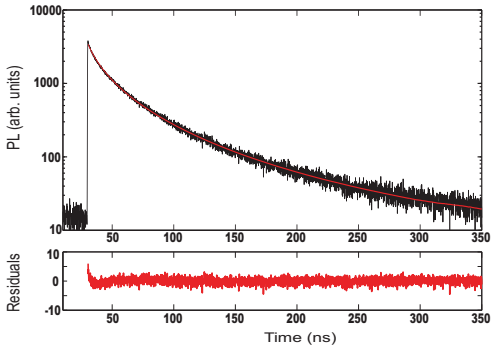

Figure 3.3: Decay curve of photoluminescence of nanocrystals with peak emission wavelength of 655 nm together with log-normal distribution of decay rates fitting curve (red line) and residuals (bottom panel).

ponents is widely used to fit decay of photoluminescence of nanocrystals with good results. It has been shown, that a careful analysis of all exponential decay components can be successfully used to get an insight into the internal structure of the nanocrystals [38, 54]. The results of fitting with this method can be used to compare different sets of nanocrystals and might give more intuitive picture of the processes responisble for recombination of carriers. Care has to be taken though, since a presence of the certain decay rate range indicate only a presence of certain states rather than gives the values of the recombination rates. The fitting function has a form:

$$\frac{y(t)}{y(0)} = \sum_{i=1}^{n} A_i \cdot e^{-k_i \cdot t}, \tag{3.7}$$

where n is number of exponents and $\sum_{i=1}^{n} A_i = 1$. The same decay curve as used for demonstration of the log-normal distribution fitting was fitted with the three exponents as shown in figure 3.4 together with residuals to the fitting. The fit was good as the $\chi^2 = 0.998$ and gave the following results: $A_1 = 0.5$, $A_2 = 0.32$, $A_3 = 0.18$, $k_1 = 5.5 \cdot 10^7 s^{-1}$, $k_2 = 2.8 \cdot 10^8 s^{-1}$, $k_3 = 1.6 \cdot 10^7 s^{-1}$. The average decay rate calculated from the formula:

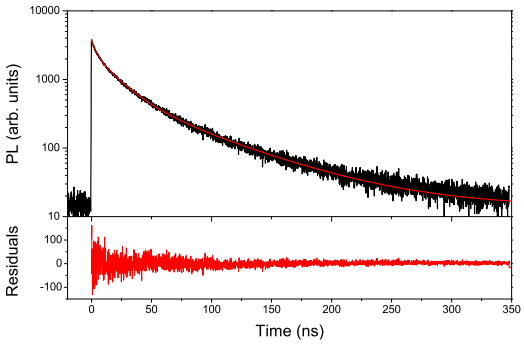

Figure 3.4: Decay curve of photoluminescence of nanocrystals with peak emission wavelength of 655 nm together with three exponential fitting curve (red line) and residuals (bottom panel).

$$k_{ave}^{-1} = \frac{\sum_{i=1}^{n} A_i/k_i}{\sum_{i=1}^{n} A_i/k_i^2} \tag{3.8}$$

and result in $k_{ave} = 2.38 \cdot 10^7 s^{-1}$. Note that the value of k_{ave} is close to the value of k_{mf}.

The log-normal distribution of lifetimes gave equally good quality fitting results to the three exponential functions and we have chosen the later to describe data in this document for the reasons mentioned above.

Chapter 4

InP/ZnS nanocrystals as light emitters

In this chapter optical characterization of the InP/ZnS colloidal nanocrystals purchased from NN-labs is presented. In time of writing those are the only non-toxic nanocrystals with a tunable emission wavelength between 500 and 700 nm.

In order to investigate the applicability of InP/ZnS nanocrystals as colour converting medium in white light emitting diodes it is most important to measure their quantum efficient of photon emission. Quantum efficiency of photoluminescence has been determined from the absorption and emission measurements and through modification of local densities of optical states. Based on the temperature and/or wavelength resolved time resolved photoluminescence (TRPL) carrier dynamics are discussed and four energy level diagram is proposed.

4.1 Quantum efficiency of InP/ZnS nanocrystals

In order to study the emissive properties of InP/ZnS nanocrystals we have measured a set of samples with the peak emission wavelength covering the range from 530 nm, through 570, 615, 630 nm to 655 nm with full width half maxima of 50, 60, 75, 90 and 105 nm, respectively. Samples, one by one, were placed in the centre of a 6-inch integrating sphere and were excited with a collimated light beam from a pulsed diode laser with the excitation power which was kept well below 10^{-6} photons per NC per pulse. The absorption was not saturated as evident by the linear change with excitation power, shown in table 4.1 and figure 4.1. Radiant fluxes of the photoluminescence spectra of all samples in a visible range were converted to a number of emitted photons, based on the following equation:

$$N_{em} = \frac{1}{h \cdot c} \int \Phi_R(\lambda) \cdot \lambda d\lambda \tag{4.1}$$

shown in the figure 4.2.

Power (mW)	530 nm	570 nm	615 nm	630 nm	655 nm
0.38	$1.41 \cdot 10^{-9}$	$6.58 \cdot 10^{-9}$	$2.27 \cdot 10^{-8}$	$4.15 \cdot 10^{-8}$	$5.09 \cdot 10^{-8}$
0.25	$5.37 \cdot 10^{-10}$	$4.59 \cdot 10^{-9}$	$1.42 \cdot 10^{-8}$	$2.91 \cdot 10^{-8}$	$3.25 \cdot 10^{-8}$
0.20	$4.86 \cdot 10^{-10}$	$3.60 \cdot 10^{-9}$	$1.13 \cdot 10^{-8}$	$2.30 \cdot 10^{-8}$	$2.50 \cdot 10^{-8}$
0.14	$3.73 \cdot 10^{-10}$	$2.52 \cdot 10^{-9}$	$8.02 \cdot 10^{-9}$	$1.59 \cdot 10^{-8}$	$1.79 \cdot 10^{-8}$
0.10	$2.32 \cdot 10^{-10}$	$1.80 \cdot 10^{-9}$	$5.89 \cdot 10^{-9}$	$1.16 \cdot 10^{-8}$	$1.32 \cdot 10^{-8}$

Table 4.1: Absorption per nanocrystal per laser pulse for all the sizes of nanocrystals for five different excitation powers.

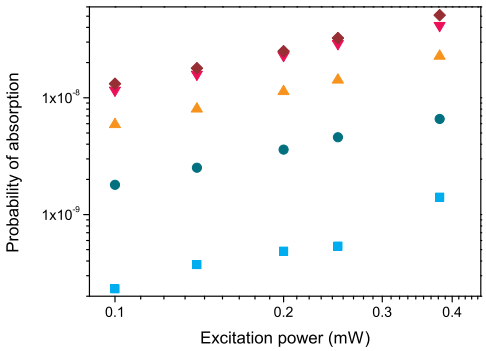

Figure 4.1: Absorption probability versus excitation power for nanocrystals with peak emission wavelength of 530 nm (cyan line), 570 nm (green line), 615 nm (orange line), 630 nm (pink line) and 655 nm (brown line).

Note that the long wavelength part of the spectrum of nanocrystals with peak emission wavelength of 530 nm drops nearly to 0 while other nanocrystals show signal at the level of $\sim 1.2 \cdot 10^{10}$ photons. This indicates that the bigger nanocrystals have higher level of sub-bandgap states than the 530 nm nanocrystals.

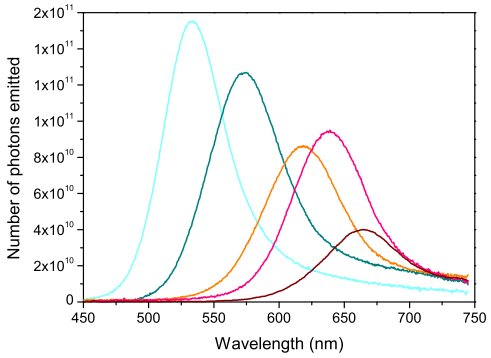

Figure 4.2: Photoluminescence spectrum expressed as a number of emitted photons of InP/ZnS nanocrystals with peak emission wavelength of 530 nm (cyan line), 570 nm (green line), 615 nm (orange line), 630 nm (pink line) and 655 nm (brown line).

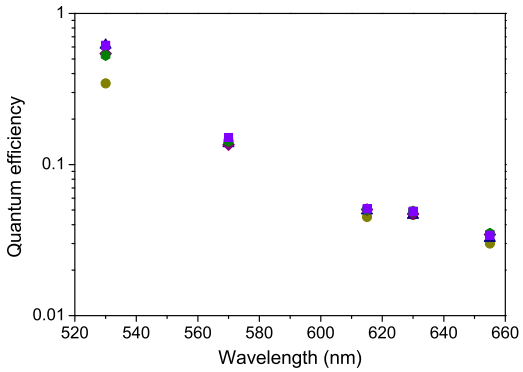

Figure 4.3: Quantum efficiency of InP/ZnS nanocrystals for following excitation powers: 0.38 (mustard dot), 0.25 (navy triangle), 0.20 (brown diamond), 0.14 (green hexagon), 0.10 (lilac square) mW as a function of peak emission wavelength.

The amplitudes of photoluminescence spectra of nanocrystals with peak emission wavelengths of 615 nm and 655 nm (orange and brown curve respectively) are lower than the trend in the curves suggesting that these NCs are of worse quality than expected. The quantum efficiency (QE_{NC}) defined in equation 3.1, presented in figure 4.3 for all of the samples, did not change within experimental error for the excitation powers change by the factor of four, shown in the figure 4.3. The quantum efficiency drops by an order of magnitude between the shortest and longer wavelengths ($\sim$50% PL quantum efficiency of 530 nm InP/ZnS nanocrystals and $\sim$5% QE of 655 nm nanocrystals [55]). This result seems counter-intuitive because nanocrystals' surface is believed to be the main source of non-radiative recombination [56] and it should become less important in larger nanocrystals [57].

In order to get insight into the origin of the efficiency drop with the emission wavelength we studied carrier's dynamics in the nanocrystals using time-resolved photoluminescence (TRPL) measurements. Figure 4.4 shows photoluminescence decay curves for peak wavelengths of all samples.

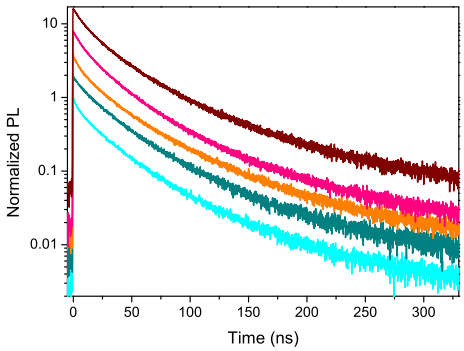

Figure 4.4: Photoluminescence decay curves for of nanocrystals (each normalized to 1) with peak emission wavelength of 530 nm (cyan line), 570 nm (green line), 615 nm (orange line), 630 nm (pink line) and 655 nm (brown line), shifted vertically for clarity.

All the curves, shown in the figure, were normalized to 1 and shifted vertically for clarity. One can see that the photoluminescence decay curves for all samples are very similar in the period of measurement, which corresponds to three orders of magnitude change in the signal.

PL decay is multiexponential and in the measured period it can be well fitted with three exponential components as discussed in chapter 3. Average decay rate k_{ave}, shown in figure 4.5 for all five samples, varies in the range between $3.16 \cdot 10^7$ s^{-1} and $3.87 \cdot 10^7$ s^{-1} which is too small to explain the change of quantum efficiency especially that variations are not correlated with the trend in QE. If we compare QE for all samples calculated from the standard equation that couples recombination rates and QE:

$$QE = \frac{k_{rad}}{k_{rad} + k_{nrad}} = \frac{k_{rad}}{k_{tot}}, \tag{4.2}$$

where k_{rad} and k_{nrad} are radiative and non-radiative decay rates, respectively, we would expect very similar values for all samples. This conclusion is based on the fact the the measured decay rates are very similar and accord-

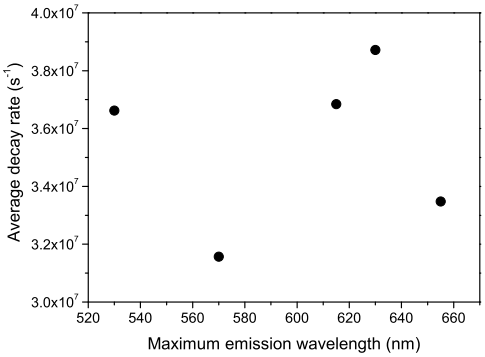

Figure 4.5: Average decay rate for the peak emission wavelength for all NCs samples.

ing to calculations presented below the k_{rad} weakly changes as a function of emission wavelength (see figure 4.6).

The k_{rad} shown in figure 4.6 is calculated from an oscillator model in which bright excitonic state is coupled to the dark excitonic state [49]. According to the oscillator model the decay rate of the bright excitons, γ_b, is:

$$\gamma_b = \frac{e^2 n F \omega^2 f}{6\pi\epsilon_0 m_0 c^3} \tag{4.3}$$

here n is a refractive index of the surrounding material (toluene in this case), F is a screening factor, ω is an photon emission frequency, c, ϵ_0, e and m_0 are speed of light in vacuum, vacuum permittivity, free electron charge and mass, respectively. As a result of coupling to dark states, which decay with the rate γ_d, the exciton decay rate is modified as follows:

$$\gamma = \frac{g_b \gamma_b e^{-\frac{\delta E}{kT}} + g_d \gamma_d}{g_b e^{-\frac{\delta E}{kT}} + g_d} \tag{4.4}$$

where $g_{b(d)}$ is the degeneracy of bright (dark) exciton state, equal to 3(5) for InP/ZnS nanocrystals [58] and δE is the energy separation between the

two states.

Results shown in figure 4.6 are calculated for the following parameters. The bright-dark exciton splitting has been assumed to follow the relationship measured in [43] and derived in [49]. The lifetime of excitons in the dark state has been taken as 1 μs [59, 60], although the calculated decay rate has not changed if the dark states lifetimes longer than this have been used. Dielectric functions of bulk InP (for the nanocrystals) and a refractive index of toluene for the surrounding medium have been used. Finally, for the full line the electron-hole overlap was taken to be equal to one and it was assumed that there is no non-radiative recombination. Such calculated decay rate is an upper limit for the radiative recombination rate in this system of coupled bright-dark excitons.

A reduction of the electron-hole overlap to more realistic value of 0.6 [52] has resulted in a calculated decay rate shown with dashed lines in figure 4.6.

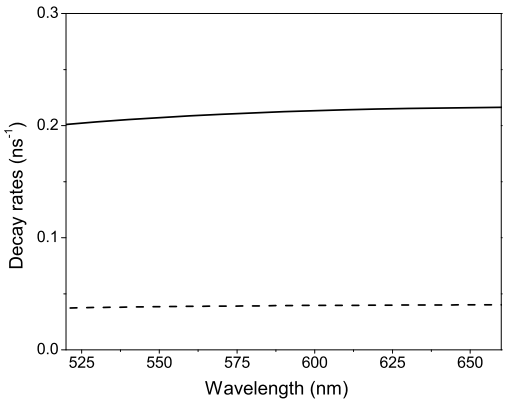

Figure 4.6: Calculated radiative decay rates as a function of wavelength for a system of coupled dark-bright excitons for the electron-hole wavefunction overlaps equal to 1 indicated as solid line and equal to 0.6 marked as dashed line.

The expected from equation 4.3 inverse dependence of the decay rate on emission wavelength is modified by the wavelength dependence of dielectric constant of InP and by wavelength dependence of the bright-dark exciton splitting. The wavelength dependence of the dielectric constant results in a weakly changing linear dependence of the decay rate on the wavelength. The dark-bright exciton splitting has been shown to increase at shorter wavelength with the dark exciton lower in energy [49, 58, 61]. Under these assumptions the linear dependence of the decay rate on wavelength is further enhanced.

As a result of the k_{rad} and k_{tot} being similar for all of the nanocrystals, the only way to reconcile the results of the QE and TRPL measurements is to assume that each nanocrystals' sample contains two populations of nanocrystals: one which emits light (bright) and one in which luminescence is quenched (dark). In such a case, QE becomes:

$$QE = \frac{k_{rad}}{k_{tot}} \cdot \frac{N}{N_{abs}}, \tag{4.5}$$

where N and N_{abs} are number of photons absorbed in emissive nanocrystals and number of absorbed photons in all nanocrystals, respectively. The ratio of N/N_{abs}, is effectively the fraction of bright nanocrystals in the whole population. Since we assumed that k_{rad}/k_{tot} is the same for all of five samples, if we also assume that for the smallest nanocrystals, emitting at 530 nm, $N = N_{abs}$, we can calculate the ratio of N/N_{abs} for all of the nanocrystal' samples, as shown in the table 4.2. Even though the assumption that k_{rad} and k_{nrad} are not changing between samples and that all NCs in 530 nm sample are emissive is only an approximation, it is clear that nanocrystals of larger sizes have much lower fraction of emissive nanocrystals.

λ_{max}	QE_{NC}	N_{abs}	N/Nabs
530	0.52	$1.77 \cdot 10^{14}$	1
570	0.15	$1.11 \cdot 10^{14}$	0.3
615	0.05	$6.11 \cdot 10^{13}$	0.1
630	0.05	$4.22 \cdot 10^{13}$	0.1
655	0.03	$2.12 \cdot 10^{13}$	0.06

Table 4.2: Results of the calculations of bright population of nanocrystals N/N_{abs} based on the assumption that the NCs emitting at 530 nm have 100% of bright nanocrystals and that the quality of nanocrystals does not change with their size (emission wavelength).

It is well known that colloidal nanocrystals exhibit blinking, a phenomenon which leads to the repeated switching of the nanocrystal between light emitting and light quenched states over time [62] and that off-time can last in the range from milliseconds to minutes while an on-time can be anywhere between few milliseconds to few hundred seconds [63]. Although there is no universally accepted explanation of this behaviour [64, 65], it has been shown that there is no correlation between the quantum efficiency and on-time of the blinking nanocrystals [64, 66]. Report on the size dependant intermittency shows that the on-time fraction for larger nanocrystals emitting at 649 nm was 70 % while for the smaller nanocrystals, emitting at 565 nm it was around 30% [64]. If we assume that blinking is responsible for the observed quantum efficiency then the later would be expected to be higher for larger nanocrystals. It leads to a conclusion that there must be a population of the permanently dark nanocrystals present in the samples [64].

Since the exciton Bohr radius of InP ($\sim$ 11.5 nm) is much larger than the radius of the InP cores, even a single defect acting as a non-radiative recombination centre can quench the PL of the nanocrystal. In uniform nanocrystals, an interface between InP core and ZnS shell is the most likely

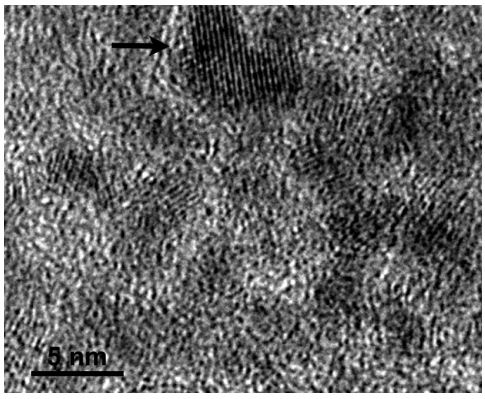

Figure 4.7: TEM image of nanocrystals emitting at 615 nm, black bar represents 5 nm. Black arrow points at particularly clear coalesced nanocrystal.

location of defects. As the average radius of NCs increases only from 1.5 nm to 2.1 nm between the smallest and largest nanocrystals, as imaged on transmission electron micrograph (shown in the chapter 5), in order to explain the order of magnitude change in efficiency with surface states we need to assume that as the reaction time is extended, surface area increases more than 10 times. Such situation is expected for nanocrystals grown in the Oswald ripening growth mode where the smaller particles disintegrate to provide material for growth of the larger particles resulting in surface disorder and grain boundaries. This is believed to influence the quantum efficiency of the measured nanocrystals [67].

Transmission electron microscopy of the nanocrystals emitting at 615 nm confirms that during the reaction leading to the formation of these nanocrystals, Oswald ripening was taking place. Images, example of which is shown in figure 4.7, have shown that a fraction of the nanocrystals has a form characteristic for particles created by coalescence of smaller nanocrystals. Coalesced nanocrystals tend to be irregular, often elongated, and are typically polycrystalline. This results in much larger surface/volume ratios than for regular shaped nanocrystals and adds internal grain boundaries. The log-

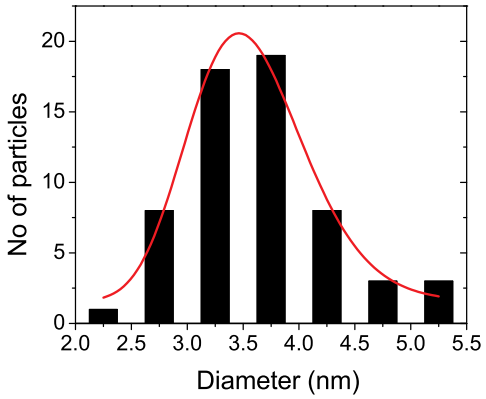

Figure 4.8: The size distribution of the NCs size determined from HRTEM image fitted with log-normal distribution function (red line).

normal distribution of the nanocrystals sizes, shown in figure 4.8 indicates further a presence of clustering. Although difficult to observe directly, another result of Oswald ripening is the surface roughening, which would also contribute to the luminescence quenching.

Summarizing, we have shown that although colloidal InP/ZnS nanocrystals emitting below 600 nm achieve high quantum efficiency of photoluminescence, it is not the case for nanocrystals emitting at longer wavelengths. During the synthesis of bigger nanocrystals, the surface of the nanocrystals and grain boundaries increase, so does the probability of creating defect that affects the luminescence.

4.2 Quantum efficiency of the nanocrystal's bright population

Measurements of quantum efficiency based on the relationship between nanocrystal's absorption and emission processes defined by equation 3.1 was described in the previous section (4.1). It provides information on the efficiency of the total population of nanocrystals, both bright and dark, and as such is the most important parameter for applications such as solid state lighting [22], solar cells [68], sensors [69] or lasers [70]. However, it is also important to quantify the efficiency of bright population of nanocrystals to better understand the dynamics of excitons and further improve synthesis.

In order to perform such study a controlled modification of local density of optical states (LDOS), a method proposed by Drexhage [71] and implemented later by others for variety of emitting materials [72, 73, 74], can be used. By placing the nanocrystals in a homogeneous medium, in a set of defined distances from a mirror, non-radiative and radiative components of the total recombination rate can be extracted. The radiative recombination is effected by the presence of the mirror while the non-radiative one remain constant. Due to the interference of the direct and the reflected beam, emission rate varies with changing the distance of the emitter to the mirror. For the constructive interference decay time of the emitter placed in the given distance from the mirror will shorten as the probability of radiation will be larger than in the case without the mirror. For the destructive interference situation will be opposite and decay time will get longer.

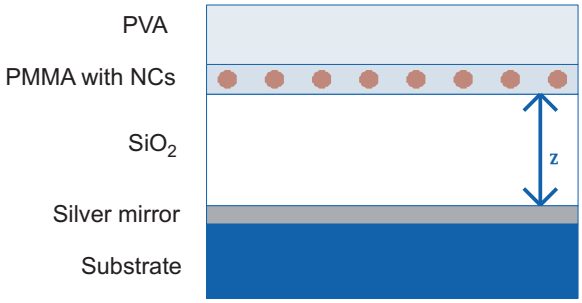

Figure 4.9: Schematic diagram of a sample used to determine quantum yield of the bright fraction of nanocrystals.

In order to study the changes of the decay times with distance to the mirror surface a set of 8 samples with the geometry shown in figure 4.9 has been fabricated. Optically thick layer of 200 nm of silver was evaporated in a vacuum chamber of an evaporator on the 1 cm^2 silicon substrate. It was followed by evaporation of the silicon dioxide SiO_2, which plays a role of a spacer between the silver mirror and emitters. Its nominal thickness between 50 nm and 300 nm with the possible error of 3 nm was controlled by adjusting the deposition time. The layer of nanocrystals immobilized in PMMA matrix was spun on such prepared substrates.

Layer	Thickness (nm)	Refractive Index at 405 nm	Deposition method
SiO_2	variable ± 3	1.469	vacuum evaporation
PMMA with NCs	10 ± 1	1.49	spin coating
PVA	∼1000	1.52	spin coating

Table 4.3: Details of the samples layers. Thickness of the SiO_2 layer for all samples are as follow: 50, 75, 100, 125, 175, 250, 275 and 300 nm.

To avoid interactions between excitons in neighbouring nanocrystals the concentration of nanocrystals in PMMA layer was chosen to be 1 per 2500 nm^2 which is equivalent to average of 50 nm distance between neighbouring nanocrystals. The thickness of the PMMA layer was measured with profile stylus with resolution of 1 nm and its surface roughness was confirmed by atomic force microscope with the tip radius curvature of 2 nm. On the basis of this measurements the error was calculated to be $\sim$1 nm. A layer of PVA was spun on the top of the sample to move the interface with air away from nanocrystals - mirror interface and maintain the homogeneous environment with refractive index $\sim$1.5 around NCs. The optical constants of the layers were determined by ellipsometry with 2 nm spectral resolution. Results are summarized in the table 4.3.

The biggest nanocrystals, with maximum emission wavelength of 655 nm, have shown the lowest quantum efficiency, indicating that there is the highest number of dark nanocrystals. We choose this size of the nanocrystals for further analysis, to establish the quality of the bright population of the total sample.

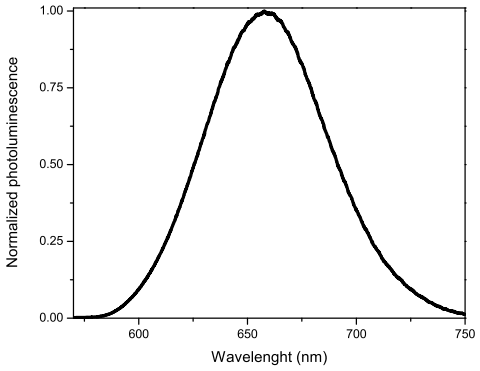

Figure 4.10: Photoluminescence spectrum of InP/ZnS nanocrystals.

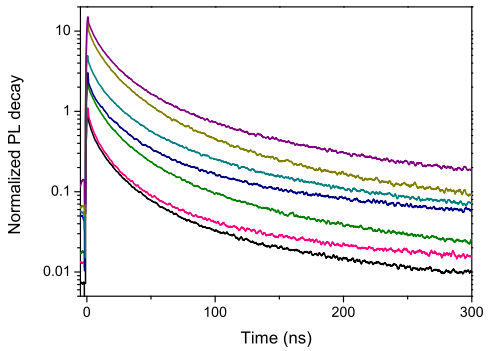

Figure 4.11: Normalized to 1 decay of photoluminescence spectrum of InP/ZnS nanocrystals for samples with 75 (black), 100 (pink), 150 (olive), 175 (navy), 250 (dark cyan), 275 (mustard) and 300 nm (purple) SiO_2 layer shifted vertically for clarity.

We investigate the quantum yield of the bright population of the large nanocrystals with peak emission wavelength of 660 nm with FWHM of 66 nm whose spectrum is shown in figure 4.10. Nanocrystals for this study have been synthesised in different batch than the previous ones and the ligands stabilizing these nanocrystals have been changed for octadecylamine. The synthesis method was the same.

Time correlated single photon counting technique was used to obtain photoluminescence decay curves as described in chapter 3. The excitation energy was $1.1 \cdot 10^{-5}$ J·cm^{-2}. Figure 4.11 shows photoluminescence decay curves normalized to one for a peak wavelength for the set of samples with the thickness of the SiO_2 layer in a range between 75 and 300 nm.

Based on a Fermi golden rule, radiative decay rate (k_{rad}) is proportional to LDOS ($\rho(\omega, z)$) and therefore k_{tot} can be expressed as:

$$k_{tot}(\omega, z) = k_{nrad}(\omega) + k_{rad}^{hom}(\omega) \cdot \frac{\rho(\omega, z)}{\rho_{hom}(\omega)} \tag{4.6}$$

where $\rho_{hom}(\omega)$ is the LDOS in homogeneous medium and $\rho(\omega, z)$, shown

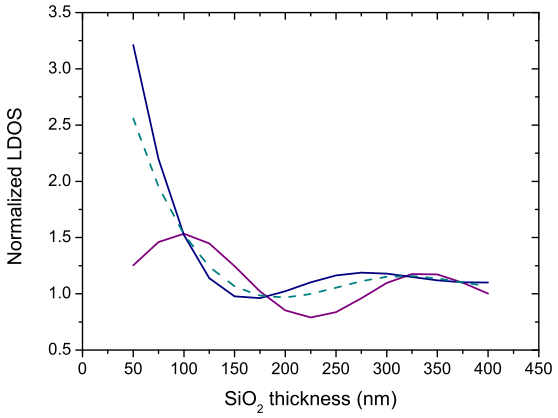

Figure 4.12: Local density of optical states as a function of thickness of SiO_2 spacer layer where LDOS for perpendicular dipole to the interface is shown as a purple curve, LDOS for parallel dipole is shown as a blue curve and LDOS used for experiment was the 1/3 the perpendicular dipole plus 2/3 parallel dipole shown as the dashed green curve.

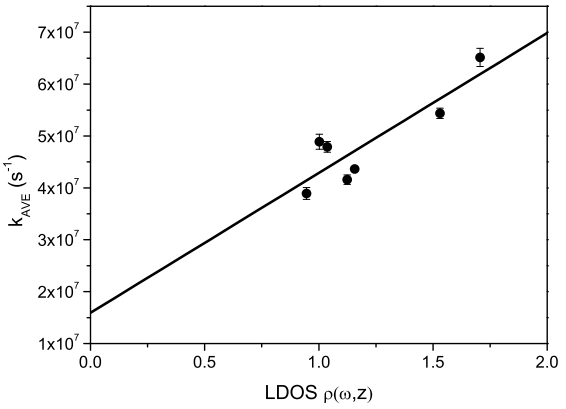

Figure 4.13: Decay rates as a function of local density of optical states.

λ_{max}	QE_{ave}	N_{abs}	N	N/N_{abs}
530	0.52	$1.77 \cdot 10^{14}$	$1.46 \cdot 10^{14}$	0.82
560	0.15	$1.11 \cdot 10^{14}$	$2.64 \cdot 10^{13}$	0.24
615	0.05	$6.11 \cdot 10^{13}$	$4.85 \cdot 10^{12}$	0.08
630	0.05	$4.22 \cdot 10^{13}$	$3.35 \cdot 10^{12}$	0.08
655	0.03	$2.12 \cdot 10^{13}$	$1.01 \cdot 10^{12}$	0.05

Table 4.4: Results of the calculation of bright population of nanocrystals and its fraction in total population.

in figure 4.12, is calculated from Green's function based on reference [75]. The formula holds when the coupling between radiative and non-radiative recombination channels is such that the total recombination rate can be expressed as a sum of the two components.

From the intercept and the slope of the fitted function, shown in figure 4.13, radiative and non-radiative decay rates have been extracted $k_{rad} = 2.7 \cdot 10^7 \pm 6.6 \cdot 10^6$ s^{-1} and $k_{nrad} = 1.6 \cdot 10^7 \pm 8.2 \cdot 10^6$ s^{-1}. The quantum yield of bright population of nanocrystals can be calculated from equation 4.2 and its value is equal to $QE_{BNC} = 0.63 \pm 0.38$.

Based on the assumption that the quality of the bright InP/ZnS nanocrystals of all sizes is the same, a fraction of bright nanocrystals in total population can be calculated with the use of equation 4.5. Results are shown in table 4.4 and being only slightly lower than the ones in table 4.2 they do not change the picture from previous section.

Care has to be taken in interpretation of the results. Although linear dependence in figure 4.13 would suggest the applicability of the method for these nanocrystals but as seen in nanocrystals spectra (and will be shown in next section) there is a strong coupling between various states in the nanocrystals. This may cause deviations, which might be hidden by a large standard deviation.

4.3 Exciton dynamics

As it has been shown in the previous section the quantum efficiency of a bright population of InP/ZnS nanocrystals is far from unity and in order to find a reason of this phenomenon further studies are necessary.

Optical studies of the colloidal nanocrystals have revealed a complex carrier dynamics, which needs to be fully understood for further improvements. Radiative recombination of photo-excited carriers competes in NCs with trapping on surface states [76] and with Auger recombination [77]. A reduction of the parasitic recombination channels is of a paramount importance for an implementation of nanocrystals in devices and it can be achieved if detailed understanding of the carrier dynamics can be gained.

We use temperature dependence of the time resolved photoluminescence of InP/ZnS colloidal nanocrystals coated with oleylamine ligands combined with multi-exponential fitting in order to identify the processes responsible for carrier recombination.

The laser power incident on the sample was set to be 15.6 μW, which corresponds to the energy density of $1.1 \cdot 10^{-5}$ J·cm^{-2}. From the probability of absorption in nanocrystals we expect an average generation of about 0.6 excitons per nanocrystal per laser pulse. Due to the Poissonian distribution of absorbed light, 10% of NCs were thus excited with more than one exciton, 33% of NCs were excited with one exciton, and 54% were not excited.

The nanocrystals were drop casted on quartz substrates and mounted on a cold finger of the helium cooled cryostat for the cryogenic measurements. Excess ligands (ligands not bound to the nanocrystals) ensured that the nanocrystals were kept on average 10 nm apart as revealed by TEM.

The photoluminescence spectrum from the nanocrystals measured on the quartz substrate at room temperature had a maximum at 642 nm. A PL spectrum at an intermediate temperature of 140 K is shown in figure 4.14. Upon cooling to 10 K the emission wavelength shifted to 632 nm reflecting increased bandgap, as shown in figure 4.15 while the FWHM decreased to 50 nm, as expected from eliminating phonon broadening [4].

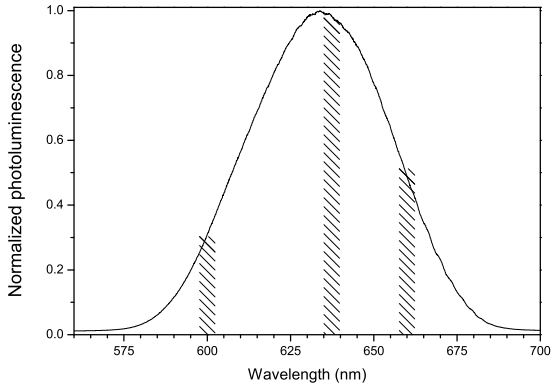

Figure 4.14: Normalized to 1 photoluminescence spectrum at 140 K. Shaded areas mark the parts of the spectrum selected for time resolved measurements.

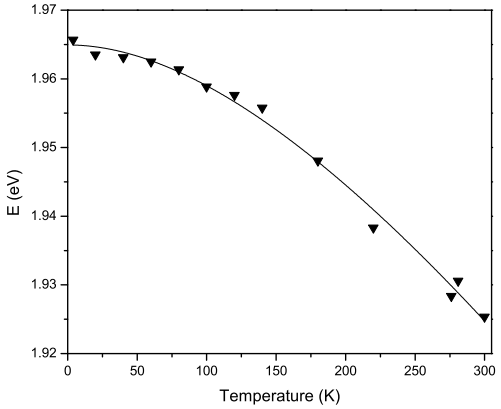

Figure 4.15: Peak emission energy (triangles) as a function of temperature together with fit (solid line) with Varshni equation.

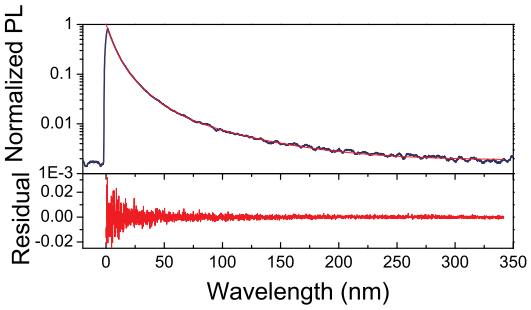

Figure 4.16: Time resolved photoluminescence following a pulse of laser light at time zero measured at 637 nm at 280 K together with the fitted curve (red line). Due to periodic excitation with 400 ns period, the signal level at t<0 indicates that not all excitons decayed before the pulse of laser at time t=0. Inset shows residuals for the fitting.

The bandgap change with the temperature was fitted with Varshni equation [78] with fitting parameters $\alpha = 3.6 \cdot 10^{-}4$ eV $\cdot$ k^{-1} and $\beta = 503$ K where the first one is close to that reported for bulk InP [79] and InP/ZnS nanocrystals [80].

Figure 4.16 shows exciton decay curve measured at 280 K. The curve can be fitted with three exponential components with rates: $k_1 = 0.25ns^{-1}$, $k_2 = 0.08ns^{-1}$ and $k_3 = 0.02ns^{-1}$ and amplitudes: $A_1 = 0.675$, $A_2 = 0.299$ and $A_3 = 0.025$. The plot of residuals in the figure inset confirms the goodness of the fit.

In our excitation scheme, only a small fraction of nanocrystals is excited with more than one exciton and since the measured signal did not change even when the excitation power was reduced by factor of 10 (with the resulting probability of multiple excitons generation of 0.17%), we can assume that the multiexciton effects can be neglected in our analysis. In this case as long as the excitons decay within one period of the laser excitation, each measured photon originates from a different nanocrystal, as a result of dif-

ferent decay processes.

The radiative recombination rate of excitons in a InP nanocrystal emitting at 637 nm on a glass slide, can be estimated as 0.2 ns^{-1} consistent with the ones shown in figure 4.6, if the electron-hole wavefunctions have overlap of unity [81]. However there is a finite energy splitting between dark and bright exciton states due to the exchange coupling [61] with the 5-fold degenerate dark exciton being the lowest energy state and the 3-fold degenerate bright exciton in InP nanocrystals as shown in figure 4.6. Since the expected energy splitting is much smaller than the thermal energy at room temperature, the presence of dark state leads to the reduced recombination rate of 0.075 ns^{-1} similar to k_2 although due to complex exciton dynamics these two are not equivalent.

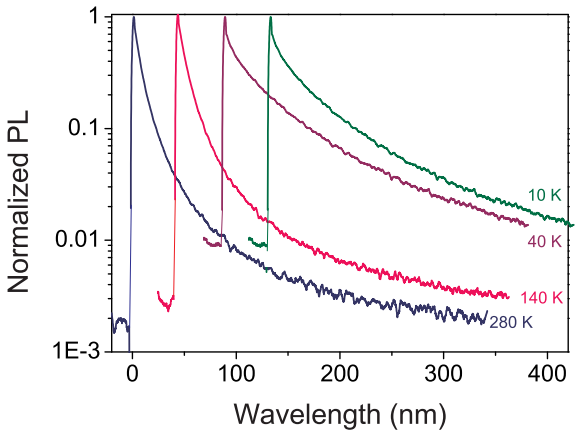

Figure 4.17: Time resolved photoluminescence following a pulse of laser light at time zero measured at 637 nm at different temperatures normalized to 1 and shifted horizontally for clarity.

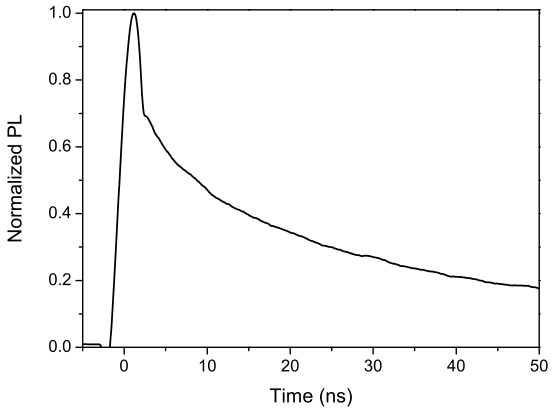

Figure 4.18: Time resolved photoluminescence at 40 K for first 50 ns. Top 25% of the peak indicate presence of the Auger recombination.

In order to differentiate between the possible decay processes, we measured temperature dependence of the TRPL. The evolution of the photoluminescence decay with temperature measured for 637 nm emission on an ensemble of nanocrystals between room temperature and 10 K is shown in figure 4.17. In the range of temperatures between room temperature and 140 K, the curves did not change much. Upon further cooling, the photoluminescence dynamics transformed drastically. The slow decay component became more pronounced leading to incomplete recombination during one period of laser excitation, seen as an increasing PL signal level just before arrival of a laser pulse at lower temperatures (e.g. PL of 0.01 of initial value at 10 K in figure 4.17). This in turn led to the appearance of Auger recombination with a very fast decay rate, k_4 (2 ns^{-1}, limited by the temporal resolution of the experiment) as shown in the figure 4.18, which gradually increased in strength as the temperature was reduced.

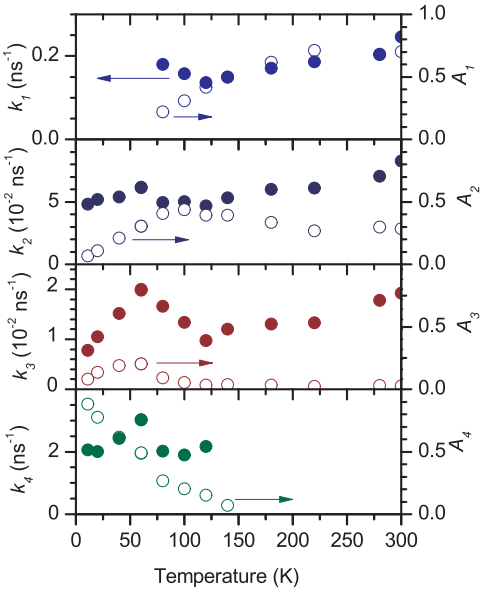

Figure 4.19: Evolution of four single exponential components: k_1, k_2, k_3, k_4 with temperature measured for emission wavelength of 637 nm. Right hand scale indicates the pre-exponential factor, A_i, in the fitting.

In order to better visualize the changes, we plot in figure 4.19 all the decay rates for 637 nm. A more familiar average decay rate is shown in figure 4.20. The values of decay rates k_1 and k_2 are only weakly changing with temperature and because of this they cannot be assigned to recombination rate of coupled bright dark exciton coupling system, k_3 and k_{ave} undergoes very strong oscillation around 50 K, a feature very characteristic of traps in resonance with the core excitonic levels [76]. For the average rate those oscillation occurs at temperature of 100 K for the wavelength of 600 nm, at 120 K for 637 nm and at 140 K for 660 nm. Low value of k_3 points to the external surface of the nanocrystal as the location of the traps. Note that this feature is clear in k_{ave} in figure 4.20.

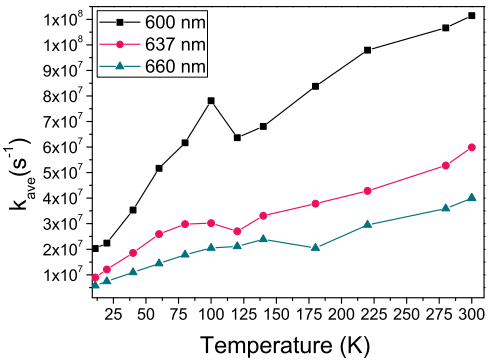

Figure 4.20: Evolution of average decay constant, k_{AVE} with temperature for emission wavelength of 600 nm, 637 nm and 660 nm.

An amplitude of k_1 component of the decay curves decreases until at about 70 K it becomes too small to be extracted by fitting. A gradual reduction of this component is associated with an increase of amplitudes of k_2 and k_3 components. Upon further cooling, the amplitude of the k_2 component starts falling while k_3 component continues to grow until finally it also decreases below 30 K while Auger recombination (k_4) steadily increases down to liquid helium temperature. It is worth noting that although the amplitude of the Auger recombination, A_4, is very high compared with other components, its contribution to the total PL signal ($= A_4/k_4$) remains small (less than 10%).

The evolution of k_1, k_2 and k_3 components can be explained as originating from a system of energy levels (see figure 4.22), with the exciton energy state (split into bright and dark exciton) and decay states with faster and slower rates. k_1, k_2 and k_3 may strongly depend on configuration of traps in the sample. Although they cannot be assigned to any specific process [54] but k_1 disappearing at 70 K means some states involved in recombination are above the lowest level. The energy separation of the state responsible for

k_1 component can be estimated as 12 meV exciton level, as it is quenched at about 70 K. We suggest that these could be interface defects because of the fast decay rate. Since we expect strong coupling between dark and bright exciton states at room temperature, the presence of long decay time (k_3) component means that there must be traps leading to such behaviour. It has to be stressed that it is not possible to relate k_1, k_2, k_3 to recombination rates of any of the states. It is not possible to perform similar estimation of the energy of the states responsible for k_2 and k_3 components due to strong presence of k_4 component in the temperature range, in which they are being quenched.

The same measurements and analysis performed for the emission centred at other wavelengths between 600 nm and 660 nm (see figure 4.14) yielded qualitatively similar results as evident in k_{ave} shown in figure 4.20 for 600, 637 and 660 nm. There are quantitative differences in the temperatures at which the different components of PL were quenched, slight difference of the temperature at which the Auger component (k_4) appeared.

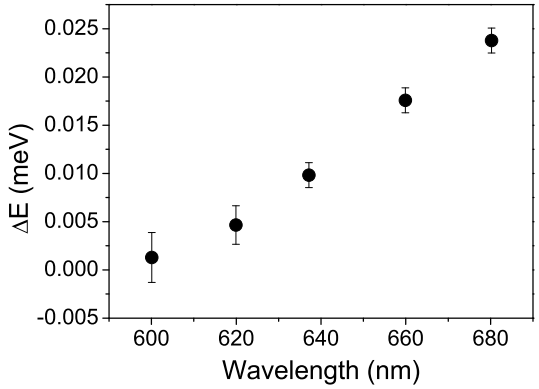

Figure 4.21: Estimated splitting between defect state (at higher energy) and lowest exciton energy (dark exciton) as a function of the energy of emission (nanocrystal size).

Analysis of the emission at these different wavelengths yielded a dependence of the energetic position of the state responsible for the decay rate k_1 as a function of emission energy, shown in figure 4.21. As the exciton energy increases the separation between the dark exciton and the analysed state decreases. Such dependence points to the defect being the origin of the k_1 component in agreement with previous studies of InP nanocrystals [82]. Note, that at the emission energy of 2.08 eV the k_1 and k_2 components are quenched in the same temperature range indicating that this state is very close in energy to the k_2 component. Defects located near the core of the nanocrystal (on the interface between the core and the shell) are the most likely origin of k_1 component as k_1 is fast. The picture of the energy states (shown in figure 4.22) of the InP/ZnS nanocrystals studied here is consistent with the one determined for etched InP nanocrystals passivated with organic ligands [82, 43]. We assumed the splitting between the bright and dark excitons to be similar to that of etched InP nanocrystals as this is an intrinsic property of the InP nanocrystals [61]. The dominant at room temperature parasitic recombination channel in the InP/ZnS (k_1) is also very similar to that of the passivated InP nanocrystals [43], proving the protective role of ZnS shell. Although thin shell may not be continuous and so InP surface may be partly exposed, numerically predicted positions of In and P dangling bonds inside the InP bandgap [83] cannot explain the results.

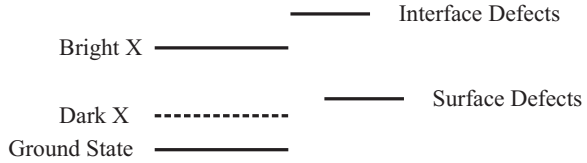

Figure 4.22: Model of the states present in the InP/ZnS nanocrystals

The hot injection synthesis method, used for the fabrication of InP/ZnS nanocrystals under study, relies on forming ZnS shells by adding the Zn and S precursors to the solution of In and P precursors after InP cores have been formed. It has been suggested [11] and later observed [82] that the shell grown under such conditions is likely to be an alloy of InP and ZnS, resulting in gradual potential transition across the interface between the core and shell rather than abrupt InP/ZnS junction. Such an interface may also be vulnerable to the formation of defects [84] or grain boundaries and extended surfaces resulting from Oswald ripening growth as shown in chapter 4.1.

The Auger recombination, (k_4) observed in the PL, relies on the transfer of energy to a third carrier (electron or hole), it is thus only possibly in nanocrystals which are charged or occupied with more than one exciton. The second case, an occupation of the nanocrystals with more than one exciton in our experiments is caused by the carriers freeze out on the long lived states (traps and dark excitons). It is clear, however, that higher levels of excitation at room temperature would also lead to Auger recombination quenching of radiative recombination. This demonstrates the detrimental effect of the presence of trap states on photon emission [85].

4.4 Conclusions

It has been shown that the quantum efficiency of smallest nanocrystals emitting at 530 nm is about 50 - 60% and it is 25 times higher than the largest particles. Further investigation revealed that nanocrystals samples contain a population of permanently non-emitting nanocrystals which are responsible for drop of efficiency with emission wavelength. Those results were confirmed when the quantum efficiency of the largest nanocrystals was mea-

sured to be 63% by modification of the local density of optical states. The bright nanocrystals fraction of 82, 24, 8, 8 and 5 % for smallest to biggest was derived. The analysis of the decay dynamics at different temperatures has indicated that initially generated exciton population decays to four energy levels, which we have assigned as dark exciton, bright exciton, surface defect and core-shell interface defect states. The interface defect states in the smallest nanocrystals, emitting at 600 nm, are very close in energy to the bright exciton state. Below about 140 K long-lived dark excitons and trapped charges lead to strong Auger recombination. The results show that while a thin ZnS shell protects the surface of InP from oxidation, it does not change the recombination dynamics in the nanocrystals and so engineering of the energy level splitting and defect elimination remain crucial factors in the design of highly emissive nanocrystals [86].

Chapter 5

InP/ZnS nanocrystals as light absorbers

In this chapter colour conversion efficiency for nanocrystals excitation via photon absorption and via resonant transfer of exciton energy (transfer of a virtual photon) has been estimated for a device consisting of layer of nanocrystals deposited on the top of the InGaN/GaN diode as shown in the figure 5.1. The carriers are injected into the active region of the diode electrically while excitation of the carriers in nanocrystals can be either by optical absorption process ($h_{\nu 1}$) or resonant energy transfer (RET). Colour conversion efficiency is a measure of how well photons from InGaN/GaN diode are converted into photons emitted from the nanocrystals. It can be defined as the product of the quantum efficiency of the photoluminescence of the nanocrystals and the efficiency of the excitation process ($\eta_{exitation}$).

$$\eta_{CC} = QE_{NCs} \cdot \eta_{exitation} \tag{5.1}$$

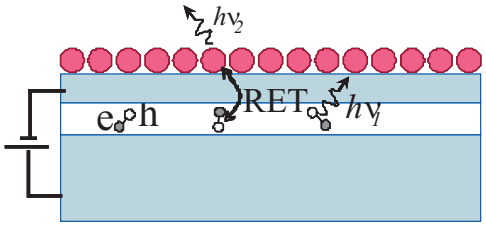

Figure 5.1: Schematic illustration of device utilizing both radiative ($h\upsilon_1$) and non-radiative (RET) excitation methods.

Based on the estimation of the colour conversion efficiency and the external quantum efficiency of the blue emitting diode the performance of the hybrid-diode can be optimized by adjusting the ratio between the blue to green, yellow and red photons. Also those efficiencies provide means for comparing the hybrid device with other white light emitting solid state devices.

Existing technology does not allow efficient direct injections of current into nanocrystals. The main problem is caused by the layer of ligands around each particle which has insulating properties, efficiently blocking any electrons. Two approaches of direct current injection have been demonstrated however none of them show external quantum efficiency of the LED higher than a percent. First concept utilizes single layer of nanocrystals sandwiched between two layers of polymer acting as electron and hole transport layers, however due to low carrier mobility the external quantum efficiency of device does not exceed 0.54% [87]. In second concept, layer of nanocrystals is assembled onto a p-type GaN and is overgrowth with n-type GaN however this method is even less efficient and it reaches values up to 0.01% [88].

5.1 Absorption

In this section colour conversion efficiency for optical absorption is estimated for the device shown in figure 5.1 and results are compared with those found in the literature.

Colour conversion efficiency η_{CC} of optical absorption (hv_1) followed by re-emission process (hv_2) for the monolayer of closely packed nanocrystals has been defined [89] as the product of absorbance (A) and quantum efficiency (QE_{NC}) of nanocrystals (eq. 5.2). This equation however does not account for the charge or the exciton transfer between the nanocrystals.

$$\eta_{CC1} = A \cdot QE_{NC} \tag{5.2}$$

where QE_{NC} is the ratio of the light emitted (Φ_E) to the absorbed one (Φ_A) by NCs as measured in chapter 4.1.

Absorbance of the InP/ZnS nanocrystals has been estimated based on the equation:

$$A = \frac{\frac{N_{abs}}{N_{NC}}}{N_{ph} \cdot \frac{S_N}{S_L} \cdot \frac{s}{S_N}} \tag{5.3}$$

where N_{abs} and $N_{ph} \cdot \frac{S_N}{S_L}$ are the number of absorbed photons per second and number of photons incident on the sample as measured in chapter 4.1 and S_N, S_L, N_{NC}, s are the size of the laser spot and the nanocrystals spot on sample, the number of nanocrystals in the S_N and area of one nanocrystal, respectively. The fraction in the nominator $\frac{N_{abs}}{N_{NC}}$ can be understood as the number of photons absorbed by one nanocrystal and the value in the denominator $N_{ph} \cdot \frac{S_N}{S_L} \cdot \frac{s}{S_L}$ as number of photons incident on the surface of one nanocrystal.

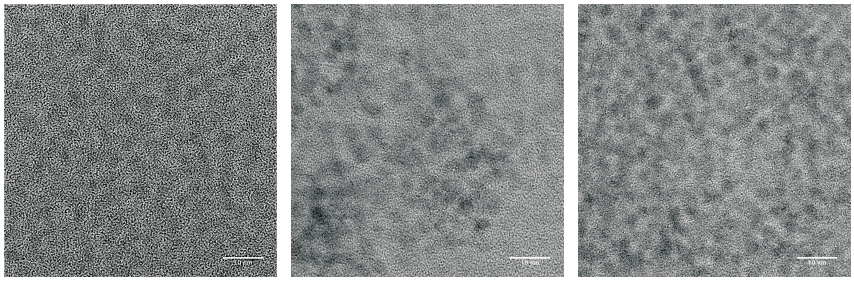

Figure 5.2: TEM image of InP/ZnS nanocrystals with the peak emission wavelength of 530 nm (left), 615 nm (middle) and 655 nm (right). The white bar on the bottom right corner of each image indicate 10 nm.

The diameter of the nanocrystals was estimated on the basis of the correlation between size of the nanocrystal core and its emission energy [4].

$$E_{PL}(d) = E_{PL}(\infty) + \frac{A_{PL}}{d^m} \tag{5.4}$$

where E_{PL} is the peak emission energy of the InP core with diameter d, $E_{PL}(\infty)$ is the PL peak energy of the InP bulk, A_{PL} is the constant equal to 1.9 $\pm$ 0.2 eV·nm and exponent m is equal to 0.9 $\pm$ 0.1 for InP nanocrystals [4].

The estimation of the size of the nanocrystals was also done based on the transmission electron micrograph for nanocrystals with emission peak wavelength of 530 nm, 615 nm and 655 nm which are shown in the figure 5.2. The results based on the analysis of 71 nanocrystals with peak emission wavelength of 530 nm, 81 nanocrystals emitting at 615 nm and 65 nanocrystals emitting at 655 nm are shown in the table 5.1. Note that only regular shapes NCs were taken into account in this analysis. The difference between measured diameter of nanocrystals and the calculated one is biggest for the small particles and decreases with increasing size of nanocrystals. The correlation between measured and the calculated values are shown in the figure 5.3.

NCs	Mean diameter (nm)	Standard deviation
530	2.91	0.71
615	4.04	0.9
655	4.16	0.98

Table 5.1: Statistical analysis of the diameter of the core/shell InP/ZnS nanocrystals based on the TEM image shown in figure 5.2.

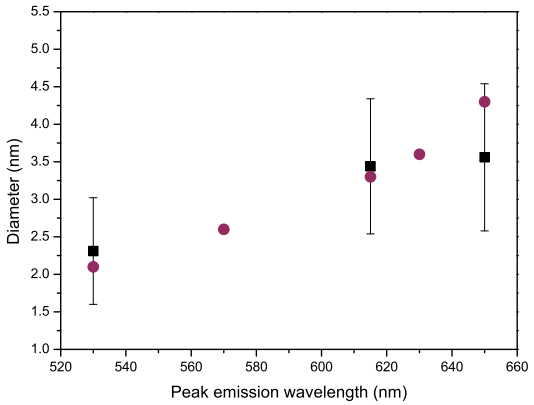

Figure 5.3: Calculated (dots) and measured values (squares) of the diameter of the core of the InP/ZnS nanocrystals.

Absorbance of five samples of nanocrystals at the wavelength of the emission of the LED (450 nm), has been estimated by scaling the probability of absorption measured in the chapter 4 at 405 nm with the normalized absorption curves obtained from table 4.1 from NN-labs [12] (shown in figure 5.4). Extrapolation of the 655 nm nanocrystals absorption curve was necessary in order to perform this scaling. The photoluminescence of the diode excites only the largest nanocrystals in the continuum of states while the other's nanocrystals absorption at 450 nm wavelength will be reduced.

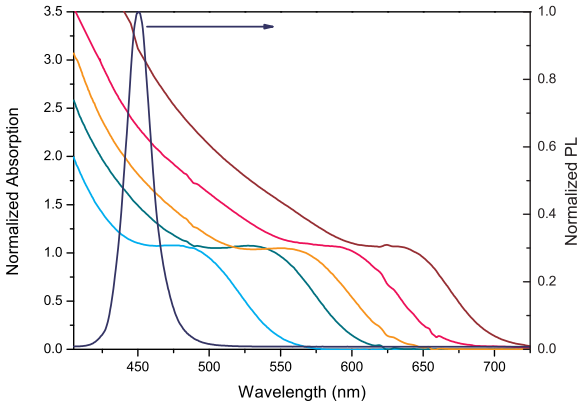

Figure 5.4: Absorption of InP/ZnS nanocrystals with peak emission wavelength of 530 (cyan), 570 (green), 615 (orange), 630 (pink) and 655 (brown) nm normalized to the maximum of the first excitonic peak (obtained from NN-Labs). Emission of the diode with peak emission wavelength of 450 nm normalized to the maximum is also shown.

The absorbance at 405 and 450 nm, together with uncertainty associated with its estimation is shown in table 5.2. The value of the errors is influenced by following factors: the uncertainty in estimation of the size of the nanocrystals, estimation of the number of nanocrystals on the measured sample, estimation of the laser spot size as well as scaling the normalized absorption spectrum and necessity of extrapolating the absorption spectrum of 655 nm curve. Absorbance values together with quantum efficiency of total population of nanocrystals QE_{NC} measured in chapter 4 have been used for the calculation of color conversion efficiency of optical absorption, results of which are shown in the column η_{CCQE} in the table 5.2. Colour conversion efficiency of nanocrystals with quantum efficiency equal 50% was also calculated and it is shown in column η_{CCQE2} in this table.

The ratio of the absorption cross-section (σ) of nanocrystals to its geometrical cross section (s) (equation 5.5) has been proposed as an alternative

way of estimating colour conversion efficiency [90].

$$\eta_{CC2} = \frac{\sigma}{s} \tag{5.5}$$

Absorption cross section has been calculated based on the equation 5.6 derived for the small particles in dielectric host [91].

$$\sigma = \frac{2 \cdot \pi}{n_s \cdot \lambda} \cdot |f_{LT}|^2 \cdot 2 \cdot n \cdot k \cdot \frac{\pi \cdot d^3}{6} \tag{5.6}$$

$$|f_{LT}|^2 = \frac{9 \cdot n_s^4}{(n^2 - k^2 + 2 \cdot n_s^2)^2 + 4 \cdot n^2 \cdot k^2} \tag{5.7}$$

where $|f_{LT}|$ denotes the local field factor, $n = 4.067$ [92] is the refractive index of InP at 450 nm, $k = 0.728$ is extinction coefficient of InP at 450 nm and $n_s = 1.25$ is the refractive index of the surrounding medium at 450 nm (averaged for n of air (1) and glass (1.5)). The absorption cross section of InP/ZnS nanocrystals is comparable to that measured [93] and calculated [94] for CdSe nanocrystals and are shown in the table 5.2.

The calculated diameter of the InP core d_{core}, absorption at 405 and 450 nm, absorption cross section σ and colour conversion efficiencies calculated with both methods are shown in table 5.2.

The results of colour conversion efficiency calculated with both methods are not the same and they show different trends: the $\eta_{CC\sigma}$ calculated from absorption cross section increases together with increasing diameter of the nanocrystals while the η_{CCQE} is varying between 0.03 and 0.05 %. This variations are directly related to the fact that the QE decreases for increasing size of nanocrystals while absorbance has opposite trend and it increases. If we assume uniform quantum efficiency for all sizes of nanocrystals trend changes and (η_{CCQE}) is increasing as shown in column $\eta_{CCQ0.5}$

λ_{max} (nm)	d_{core} (nm)	A_{405nm}	A_{450nm}	σ (m^2)	η_{CCQE} (%)	$\eta_{CC0.5}$ (%)	$\eta_{CC\sigma}$ (%)
530	2.1	$(9.5 \pm 4.2) \cdot 10^{-4}$	$(5.3 \pm 4.7) \cdot 10^{-4}$	$1.76 \cdot 10^{-20}$	0.03±0.02	0.03	0.51
570	2.6	$(4.4 \pm 1.7) \cdot 10^{-3}$	$(2.5 \pm 1.9) \cdot 10^{-3}$	$3.33 \cdot 10^{-20}$	0.04±0.03	0.1	0.63
615	3.3	$(8.8 \pm 1.3) \cdot 10^{-3}$	$(5.2 \pm 1.5) \cdot 10^{-3}$	$6.82 \cdot 10^{-20}$	0.03±0.009	0.3	0.80
630	3.6	$(1.5 \pm 0.3) \cdot 10^{-2}$	$(9.7 \pm 3.2) \cdot 10^{-3}$	$8.85 \cdot 10^{-20}$	0.05±0.02	0.5	0.87
655	4.3	$(1.7 \pm 0.3) \cdot 10^{-2}$	$(1.2 \pm 0.3) \cdot 10^{-2}$	$1.51 \cdot 10^{-19}$	0.04±0.01	0.6	1.04

Table 5.2: Results of the calculation of a diameter of the core of the InP/ZnS nanocrystal d_{core}, absorbance of InP/ZnS nanocrystals at 405 nm A_{405nm} and 450 nm A_{450nm}, absorption cross section σ and colour conversion efficiency for current quantum efficiency η_{CCQE} of nanocrystals as well as for assumed 50% QE $\eta_{CC0.5}$ together with colour conversion efficiency based on the absorption cross section $\eta_{CC\sigma}$.

for 50% quantum efficiency. The increasing trend of colour conversion efficiency is expected from the position of the PL peak of the blue emitting diode in relation to the absorption spectrum of the nanocrystals: the large nanocrystals are excited with highest probability, as shown in the figure 5.4.

The colour conversion efficiency calculated from absorption cross section gives the values for the nanocrystals with 100% quantum efficiency. If compared with the values of colour conversion efficiency calculated directly from absorption (double the ones calculated for $\eta_{CC0.5}$) the values are still not the same, however they are similar. The difference might be caused by the large uncertainty in determining the value of absorbance. Results of both ways of estimating colour conversion efficiency are thus equivalent. For the purpose of further analysis the η_{CCQE} will be used as the quantum efficiency factor will have strong effect on the results discussed.

The results obtained from calculation of colour conversion efficiency below one percent are in agreement with the values reported for CdSe colloidal

quantum dots [2] determined from the quantum efficiency of nanocrystals.

5.2 RET

In contrast to absorption, resonant energy transfer (RET) transmits the energy of excitons non-radiatively via dipole-dipole interaction. In order to utilize this process as a source of excitation energy for the colour converting layer in hybrid device as shown in figure 5.1 few conditions has to be met.

The energy transfer rate has been shown to depend sensitively on the character of dipoles of the donors and acceptors [95]. For example RET rate between QWs (donor) and organic overlayers (acceptor) have been shown to increase at the transition from localised and free excitons in the quantum well (the donor) at increasing temperature [96]. Non-radiative energy transfer from optically excited electron-hole pairs in a quantum well and excitons in the colloidal nanocrystals has also been observed with relatively high efficiency [2], followed by the demonstration of colour conversion using NCs driven by RET from blue emitting LEDs. The high efficiency of RET leads to two orders of magnitude increase of colour conversion efficiency compared with the case of the colour conversion via absorption-emission process [13].

Due to high sensitivity of RET to the character of the donor and acceptor dipoles it is however not clear if the RET will allow the generation of light with stable white colour over wide range of excitations, a condition necessary for good quality white LED.

In order to answer the last question, we study the efficiency of resonant energy transfer between an InGaN quantum well as an energy donor and a monolayer of InP/ZnS colloidal quantum dots as the acceptors over wide range of excitation levels.

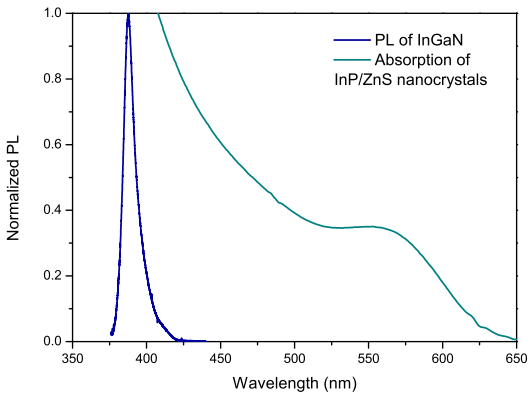

Figure 5.5: Photoluminescence spectrum of the InGaN quantum well (blue line) with absorption spectrum of InP/ZnS nanocrystals (green line).

5.2.1 Experimental determination of RET rate

The InGaN/GaN wafer used in this work was grown by metal organic chemical vapour deposition on a c-plane sapphire substrate. A single, 2.5 nm thick, InGaN quantum well was grown on an un-doped GaN layer and covered with a 3.2 ± 0.5 nm thick GaN barrier. The low indium content in the quantum well resulted in light emission from the quantum well centred at the wavelength of 390 nm, as shown in figure 5.5.

In order to obtain good spectral overlap between light emission from the quantum well and absorption of nanocrystals (both shown in figure 5.5), which is necessary for efficient RET [97], InP/ZnS nanocrystals with an absorption edge of 625 nm were chosen. With their core diameter of 3.3 nm, shell thickness of 0.3 nm and the ligands length of ∼1 nm, the separation between the donor and acceptor dipoles (the distance from the center of nanocrystal's core to the middle of the quantum well) was 7.4 nm.

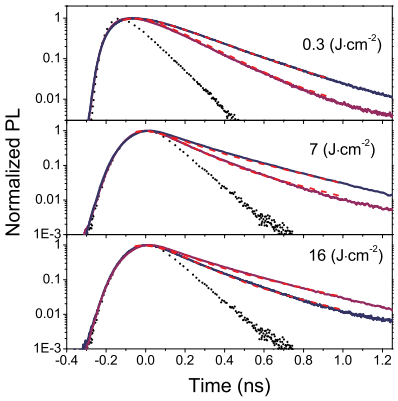

Figure 5.6: Typical photoluminescence decay curves of InGaN QWs (blue solid line), hybrid devices (purple solid line) and instrument response function (IRF) (black dotted line). Red lines show results of the fitting based on single exponential decay convoluted with the IRF.

The hybrid samples were prepared by spinning InP/ZnS nanocrystals from a solution on a clean GaN surface of the wafer. The concentration of NCs solution was adjusted to achieve a uniform layer of particles which has been evaluated in the spatially resolved confocal microscope under illumination with a laser emitting at 458 nm.

As RET between quantum well and nanocrystals in hybrid structure is expected to increase total recombination rate in the quantum well is compared with the recombination rate of the bare wafer. Typical decay curves of photocarriers in the quantum well of the bare wafer and the hybrid device together with instrument response function for the measurements are shown in figure 5.6 for three different energy densities: 0.3, 7 and 16 J·cm^{-2}. The data in the top (middle and bottom) figure were obtained by illuminating samples with a pulsed laser emitting at 365 nm (375 nm) with pulse duration of 200 ps and repetition rate of 80 MHz (250 kHz) to achieve low (high) power densities. The resulting photoluminescence from the quantum well

was measured using an avalanche photodiode with the temporal resolution of 50 ps, after filtering the desired wavelength of 390 nm with a monochromator with a 0.6 nm resolution.

In the InGaN quantum wells the photogenerated carriers decay via non-radiative and radiative recombination channels, with the former one dominating at low excitation power densities and the latter dominating after the saturation of non-radiative recombination channel [16, 98]. In the presence of nanocrystals, in a close vicinity of the quantum well another carrier recombination channel opens resulting in an increased decay rate of photocarriers in the hybrid device. The difference between the decay rates of the bare QW and hybrid device is the resonant energy transfer rate (k_{RET}). In order to determine k_{RET}, all photoluminescence decay curves were fitted with a convolution of a single exponential function and an instrument response function as shown in red in figure 5.6. For the data in figure 5.6 we find that k_{RET} is $1.4 \cdot 10^9$ s^{-1}, $1.4 \cdot 10^9$ s^{-1} and $9.4 \cdot 10^8$ s^{-1} while k_{hybrid} is $5.4 \cdot 10^9$ s^{-1}, $4.4 \cdot 10^9$ s^{-1} and $4.2 \cdot 10^9$ s^{-1} for top, middle and bottom figure. It means that the efficiency of RET, defined as:

$$\eta_{RET} = \frac{k_{RET}}{k_{RET} + k_{QW}} \tag{5.8}$$

is 26% (30% and 23%) respectively. It is consistent with previously measured transfer rates [2]. Note that the $k_{QW} = k_{QW}^{rad} + k_{QW}^{nrad}$ while literature reports $\eta_{RET} = \frac{k_{RET}}{k_{RET}+k_{QW}^{rad}}$.

We repeated the measurements for laser excitation levels from 0.01 to 148 J$\cdot$ cm^{-2}, which resulted in the initial carrier densities in the quantum well of $5.5 \cdot 10^{10}$ - $4.5 \cdot 10^{14}$ m^{-2} although due to the uncertainty in the absorption coefficient [99], it is possible that the values may vary from the calculated.

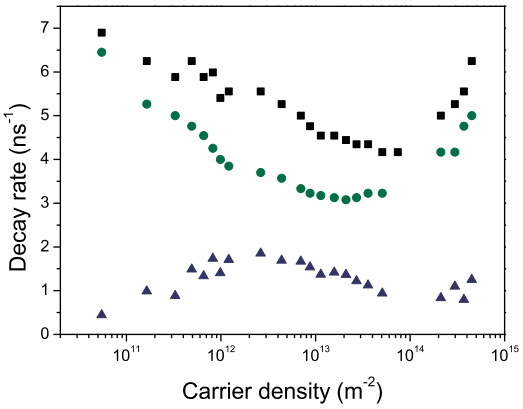

Figure 5.7: Decay rates of hybrid diode (black squares) and InGaN (green dots) and their difference being resonant energy transfer (blue triangles) as a function of carrier density.

The decay rates of bare InGaN, hybrid device and RET obtained from the measurements are shown in figure 5.7. Both the InGaN decay rate and hybrid structure decay rate are showing decreasing trend with increasing carrier concentration followed by a sharp increase at highest carrier concentration. The value of carrier density when both rates change the trend is different and it is equal to $1 \cdot 10^{13}$ m^{-2} for InGaN and $5 \cdot 10^{13}$ m^{-2} for hybrid rate. The RET rate increases in the carrier density range up to $2 \cdot 10^{12}$ m^{-2} and then it decreases to stabilize above 10^{14} m^{-2}.

Efficiency of the transfer calculated from the equation 5.8, shown in figure 5.8, increases up to 34% for carrier density range between $1.9 - 6.4 \cdot 10^{11}$ m^{-2} and then decrease to achieve value of 14% at the lowest point. Moreover since $k_{QW} = k_{QW}^{nrad} + k_{QW}^{rad}$ the drop may be due to increasing non-radiative recombination rate k_{nrad} while transfer efficiency is constant. Since the non-radiative recombination in the samples is apparent, its reduction can lead to much higher efficiencies.

The interactions between quantum well and monolayer of nanocrystals

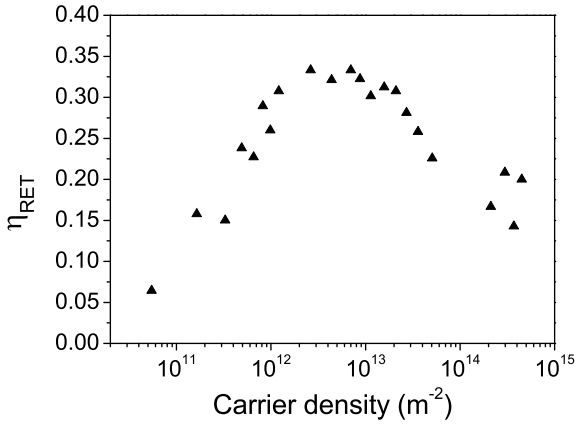

Figure 5.8: RET efficiency calculated as $k_{RET}/k_{RET} + k_{QW}$ as a function of excitation densities.

are strongly dependant on whether the carriers in the quantum well are bound into excitons or form electron-hole plasma. In the first case, RET rate is independent of the level of carrier concentration while for electron – hole pairs energy transfer rate is proportional to carrier density [2]; the later describes the behaviour of the quantum well under study at low excitation levels (up to $3 \cdot 10^{12}$ m^{-}2).

To explain the decrease of the InGaN and hybrid rates, one has to consider two competing effects: increase of k_{RET} with carrier concentration [90] and decrease with T. At low carrier concentrations, where k_{RET} increases linearly, the change of k_{QW} is due to the saturation of non-radiative recombination.

The drop of the RET rate above the value of $3 \cdot 10^{12}$ m^{-2} could be caused either by heating or transition to degenerate plasma. Degenerate plasma according to [90] requires carrier densities in a range of $8.6 \cdot 10^{11}$ m^{-2} which is close to the values where k_{RET} drops in this experiment.

In summary, it has been shown that the radiative energy transfer is present in wide range of the excitation energies and that η_{RET} is as high as

34% for the $\sim$ 7 nm distance between single InGaN/GaN quantum well and InP/ZnS nanocrystals with peak emission wavelength of 615 nm. Although, there are several processes which can possibly quench k_{RET} its efficiency does not drop below 10%.

5.2.2 Colour conversion efficiency

Based on the measurements on hybrid diode colour conversion efficiency for RET has been estimated with the use of equation [2]:

$$\eta_{CCRET} = F \cdot QE_{NC} \cdot \frac{k_{RET}}{k_{hybrid}} \tag{5.9}$$

where F is the factor reflecting degree of spectral overlap of the nanocrystals absorption and emission of the diode calculated based on the figure 5.4.

There is no evidence that the resonant energy transfer do not occur between quantum wells and the dark population of nanocrystals thus total population of nanocrystals has been used in calculation of colour conversion efficiency. The QW and RET rates have been taken from figure 5.7 for the carrier density of the commercial diode ($6.25 \cdot 10^{12}$ cm^{-2}). The results of the calculations of colour conversion efficiency of RET are shown in table 5.3 and they are compared with the efficiency of optical absorption.

The colour conversion efficiency of RET is one to two orders of magnitude larger than the optical absorption. The values of the η_{CCRET} vary between 5 % for the smallest nanocrystals and 0.6 % for the larger ones. Due to the fact that the quantum efficiency of total population of nanocrystals as well as absorption are changing with the size of nanocrystals, colour conversion efficiency of both optical absorption and resonant energy transfer is also

λ (nm)	η_{CCRET} (%)	η_{CCQE} (%)
530	4.8	0.03
570	1.7	0.04
615	0.7	0.03
630	0.8	0.05
655	0.6	0.04

Table 5.3: Comparison of colour conversion efficiency of resonant energy transfer and optical absorption.

changing. Those changes of absorbance and efficiency are, however, opposite and they compensate so they are not visible in the trend of the η_{CCQE}. The decrease of η_{CCRET} with the increase of the nanocrystal' diameter is caused by the dominant effect of dropping quantum efficiency with the emission wavelength. To maximize the η_{CCRET} efficiency, RET rate should become faster to be able to compete more efficiently with the non-radiative and radiative recombination rates which will increase possibility of carrier decay via RET channel. Improvement of the efficiency of nanocrystals is necessary to maximize the nanocrystals excitation via resonant energy transfer. Also, the emission wavelengths of blue emitting diode as well as nanocrystal has to be chosen carefully to maximize the spectral overlap as it has huge effect on the colour conversion efficiency.

5.3 Conclusions

In conclusions, the possible methods of nanocrystal's excitation have been studied. The efficiency of the process of optical absorption has been esti-

mated by two methods and the validity of the results has been discussed. The resonant energy transfer between InGaN/GaN single quantum well in proximity ($\sim$ 7 nm) of InP/ZnS nanocrystals with absorption edge of 625 nm for four orders of magnitude change of carrier density. The efficiency of RET shows that the process is sturdy and it is present at very low excitation energies where it competed with non-radiative recombination and at very high carrier densities where the heating reduce it. The colour conversion efficiency for optical absorption and resonant energy transfer was estimated. It has been shown that the later one is one to two orders of magnitude higher for all the nanocrystals' sizes than the η_{CCQE} and that the spectral overlap is crucial for both excitation processes. Both efficiencies can be improved by choosing the diode with lower emission wavelength to improve the spectral overlap between absorption of nanocrystals and the emission of the diode and by using nanocrystals with higher quantum efficiency of photoluminescence.

Chapter 6

Colour mixing

In order to investigate the performance of the InP/ZnS nanocrystals as a down-converting material for generation of white light, simulation of emission from the hybrid white light emitting diode has been performed. The goal of the calculation was to assess if the high values of luminous efficacy of radiation can be achieved with simultaneous high colour rendering in a wide range of correlated colour temperatures for the white light emitted by the hybrid diode. Fulfilling this conditions would allow for replacement of conventionally used light sources in a wide range of applications.

6.1 Model of hybrid white light emitting diode

The simulation of white light emission was based on the hybrid-diode consisting of a multi-quantum well InGaN/GaN diode with a layer of mixture of nanocrystals with peak emission wavelength of 530, 570, 615, 630 and 655 nm embedded in PMMA. The diode was fixed inside the heat transmitting metal housing in the shape of a square "well" so that all the light emitted by the diode could escape only trough the top of the "well". The housing was

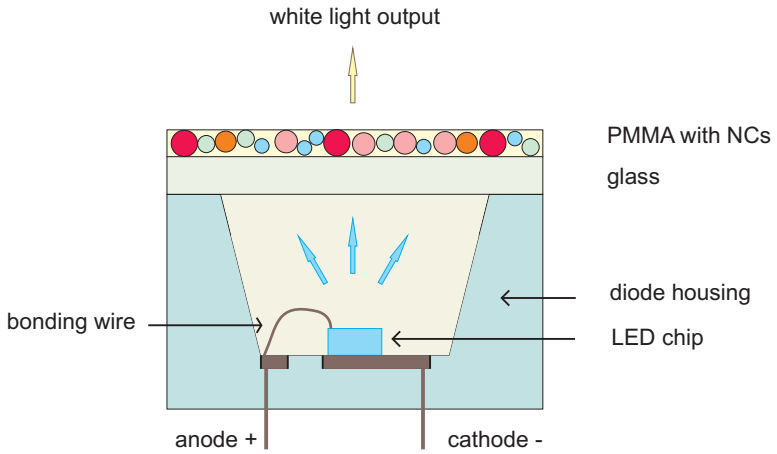

Figure 6.1: Schematic illustration of WLED with layer of nanocrystals.

closed at the top by a glass plate, on which a layer of PMMA with a mixture of nanocrystals was spun. The device on which the modelling was based is shown in figure 6.1. The number of each type of nanocrystals (with different emission wavelengths) was chosen on the basis of the CRI and CCT values of resulting white light.

In order to generate white light of high quality, the composition of the total spectrum of the LED was varied by adjusting the number of nanocrystals of different wavelengths. The resulting spectra were analysed for their CCT and CD as well as CRI index. According to CIE document [100] the light is considered to be of a good quality if $CRI > 80$, CCT value is between 2500 and 8800 K and $CD < 5.4 \cdot 10^{-3}$. The radiant flux $\Phi_R(\lambda)$ (μW), for nanocrystals and the InGaN/GaN diode, was varied with a step of 5% for each component. The resulting white light radiant flux $\Phi_R^W(\lambda)$ can be described by the equation:

$$\Phi_R^W(\lambda) = \sum_{i=1}^{n} A_i \cdot \Phi_R(\lambda)_i \tag{6.1}$$

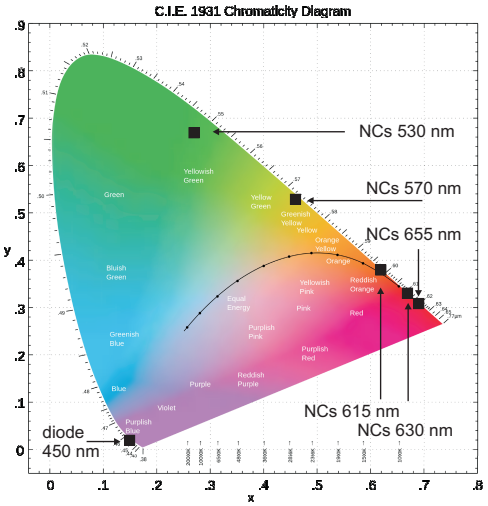

Figure 6.2: Chromaticity diagram with marked coordinates of diodes and all nanocrystals.

where $\sum_{i=1}^{n} A_i = 1$ and $n = 6$ for InP/ZnS nanocrystals with peak emission wavelength of 530, 570, 615, 630 and 655 nm and the InGaN/GaN diode with peak emission wavelength of 450 nm. The chromaticity coordinates of each of these hybrid diode components are shown in figure 6.2.

The electroluminescence (EL) of the diode driven by 700 mA current and photoluminescence for all types of nanocrystals, obtained from integrating sphere measurements described in chapter 3, were normalized to the total photoluminescence of 1 (integrated area under the EL/PL curve = 1). Results of normalization are shown in figure 6.3).

In order to correlate the results of the simulations of the hybrid white light emitting diode with the experimentally measured total photoluminescence of nanocrystals and electroluminescence of the diode, as described in section 3, number of each size of nanocrystals (N_{NC}^{need}) generating required amount of light was calculated from following formula:

$$N_{NC}^{need} = \frac{N_{NC}^{sample} \cdot N_{ph}^{need}}{N_{ph}^{sample}} \tag{6.2}$$

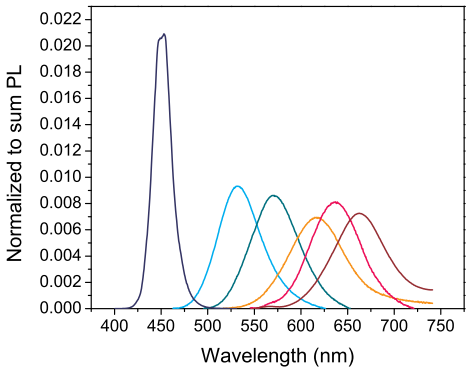

Figure 6.3: Spectra used for modelling of the light quality of hybrid diode normalized to the total photoluminescence of 1.

where N_{NC}^{sample} is the number of nanocrystals on the sample measured as described in chapter 4.1 and N_{ph}^{sample} and N_{ph}^{need} are the number of photons emitted by the nanocrystals on the measured sample and needed to generate desired white light, respectively.

The structure of the hybrid diode allows blue light emitted from the diode to be either transmitted trough the layer of nanocrystals or reflected from the surface of the glass substrate, nanocrystals or PMMA back into the diode housing. The latter together with the light which is emitted in the angle $> 70^o$ from the normal is getting reflected from the surface of the metal housing and part of it is eventually absorbed by one of the surfaces (diode, glass, nanocrystals, PMMA, metal housing, bonding wires) while the rest is transmitted through a layer of nanocrystals. Thickness of the colour converting layer of nanocrystals was calculated assuming that around each nanocrystal (for the required number of nanocrystals) there is 10 nm free space (which results in 20 nm space between two neighbouring nanocrystals) and that the required contribution of blue light is transmitted through the layer of nanocrystals.

6.2 Results of modelling

Varying each spectrum by 5% results in 53130 different variations of resulting light. Calculations of chromaticity distance (CD), colour rendering index (CRI) and correlated colour temperature (CCT) have been performed for all of those variations. All the combinations, with $CD < 5.4 \cdot 10^{-3}$ were rejected as they were not classified as white light. An assessment of quality of light based on CRI index was performed on all remaining combinations. After rejecting all the variations with poor colour rendering $CRI < 80$, and after ignoring variations with CCT outside the region of interest (2500 - 8800 K) 1821 variations remained (shown in Subsidiary Information) of which 36 fulfilling additional condition of $CD < 10 \cdot 10^{-4}$ are shown in the figure 6.4 and the table 6.1. The last condition was added in order to display the representative sample of the results, however all further analysis is based on the 1821 variations.

Figure 6.4 shows the spectral distribution of radiant flux for all 36 variations from table 6.1. For clarity they are divided in four groups sorted by the contribution of the blue light towards the resulting spectrum. Top left graph shows the 15% contribution, the top right graph shows 20% contribution, the bottom left graph shown the 25% and the bottom right graph shown the 30, 35, 40, 45, 50 and 55% contribution of the blue light. Generally we can see three trends: there is either majority of the red light (top left graph - 15% contribution of the blue and 45 - 60 % of contribution from 630 and 655 nm nanocrystals) or the blue light (bottom right graph - minimum 30% contribution of the blue and maximum 25% of red light with exception of curve no. 29 which has 40% of red light) or the third option where the contributions are more balanced (top right and bottom left graphs - 20 and 25% contributions of the blue and between 10 an 50% of the red light).

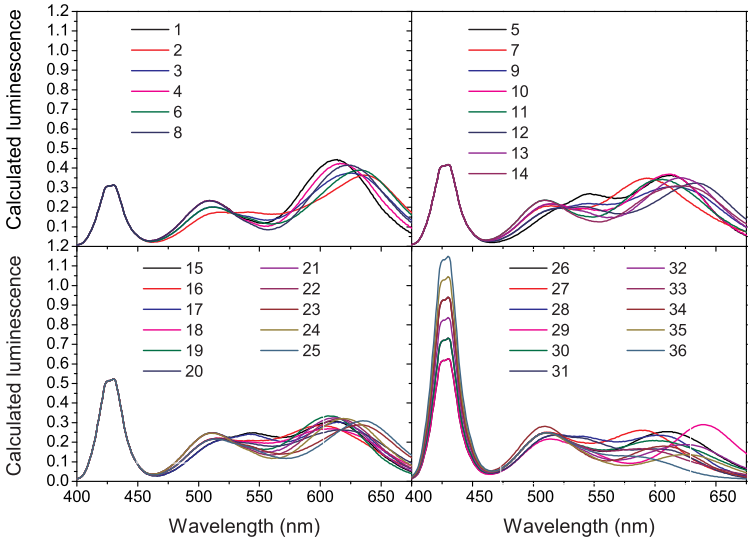

Figure 6.4: Calculated luminescence spectrum of hybrid white light emitting diode consisting of layer of InP/ZnS nanocrystals and the electrically driven blue emitting diode. Legend correlates the spectrum with the row in the table 6.1. Note, that the higher number corresponds to higher CCT. Top left graph shows the 15% contribution of the light from the blue diode towards the white light spectrum, the top right graph shows 20% contribution, the bottom left graph shown the 25% and the bottom right graph shown the largest 30, 35, 40, 45, 50 and 55% contribution of the blue light.

For the first three graphs, with contribution of blue light between 15 and 25%, the white light spectra are weakly varying suggesting that for colour temperature below 3500 K this is the optimal spectrum. Moreover the contribution from smallest nanocrystals emitting at 530 nm (in a green region) is smaller than the red and blue peaks at these graphs. For the graphs showing spectra with highest contribution of blue, the green emission peak is comparable to the red one however its contribution towards the white light spectrum did not change between all four graphs. The reason why the green peak contribution is constant and it is smaller than the other peaks

is high sensitivity of human eye in the yellow to green spectral region.

Columns II-VII of the table 6.1 show contribution from the diode and the nanocrystals to the total spectrum. Note that 16 out of 36 variations have only contribution from four sizes of nanocrystals and five has contribution from only three, showing that only four colours of emission spectra are enough to generate good quality white light in wide range of correlated colour temperatures (based on the results from table 6.1). It is partly due to the broad spectrum of emission of the NCs compared with the LED emission. This is still one colour more than in popular WLEDs where tricolour phosphors or RGB LED systems are used. The light emitted by 530 nm is present in every variation while 570, 630 and 655 nm light are missing in 6 variations and 615 nm light is missing in 8 variations. It would suggest that the least important component is the 615 nm light source and the contribution from green component is crucial. Out of all the variations, 15 represent white light with CRI value equal to 90 and only four of the variations have CRI lower than 85 confirming that excellent light quality can be obtained with InP/ZnS nanocrystals. These results are comparable to the ones obtained for CdSe nanocrystals [23] which is not surprising as the light quality should not depend on the composition of nanocrystals. The thickness of the colour converting layer, has been calculated for the nanocrystals under study and with 50% QE and is shown in column d and $d_{0.5}$ of the table 6.1, respectively. As the quality of nanocrystals improves, its colour conversion efficiency increases which results is smaller number of nanocrystals needed in order to generate white light. The thickness for the current quality of nanocrystals is 2 to 7 times larger than the more efficient ones. It is very interesting that for the latter nanocrystals the thickness increases for the higher correlated colour temperature which would suggest that in

No	450 nm	530 nm	570 nm	615 nm	630 nm	655 nm	*CRI*	*CCT*	d (mm)	$d_{0.5}$ (mm)	η_R lm/W
1	15	25	0	10	45	5	91	2501	6.2	1.8	253
2	15	15	10	15	0	45	93	2511	10.4	1.6	220
3	15	20	5	10	20	30	92	2536	8.9	1.7	229
4	15	25	0	5	40	15	88	2560	7.5	1.8	238
5	20	10	25	0	40	5	82	2586	7.1	1.6	277
6	15	20	5	5	15	40	89	2604	10.2	1.8	214
7	20	20	5	45	0	10	90	2614	5.2	1.5	278
8	15	25	0	0	35	25	84	2630	8.7	1.9	223
9	20	15	15	15	15	20	88	2679	7.9	1.6	257
10	20	20	10	10	35	5	93	2702	6.3	1.8	266
11	20	25	0	30	15	10	95	2733	5.8	1.8	262
12	20	15	15	5	10	35	89	2795	10.0	1.7	232
13	20	20	10	0	30	20	91	2821	8.4	1.9	241
14	20	25	0	20	10	25	91	2858	7.9	1.8	236
15	25	15	20	5	30	5	85	2913	6.7	1.8	274
16	25	20	10	25	10	10	89	2948	6.1	1.8	269
17	25	15	20	0	30	10	86	2960	7.5	1.9	264
18	25	20	10	20	10	15	90	2997	7.0	1.8	259
19	25	25	5	15	30	0	94	3022	5.3	2.0	268
20	25	20	10	15	10	20	91	3052	7.8	1.9	249
21	25	25	5	10	30	5	92	3078	6.1	2.0	258
22	25	25	5	5	30	10	90	3141	7.0	2.1	248
23	25	20	10	5	10	30	90	3183	9.5	1.9	228
24	25	25	5	0	30	15	88	3211	7.8	2.1	238
25	25	20	10	0	10	35	88	3261	10.3	2.0	218
26	30	25	5	15	15	10	92	3418	6.4	2.1	251
27	35	25	5	35	0	0	89	3531	3.9	2.0	274
28	35	20	15	10	20	0	85	3573	5.5	2.1	269
29	30	20	10	0	0	40	86	3733	11.2	2.1	206
30	35	25	5	20	5	10	91	3755	6.1	2.2	249
31	45	20	15	5	15	0	83	4492	5.6	2.4	249
32	40	25	5	5	10	15	88	4502	7.7	2.4	221
33	45	25	5	20	0	5	88	4638	5.2	2.4	239
34	45	30	0	10	15	0	89	5079	4.9	2.7	233
35	50	25	5	0	10	10	85	6206	7.4	2.7	206
36	55	25	5	15	0	0	84	6282	4.2	2.8	224

Table 6.1: Results of the light quality calculations where first 6 columns show the contribution of the diode and each of the nanocrystals towards the white light spectrum. Column d shows the thickness of the nanocrystals layer under study while $d_0.5$ for the nanocrystals with 50% quantum efficiency; η_R indicates the luminous efficacy of radiation. Note, that the thickness is expressed in millimetres.

order to generate such temperatures more nanocrystals are needed. This is the results of the smaller absorption probability of the smaller nanocrystals as shown in the table 5.2. In order to generate cool white light more blue photons are needed and less red photons, however the missing part of red spectrum has to be substituted with photons from 530, 570 and 615 nm. This effect cannot be seen in the case of nanocrystals under study because their quantum efficiency changes with their size. Also the highest achieved value of CCT (shown in the table 6.1) is 6200 K which is much smaller than set in requirements. Note that the CCT of 8800 K is obtained for the $CD < 5.4 \cdot 10^{-}3$. This can be explained by the conditions which need to be met in order to achieve white light with $CD < 10^{-}4$ and high CRI index: there should be balanced contribution from blue, green and red spectral region.

Luminous efficacy of radiation η_R for the hybrid diode for nanocrystals under study is shown in table 6.1. If we assume that all nanocrystals have quantum efficiency of photoluminescence equal to 50% then, in this model, number of nanocrystals will be reduced in order to meet the requirements. The luminous efficacy of radiation thus would not change. Those values of achieved efficacies would exceed most efficient source of light which is high discharge sodium vapour lamp and would approach the theoretically predicted limit for the WLED based on the phosphors as colour conversion material (300 lm/W). United States National Institute of Standard and Technology (NIST) has shown that the maximum theoretical value of luminous efficacy of radiation for RGB based white light emitting diode is over 400 lm/W [101].

6.3 Analysis of the WLED components contribution

In order to understand how the contributions of the emission of each white LED component influence the resulting light quality further analysis is necessary. The discussion is based on the relations between CCT, CRI and luminous efficacy of radiation and light contribution from each of the hybrid WLED component. Care has to be taken in this analysis as the presence of the contribution of each of the component of the WLED is strongly correlated with the rest of them. For example, white light with $CCT \sim 3500$ K could not be reached without the presence of the contribution of red light and by looking at the row 27 in the table 6.1, one could draw misleading conclusions looking just at the contribution from 630 and 650 nm nanocrystals (which is 0 for both) and not at the 615 nm (which is 35%).

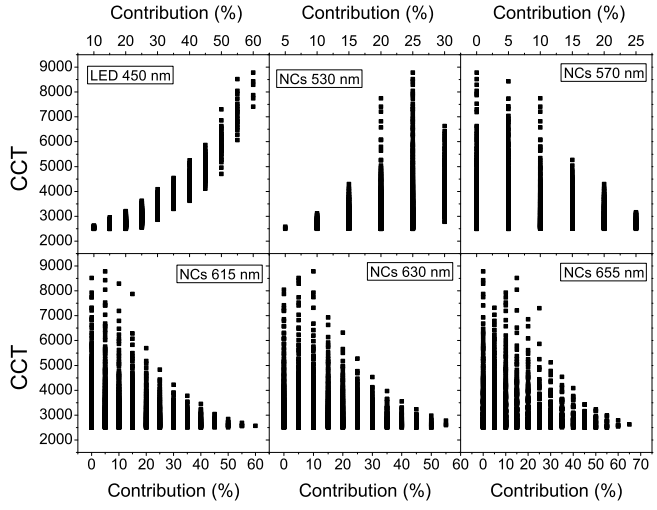

Figure 6.5: Influence of the contribution from the emission of the diode and all the nanocrystal' sizes on correlated colour temperature of resulting white light based on table 6.1. Note that low sensitivity of CCT to a single component means there are other components that can replace it.

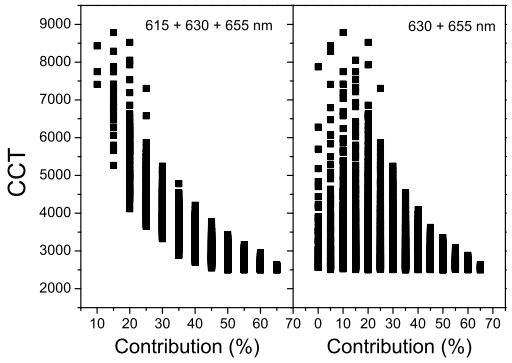

Figure 6.6: Influence of the contribution from the red and orange - red emission on correlated colour temperature of resulting white light based on table 6.1.

As expected, there is a clear correlation between percentage of the blue light in the white light spectrum of the hybrid diode and the correlated colour temperature: for bigger contribution of the blue light the higher is the correlated colour temperature of the resulting white light, see table 6.1. It is interesting to see how emission of each size of nanocrystals influences the CCT of the white light spectrum. Figure 6.5 shows the CCT as a function of the contribution of the emission of the diode and five sizes of nanocrystals to white light spectrum. The subfigure on the top left, showing CCT of the diode with peak emission wavelength of 450 nm confirms the correlation described above. Similar trend can be seen for the nanocrystals with maximum emission wavelength of 530 nm; however the range of CCT of the resulting white light which can be reached with increasing contribution of the light from these nanocrystals is broader. The influence of the nanocrystals with maximum emission wavelength of 570, 615, 630 and 655 nm is opposite and wider CCT range is achievable at lower contributions. The joint contribution from nanocrystals emitting above 600 nm is plotted against CCT values as shown in figure 6.6. It shows that only one of red

emitting nanocrystals (615 nm) is necessary to achieve wide range of CCT.

The effect of the contribution of the diode and nanocrystals on the colour rendering index of resulting white light is shown on the figure 6.7. For the nanocrystals with peak emission wavelength above 600 nm (bottom three graphs) almost any CRI can be reached (from 80 to 96), however the sum of this contributions from red light should not be smaller than 10% and bigger than 65% (as there is also need for blue to yellow light). The CRI however increases with the sum from 615, 630 and 655 nm nanocrystals as shown in figure 6.8. The opposite trend is for the 570 nm nanocrystals where its bigger contribution reduces CRI. This is similar to the joint contribution from 530 and 570 nm nanocrystals: bigger the contribution, lower the CRI, as shown in figure 6.8. The green and yellow light should be kept in the region between 20 and 40%.

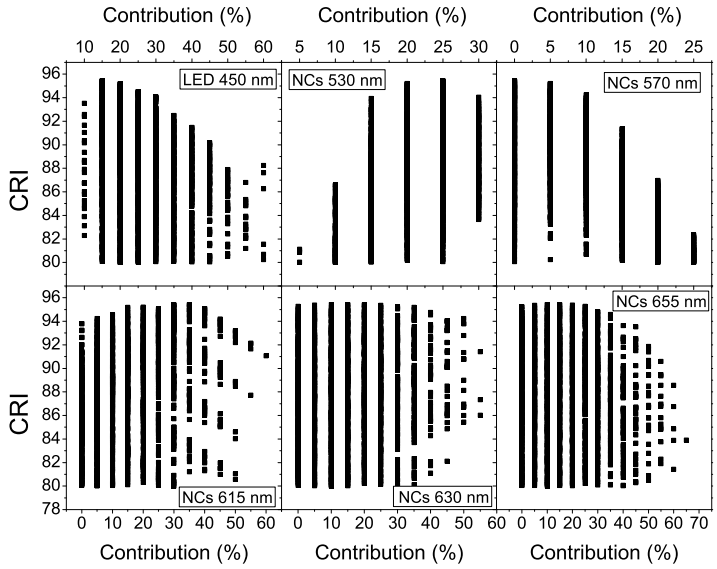

Figure 6.7: Influence of the contribution from diode and all sizes of nanocrystals on colour rendering index of resulting white light.

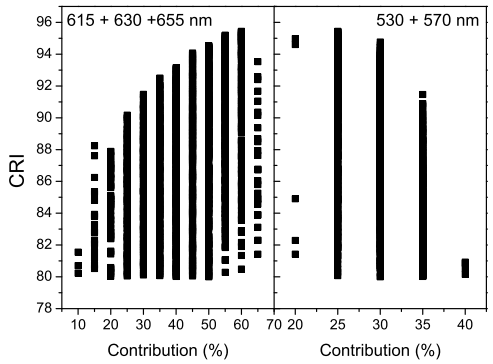

Figure 6.8: Influence of the contribution from nanocrystals emitting in red region (615, 630 and 655 nm) and green to yellow (530 and 570 nm) on colour rendering index of resulting white light.

For the contribution of the diode emission higher than 55% CRI > 90 cannot be obtained from the same reasons why there should be no more than 65% of red light. Opposite influence has contribution of nanocrystals with peak emission wavelength of 530 nm - for its low value below 10% only CRI of 86 can be obtained and for increase of 530 nm emitting nanocrystals higher CRI values can be reached. The fact that the CRI between 80 and 90 (which is highly desirable) can be achieved by any contribution from diode and the nanocrystals might lead to the conclusion that the CRI value is not influenced by the size of the contribution from each components but by the presence of that component in the white light spectrum.

The effect of the contribution of each type of nanocrystals and the diode on luminous efficacy of radiation is very strong. The luminous efficacy decreases for higher contribution of diode or nanocrystals with peak emission wavelength of 655 nm and it increases for nanocrystals emitting at 615 nm. Moreover the high values of efficacy can be generated by the diode with contribution in a range 15 - 35% of 530 nm nanocrystals, 0 to 25% of 570 nm nanocrystals and 0 - 50% of 630 nm nanocrystals. These trends have

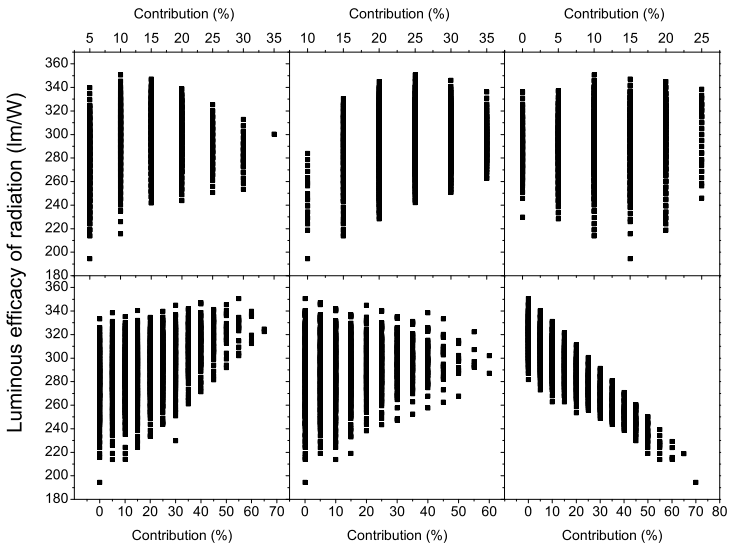

Figure 6.9: Influence of the contribution from diode and all sizes of nanocrystals on luminous efficacy of radiation of resulting white light.

resulted from the eye response function: more light in the area where the eye is not sensitive leads to luminous efficacy decrease.

In order to confirm how many nanocrystals are necessary for the white light fulfilling quality conditions set at the beginning of this chapter calculations for different sets of nanocrystals and the diode has been performed. Tables 6.2 - 6.7 shows the results of the calculations. The choice of the components for these calculations has been made on the basis of the knowledge gained from the previous analysis: table 6.1 shows that the 530 nm nanocrystals are crucial in order to obtain good CRI and high luminous efficacy of radiation so those nanocrystals together with diode are obligatory. For the sets which has contribution from 570 nm nanocrystals the contribution from only one red emitting nanocrystals was added. Those calculations were followed by the obligatory contribution of 615 nm nanocrystals and one of the remaining red emitting nanocrystals. From the sets with only three

emission colours only the one with 615 nm produced the variations fulfilling light quality conditions. Note that the CRI values are around 90 which are comparable to ones in table 6.1 however the luminous efficacy of radiation is higher as expected from reducing the number of components. The CCT values above $\sim$ 4500 K could not be reached. If four colours of hybrid diode components are considered the efficacy is still higher that the one shown in the table 6.1 however its value depends on the presence of different components. It is the highest for the sets with 570 and 615 nm nanocrystals (see table 6.3), it gets lower when 630 nm are used (see table 6.4) and is the lowest for 655 nm nanocrystals (see table 6.5). As it has been mentioned before it is related to the sensitivity of an eye in the region of emission of these nanocrystals. The CRI shows opposite effect and it increases with increasing fraction of contribution from red emitting nanocrystals. The CCT shows similar effect which can be explained by the need of balancing the blue and red contributions in order to meet the CRI requirement. It feels counter-intuitive to add deep red to achieve cooler correlated colour temperature however the chromaticity diagram (figure 6.2) shows that this is necessary. This is also clearly visible if one compares row 1 of table 6.2 and rows 2 and 3 of table 6.3. Reducing amount of red light (615 nm) from 65% to 60% and then 55% and replacing it by 5% and than 10% of 570 nm light causes increase of CCT and efficacy but reduction of CRI. By adding 655 nm component (table 6.7) gives the chance to increase CCT beyond 4500 K.

450 nm	530 nm	615 nm	*CRI*	*CCT*	η lm/W
10	25	65	92	2688	323
10	30	60	91	3066	336
15	30	55	92	3411	323
15	35	50	89	3888	336
20	35	45	89	4478	324

Table 6.2: Results of the light quality calculations for diode (1st column) and two sizes of nanocrystals (2nd and 3rd columns); η indicates the luminous efficacy of radiation.

450 nm	530 nm	570 nm	615 nm	*CRI*	*CCT*	η lm/W
10	20	10	60	83	2677	338
10	25	5	60	88	2862	337
10	25	10	55	83	3033	351
15	25	10	50	84	3350	338
15	30	5	50	87	3609	337
20	30	5	45	88	4126	325
20	30	10	40	82	4326	339
25	35	5	35	83	5510	325
30	35	5	30	82	6773	313
35	35	5	25	80	8809	300

Table 6.3: Results of the light quality calculations for diode (1st column) and three sizes of nanocrystals (2nd to 4th columns); η indicates the luminous efficacy of radiation.

450 nm	530 nm	570 nm	630 nm	*CRI*	*CCT*	η lm/W
10	15	25	50	86	2762	315
10	20	20	50	89	2971	314
10	25	10	55	84	3000	294
10	20	25	45	83	3159	333
10	25	15	50	88	3202	313
15	20	25	40	83	3522	326
15	25	15	45	87	3608	306
15	25	20	40	85	3805	325
15	30	10	45	84	3924	305
20	25	20	35	84	4371	318
20	30	10	40	84	4580	297
20	30	15	35	84	4743	317
20	35	5	40	81	5001	296
25	30	15	30	82	5631	309
25	35	5	35	81	6066	289
30	30	15	25	81	6917	302
30	35	5	30	82	7677	282

Table 6.4: Results of the light quality calculations for diode (1st column) and three sizes of nanocrystals (2nd to 4th columns); η indicates the luminous efficacy of radiation.

450 nm	530 nm	570 nm	655 nm	*CRI*	*CCT*	η lm/W
10	15	15	60	81	3426	216

Table 6.5: Results of the light quality calculations for diode (1st column) and three sizes of nanocrystals (2nd to 4th columns); η indicates the luminous efficacy of radiation.

450 nm	530 nm	615 nm	630 nm	*CRI*	*CCT*	η lm/W
10	30	20	40	81	3047	294
10	30	25	35	84	3049	299
10	30	30	30	87	3052	305
10	30	35	25	89	3054	310
10	30	40	20	91	3057	315
10	30	45	15	92	3059	320
10	30	50	10	93	3061	325
10	30	55	5	92	3063	330
15	35	45	5	90	3902	331
15	35	40	10	90	3918	326
15	35	35	15	89	3934	321
15	35	30	20	88	3950	316
15	35	25	25	86	3968	310
15	35	20	30	84	3986	305
15	35	15	35	82	4006	300
20	35	40	5	90	4510	319
20	35	35	10	89	4544	313
20	35	30	15	88	4580	308
20	35	25	20	86	4618	303
20	35	20	25	84	4658	298
20	35	15	30	82	4701	293

Table 6.6: Results of the light quality calculations for diode (1st column) and three sizes of nanocrystals (2nd to 4th columns); η indicates the luminous efficacy of radiation.

450 nm	530 nm	615 nm	655 nm	*CRI*	*CCT*	η lm/W
10	25	60	5	93	2740	312
10	25	55	10	93	2798	302
10	25	50	15	93	2862	292
10	25	45	20	92	2934	282
10	25	40	25	89	3014	271
10	25	35	30	87	3105	261
10	30	55	5	92	3139	325
10	25	30	35	83	3209	251
10	30	50	10	92	3221	315
10	30	45	15	92	3311	305
10	30	40	20	90	3411	295
15	30	50	5	92	3519	313
15	30	45	10	91	3639	303
15	30	40	15	90	3774	292
15	30	35	20	88	3926	282
15	30	30	25	85	4099	272
15	30	25	30	83	4294	262
15	30	20	35	80	4518	251
20	35	40	5	89	4673	313
20	35	35	10	88	4891	303
20	30	25	25	83	4999	259
20	35	30	15	86	5136	293
20	35	25	20	84	5411	283
25	35	35	5	88	5640	301
25	35	30	10	86	5979	291
25	35	25	15	85	6367	281
25	35	20	20	83	6814	270
30	35	30	5	86	7162	289
30	35	25	10	85	7734	278
30	35	20	15	83	8414	268

Table 6.7: Results of the light quality calculations for diode (1st column) and three sizes of nanocrystals (2nd to 4th columns); η indicates the luminous efficacy of radiation.

6.4 Conclusions

From the analysis of over $5 \cdot 10^4$ variations of spectral distribution of radiant energy of white light we can conclude that high values (> 80) of colour rendering index for wide range of colour temperatures (2500 - 8800 K) can be generated from hybrid diode consisting of electrically driven InGaN/GaN chip and 10 x 10 cm layer of nanocrystals of different sizes. In order to generate such quality light, from nanocrystals under study, thickness of colour converting layer should be in the range between 4 and 11 mm. Luminous efficacy of radiation varies between 200 and 350 lm/W. The CRI $\sim$ 90 for warm white light and high luminous efficacy of radiation can be achieved from only two sizes of nanocrystals (530 nm and 615 nm). If higher values of CCT are required the additional 630 nm nanocrystals needs to be added. Using five sizes of nanocrystals improves only slightly CRI index from 92 to 96 (for $\sim$ 2700 K) however the luminous efficacy drops from 323 to 262 lm/W.

Chapter 7

Conclusions

In this work, InP/ZnS colloidal nanocrystals as colour converting material in white light emitting diodes have been investigated. The studied nanocrystals have been synthesized using a one pot, hot injection method that allows size tuning by adjusting time and precursors ratios.

Experiments described in this thesis show that the studied nanocrystals consist of two populations: nanocrystals that emit light (bright) and the ones that do not non-emit light (dark). The fraction of bright nanocrystals in the total population is one order of magnitude bigger for the small particles (emitting at shorter wavelength) than for the large nanocrystals (with an emission wavelength above 600 nm). Correlation of the optical investigations with structural characterization points to the presence of extended surfaces and interfaces between coalesced nanocrystals as the origin of the defects responsible for the emission quenching. The quantum efficiency of the bright population of nanocrystals is determined to be 64% at 660 nm. Based on TRPL studies carrier dynamics in the nanocrystals is discussed and the diagram illustrating energy levels is proposed. Bright and dark exitonic levels coexist with trap states which are most likely located at the

surface and at the core-shell interface. The long lived trapped carriers and dark excitons lead to the Auger recombination at the temperature below 140 K. We expect thus that Auger recombination can cause problem in applications where NCs are strongly excited even at room temperature.

Two methods of exciting the nanocrystals have been considered: photon absorption and resonant energy transfer. A very low absorption probability combined with low quantum efficiency leads to colour conversion efficiencies lower around 1%. The colour conversion efficiency for resonant energy transfer is one order of magnitude higher than for the optical absorption however due to low quantum efficiency of larger nanocrystals it is still below 5%. Although resonant energy transfer enhances the photon transfer from blue LED to the NCs compared with absorption, the need to keep nanocrystals in close proximity of the quantum well renders the effect unsuitable for light sources using standard blue LEDs. It may however be considered in a combination with nanowire blue LEDs, where it could compete with the surface recombination.

The simulation of the emission from hybrid white light emitting diode consisting of layer of nanocrystals of different sizes deposited on the InGaN/GaN diode has shown that the white light in a wide range of correlated colour temperatures (2500 - 8800 K) can be generated with colour rendering index above 80 (and even close to the ideal CRI, with value of 96) and high luminous efficacy. It is theoretically possible to achieve high luminous efficacy of radiation comparable to that theoretically predicted for phosphor based WLED. Due to the low colour conversion efficiency, in order to obtain a desired colour conversion the number of nanocrystals is learned to be large. It is found that it is enough to use LED with only two nanocrystals (green and red) to produce high quality light while adding additional components

can be used to tune the CCT and luminous flux or CRI.

An obvious extension of this work is to characterize experimentally InP/ZnS nanocrystals based white light emitting diode. The important factor to check is the colour stability over extended working hours and/or at elevated temperatures. As discussed in chapter 2.1 the white light emitting diodes experience the colour shift caused by the rise of the temperature. An important factor which will influence the spectrum of white light and which should be investigated in future both theoretically and experimentally is the possibility of absorption and resonant energy transfer between nanocrystals. As the RET rate scales with the distance to the power of 6 between zero-dimensional donor and zero dimensional acceptor (nanocrystal to nanocrystal), even 2 nm distance between nanocrystals is enough to prevent it. Absorption of light emitted at shorter wavelengths by the larger nanocrystals cannot be avoided easily. Unless a method of preventing such cross-absorption by optical engineering is developed (e.g. by spatially separating the nanocrystals, followed by light remixing), it should be included in WLED analysis. For a design of white LED one should also include an analysis of the optimal peak emission wavelengths for nanocrystals. In the analysis performed here it is clear that removing one of the nanocrystal samples (either 630 nm or 655 nm) result in only a small decrease of CRI and a large increase of luminous efficacy of radiation.

In order to improve colour conversion efficiency, which is currently the major drawback of the InP/ZnS nanocrystals for solid state lighting, future work should focus on improving the quantum efficiency of InP/ZnS nanocrystals to at least 50% for the required emission wavelengths. Since

the efficiency of the InP/ZnS nanocrystals seems to decrease with increase of size, it may be an option to change the material for the efficient red emitters to, for example, InAs. With a smaller bandgap than InP, smaller nanocrystals of InAs would be needed to achieve the same wavelength of emission. Further improvements could be considered that would lead to increase of the absorption probability of the nanocrystals. One possibility would be to grow thicker shell of the material which would absorb but not emit light (excitons would decay to the core where they would recombine). Even more attractive geometry would require a growth of two shells in order to even extend the nanocrystals absorption area in the inner shell and protect the excitons from the surface states with the outer shell.

Subsidiary Information

Table 7.1: Results of the light quality calculations where first 6 columns show the contribution of the diode and each of the nanocrystals towards the white light spectrum; η_R indicates the luminous efficacy of radiation.

No	450 nm	530 nm	560 nm	615 nm	630 nm	655 nm	*CRI*	*CCT*	d (mm)	$d_{0.5}$ (mm)	η lm/W
1	15	25	0	10	45	5	91	2501	5.3	1.5	138
2	15	20	5	25	15	20	95	2501	6.2	1.4	233
3	10	20	5	0	15	50	87	2501	10.1	1.6	343
4	15	20	0	5	5	55	82	2502	10.0	1.5	324
5	15	25	0	25	35	0	95	2502	4.3	1.4	122
6	20	5	25	0	10	40	81	2502	8.9	1.2	299
7	15	20	5	40	5	15	92	2502	5.2	1.3	223
8	10	25	0	0	35	30	85	2502	8.2	1.7	259
9	10	20	5	15	5	45	92	2503	9.1	1.5	352
10	20	10	20	0	30	20	87	2503	7.0	1.3	206
11	10	25	0	15	25	25	91	2504	7.2	1.6	258
12	15	10	25	10	30	10	80	2504	6.1	1.3	186
13	20	15	15	0	50	0	91	2504	5.1	1.3	101
14	20	10	20	15	20	15	83	2504	6.0	1.2	197
15	20	10	20	30	10	10	80	2505	5.0	1.1	183
16	15	10	20	5	10	40	85	2506	8.9	1.3	322
17	15	15	15	5	30	20	90	2507	7.0	1.4	223
18	15	10	20	20	0	35	82	2507	7.9	1.2	323
19	15	15	15	20	20	15	87	2508	6.0	1.3	214
20	15	20	10	5	50	0	94	2508	5.2	1.5	114
21	20	15	10	10	20	25	94	2508	6.9	1.3	225
22	15	15	15	35	10	10	84	2508	5.0	1.2	200
23	20	15	10	25	10	20	90	2509	5.9	1.2	220
24	20	20	5	10	40	5	95	2509	5.1	1.4	128
25	15	15	15	50	0	5	81	2509	4.0	1.2	182
26	20	15	10	40	0	15	87	2509	4.9	1.1	211
27	20	20	5	25	30	0	94	2509	4.1	1.3	112
28	15	15	10	0	10	50	90	2510	9.8	1.4	327
29	15	15	10	15	0	45	93	2511	8.8	1.3	336
30	15	20	5	0	30	30	89	2511	8.0	1.5	246
31	15	20	5	15	20	25	94	2512	7.0	1.4	244
32	15	25	0	0	50	10	86	2512	6.1	1.6	154

33	15	20	5	30	10	20	94	2512	6.0	1.3	239
34	15	25	0	15	40	5	92	2512	5.1	1.5	142
35	15	20	5	45	0	15	90	2512	5.0	1.3	229
36	15	25	0	30	30	0	95	2512	4.1	1.4	126
37	15	10	25	0	35	15	82	2513	6.9	1.4	204
38	20	20	0	35	0	25	95	2513	5.9	1.2	241
39	10	20	5	5	10	50	88	2514	9.9	1.5	352
40	10	20	5	20	0	45	94	2514	8.9	1.5	361
41	20	5	25	5	5	40	80	2515	8.7	1.2	307
42	10	25	0	5	30	30	87	2515	8.0	1.6	266
43	10	25	0	20	20	25	93	2515	7.0	1.6	264
44	20	10	20	5	25	20	85	2515	6.8	1.2	211
45	20	10	20	20	15	15	82	2515	5.8	1.2	202
46	20	15	15	5	45	0	90	2515	4.9	1.3	105
47	15	20	0	10	0	55	85	2516	9.8	1.4	334
48	15	15	15	40	5	10	83	2518	4.8	1.2	205
49	15	10	20	10	5	40	84	2518	8.7	1.3	330
50	15	15	15	25	15	15	86	2518	5.8	1.3	219
51	15	15	15	10	25	20	89	2518	6.8	1.4	229
52	15	20	10	10	45	0	93	2518	5.0	1.5	117
53	20	15	10	30	5	20	89	2520	5.8	1.2	226
54	20	20	5	30	25	0	93	2520	3.9	1.3	116
55	20	15	10	15	15	25	93	2520	6.8	1.3	232
56	20	20	5	15	35	5	95	2520	4.9	1.3	132
57	15	20	5	35	5	20	93	2523	5.8	1.3	245
58	15	25	0	35	25	0	95	2523	3.9	1.4	129
59	15	20	5	20	15	25	95	2523	6.8	1.4	251
60	15	25	0	20	35	5	94	2523	4.9	1.5	146
61	15	10	25	5	30	15	81	2524	6.7	1.3	209
62	15	25	0	5	45	10	88	2524	5.9	1.6	159
63	15	20	5	5	25	30	91	2524	7.8	1.5	253
64	15	15	10	5	5	50	91	2524	9.7	1.4	336
65	20	10	20	25	10	15	81	2525	5.6	1.1	207
66	20	15	15	10	40	0	89	2526	4.7	1.3	108
67	20	10	20	10	20	20	84	2526	6.6	1.2	217
68	10	25	0	10	25	30	89	2526	7.8	1.6	273
69	10	20	5	10	5	50	90	2527	9.7	1.5	362
70	15	15	15	45	0	10	82	2527	4.7	1.2	209
71	15	15	15	30	10	15	85	2528	5.7	1.3	224
72	15	20	10	15	40	0	93	2528	4.8	1.4	121
73	15	15	15	15	20	20	88	2529	6.7	1.4	235
74	15	10	20	15	0	40	83	2529	8.5	1.3	338
75	15	20	10	0	50	5	94	2529	5.8	1.5	138
76	15	15	15	0	30	25	91	2530	7.7	1.4	241
77	15	10	20	0	10	45	86	2530	9.5	1.3	334
78	20	20	5	35	20	0	92	2530	3.7	1.2	119
79	20	15	10	35	0	20	88	2531	5.6	1.2	232
80	20	20	5	20	30	5	95	2532	4.7	1.3	136
81	20	15	10	20	10	25	92	2532	6.6	1.2	238
82	15	25	0	40	20	0	95	2532	3.7	1.4	132
83	15	20	5	40	0	20	92	2533	5.6	1.3	251

84	20	20	5	5	40	10	93	2533	5.7	1.4	148
85	15	10	25	10	25	15	80	2533	6.5	1.3	215
86	15	25	0	25	30	5	95	2534	4.7	1.5	150
87	15	20	5	25	10	25	95	2534	6.6	1.4	257
88	15	25	0	10	40	10	90	2535	5.7	1.5	163
89	15	20	5	10	20	30	92	2536	7.6	1.4	260
90	20	15	15	15	35	0	88	2536	4.6	1.3	111
91	15	15	10	10	0	50	92	2536	9.5	1.4	346
92	15	15	15	35	5	15	84	2537	5.5	1.3	230
93	20	10	20	15	15	20	83	2537	6.4	1.2	222
94	10	25	0	15	20	30	90	2538	7.6	1.6	281
95	15	20	10	20	35	0	91	2538	4.6	1.4	124
96	20	15	15	0	45	5	91	2538	5.6	1.4	128
97	20	20	0	30	0	30	95	2538	6.5	1.3	256
98	10	20	5	15	0	50	92	2538	9.5	1.5	372
99	15	15	15	20	15	20	87	2539	6.5	1.3	241
100	20	10	20	0	25	25	87	2539	7.4	1.3	229
101	10	25	0	0	30	35	84	2540	8.6	1.7	280
102	15	20	10	5	45	5	94	2540	5.6	1.5	141
103	20	5	25	0	5	45	81	2540	9.3	1.2	319
104	20	20	5	40	15	0	91	2540	3.5	1.2	122
105	10	20	5	0	10	55	86	2541	10.5	1.6	360
106	15	15	15	5	25	25	90	2541	7.5	1.4	248
107	15	25	0	45	15	0	94	2542	3.5	1.4	136
108	15	10	20	5	5	45	85	2542	9.3	1.3	343
109	20	20	5	25	25	5	94	2542	4.5	1.3	139
110	20	15	10	25	5	25	91	2543	6.4	1.2	244
111	15	25	0	30	25	5	95	2544	4.5	1.4	154
112	15	15	20	0	50	0	87	2544	5.5	1.5	116
113	15	20	5	30	5	25	94	2545	6.4	1.4	264
114	20	20	5	10	35	10	94	2545	5.5	1.4	152
115	15	10	25	0	30	20	82	2545	7.3	1.4	231
116	20	15	10	10	15	30	94	2546	7.4	1.3	247
117	15	25	0	15	35	10	92	2546	5.5	1.5	168
118	15	15	15	40	0	15	83	2546	5.3	1.2	235
119	20	15	15	20	30	0	87	2546	4.4	1.3	114
120	15	20	0	5	0	60	81	2547	10.4	1.5	338
121	15	20	5	15	15	30	94	2547	7.4	1.4	267
122	15	20	10	25	30	0	90	2547	4.4	1.4	127
123	20	10	20	20	10	20	82	2548	6.2	1.2	228
124	15	15	15	25	10	20	86	2549	6.3	1.3	247
125	25	15	10	40	10	0	86	2549	3.3	1.1	112
126	15	25	0	0	45	15	85	2549	6.5	1.6	177
127	20	15	15	5	40	5	90	2549	5.4	1.3	131
128	20	20	5	45	10	0	90	2550	3.3	1.2	125
129	15	20	10	10	40	5	93	2550	5.4	1.5	145
130	20	10	20	5	20	25	85	2550	7.2	1.3	235
131	15	20	5	0	25	35	88	2550	8.4	1.5	266
132	15	25	0	50	10	0	93	2551	3.4	1.3	139
133	15	15	15	10	20	25	89	2551	7.3	1.4	254
134	10	25	0	5	25	35	86	2551	8.4	1.6	287

135	15	15	10	0	5	55	89	2552	10.3	1.4	343
136	20	20	5	30	20	5	93	2553	4.3	1.3	143
137	20	10	25	0	45	0	82	2553	5.2	1.3	106
138	15	10	20	10	0	45	84	2553	9.1	1.3	352
139	10	20	5	5	5	55	88	2553	10.3	1.6	370
140	15	25	0	35	20	5	95	2553	4.4	1.4	158
141	15	15	20	5	45	0	86	2553	5.3	1.4	119
142	20	15	10	30	0	25	89	2554	6.2	1.2	251
143	15	20	5	35	0	25	93	2555	6.2	1.3	270
144	15	10	25	5	25	20	81	2555	7.1	1.3	237
145	25	10	20	20	25	0	82	2555	4.2	1.1	104
146	20	20	5	15	30	10	95	2556	5.3	1.4	157
147	20	15	15	25	25	0	86	2556	4.2	1.2	117
148	15	20	10	30	25	0	89	2557	4.2	1.4	131
149	15	25	0	20	30	10	94	2557	5.4	1.5	172
150	20	10	20	25	5	20	81	2558	6.1	1.2	234
151	20	15	10	15	10	30	93	2558	7.2	1.3	254
152	15	15	15	30	5	20	85	2558	6.1	1.3	252
153	15	20	5	20	10	30	95	2558	7.2	1.4	274
154	25	15	10	45	5	0	85	2559	3.1	1.0	115
155	20	20	5	50	5	0	89	2559	3.1	1.2	129
156	20	15	15	10	35	5	89	2559	5.2	1.3	135
157	15	25	0	55	5	0	92	2559	3.2	1.3	143
158	15	20	10	15	35	5	93	2560	5.2	1.4	149
159	15	25	0	5	40	15	88	2560	6.4	1.6	182
160	20	10	20	10	15	25	84	2561	7.1	1.2	241
161	15	15	15	15	15	25	88	2562	7.1	1.4	260
162	20	10	25	5	40	0	81	2562	5.1	1.3	109
163	15	20	5	5	20	35	90	2562	8.2	1.5	273
164	15	15	20	10	40	0	85	2563	5.1	1.4	122
165	20	20	5	35	15	5	92	2563	4.1	1.3	147
166	10	25	0	10	20	35	88	2563	8.3	1.6	295
167	15	25	0	40	15	5	95	2563	4.2	1.4	162
168	15	20	10	0	45	10	93	2564	6.2	1.5	163
169	15	10	25	10	20	20	80	2564	7.0	1.3	242
170	15	15	10	5	0	55	91	2565	10.1	1.4	353
171	10	20	5	10	0	55	89	2565	10.1	1.5	380
172	25	10	20	25	20	0	81	2565	4.0	1.1	107
173	20	15	15	30	20	0	85	2565	4.0	1.2	120
174	15	20	10	35	20	0	88	2565	4.0	1.3	134
175	15	15	15	0	25	30	90	2566	8.1	1.4	264
176	15	25	0	25	25	10	95	2567	5.2	1.5	177
177	20	20	5	20	25	10	95	2567	5.1	1.3	161
178	15	15	15	35	0	20	84	2567	5.9	1.3	258
179	15	25	0	60	0	0	91	2568	3.0	1.3	147
180	20	20	5	55	0	0	88	2568	2.9	1.2	132
181	15	10	20	0	5	50	86	2568	10.0	1.4	353
182	25	15	10	50	0	0	84	2568	2.9	1.0	119
183	15	20	5	25	5	30	95	2569	7.0	1.4	281
184	20	15	10	20	5	30	92	2569	7.0	1.2	260
185	15	20	10	20	30	5	92	2569	5.0	1.4	153

186	20	15	15	15	30	5	88	2569	5.0	1.3	139
187	15	15	20	15	35	0	84	2571	4.9	1.4	125
188	15	15	15	20	10	25	87	2571	6.9	1.3	267
189	15	25	0	10	35	15	90	2571	6.2	1.5	187
190	20	10	25	10	35	0	80	2572	4.9	1.3	112
191	20	10	20	15	10	25	83	2572	6.9	1.2	247
192	20	20	5	5	35	15	92	2572	6.1	1.4	171
193	15	25	0	45	10	5	94	2572	4.0	1.4	166
194	20	20	5	40	10	5	91	2572	3.9	1.2	151
195	15	20	10	5	40	10	94	2574	6.0	1.5	168
196	15	20	10	40	15	0	87	2574	3.8	1.3	137
197	15	20	5	10	15	35	92	2574	8.0	1.5	281
198	20	15	15	0	40	10	91	2574	6.0	1.4	153
199	20	15	15	35	15	0	84	2574	3.8	1.2	123
200	20	15	10	5	15	35	93	2575	8.0	1.3	260
201	15	15	20	0	45	5	87	2576	5.9	1.5	144
202	15	15	15	5	20	30	90	2576	7.9	1.4	271
203	15	25	0	30	20	10	95	2576	5.0	1.4	181
204	20	10	20	0	20	30	86	2577	7.9	1.3	251
205	20	20	5	25	20	10	95	2577	4.9	1.3	166
206	15	20	10	25	25	5	90	2578	4.8	1.4	157
207	15	10	25	0	25	25	82	2578	7.8	1.4	257
208	20	15	15	20	25	5	87	2579	4.8	1.3	142
209	15	20	5	30	0	30	94	2579	6.9	1.4	288
210	15	10	20	5	0	50	85	2579	9.8	1.3	363
211	10	25	0	0	25	40	83	2579	9.1	1.7	299
212	25	10	20	15	25	5	83	2580	4.8	1.1	128
213	20	15	10	25	0	30	91	2580	6.8	1.2	267
214	20	5	25	0	0	50	81	2580	9.7	1.2	338
215	15	25	0	50	5	5	93	2581	3.8	1.3	170
216	15	15	15	25	5	25	86	2581	6.7	1.3	273
217	20	20	5	45	5	5	90	2581	3.8	1.2	155
218	20	10	20	20	5	25	82	2582	6.7	1.2	253
219	15	25	0	15	30	15	92	2582	6.0	1.5	192
220	15	20	10	45	10	0	86	2582	3.7	1.3	141
221	25	15	10	40	5	5	86	2582	3.7	1.1	140
222	10	20	5	0	5	60	85	2583	10.9	1.6	376
223	20	15	15	40	10	0	83	2583	3.6	1.2	127
224	20	20	5	10	30	15	94	2583	5.9	1.4	176
225	15	20	10	10	35	10	93	2583	5.8	1.5	172
226	20	15	15	5	35	10	90	2584	5.8	1.3	157
227	15	15	20	5	40	5	86	2585	5.7	1.4	148
228	15	20	5	15	10	35	93	2585	7.9	1.4	288
229	15	25	0	35	15	10	95	2586	4.8	1.4	186
230	20	10	25	0	40	5	82	2586	5.7	1.3	134
231	20	15	10	10	10	35	93	2586	7.8	1.3	267
232	15	15	15	10	15	30	89	2586	7.7	1.4	278
233	15	20	10	30	20	5	89	2587	4.7	1.4	161
234	20	20	5	30	15	10	94	2587	4.8	1.3	170
235	15	10	25	5	20	25	81	2588	7.6	1.4	263
236	20	10	20	5	15	30	85	2588	7.7	1.3	257

237	20	15	15	25	20	5	86	2588	4.6	1.2	146
238	15	25	0	0	40	20	85	2588	7.0	1.6	199
239	15	25	0	55	0	5	92	2589	3.6	1.3	174
240	25	10	20	20	20	5	82	2589	4.6	1.1	132
241	15	15	15	30	0	25	85	2590	6.5	1.3	280
242	20	20	5	50	0	5	89	2590	3.6	1.2	159
243	10	25	0	5	20	40	85	2590	8.9	1.6	307
244	20	15	15	45	5	0	82	2591	3.4	1.1	130
245	20	10	20	25	0	25	81	2591	6.5	1.2	260
246	25	15	10	45	0	5	85	2592	3.5	1.1	144
247	15	25	0	20	25	15	93	2592	5.8	1.5	197
248	15	20	5	0	20	40	88	2592	8.9	1.5	285
249	15	20	10	15	30	10	93	2593	5.7	1.5	177
250	15	15	20	10	35	5	85	2593	5.5	1.4	152
251	20	20	5	15	25	15	95	2594	5.8	1.4	181
252	10	20	5	5	0	60	87	2594	10.8	1.6	387
253	20	15	15	10	30	10	89	2594	5.6	1.3	161
254	15	25	0	40	10	10	95	2595	4.6	1.4	191
255	20	10	25	5	35	5	81	2595	5.5	1.3	138
256	15	20	10	35	15	5	88	2595	4.5	1.4	165
257	15	20	5	20	5	35	94	2596	7.7	1.4	296
258	15	15	15	15	10	30	88	2596	7.5	1.4	285
259	20	20	5	35	10	10	92	2596	4.6	1.3	174
260	15	15	10	0	0	60	89	2597	10.7	1.4	359
261	15	10	25	10	15	25	80	2597	7.4	1.3	269
262	20	15	15	30	15	5	85	2597	4.4	1.2	150
263	20	25	0	0	55	0	86	2597	4.9	1.5	93
264	20	15	10	15	5	35	93	2598	7.6	1.3	274
265	20	10	20	10	10	30	84	2598	7.5	1.2	264
266	25	10	20	25	15	5	81	2599	4.4	1.1	136
267	20	15	15	50	0	0	81	2599	3.2	1.1	133
268	15	25	0	5	35	20	87	2599	6.8	1.6	205
269	15	20	10	0	40	15	93	2600	6.7	1.5	188
270	15	25	0	25	20	15	95	2602	5.6	1.5	203
271	20	20	5	0	35	20	90	2602	6.8	1.4	187
272	15	20	10	20	25	10	92	2602	5.5	1.4	181
273	15	25	0	45	5	10	94	2603	4.4	1.4	195
274	15	20	10	40	10	5	87	2603	4.3	1.3	169
275	15	20	5	5	15	40	89	2604	8.7	1.5	293
276	15	15	15	0	20	35	90	2604	8.5	1.4	286
277	20	20	5	20	20	15	95	2604	5.6	1.3	186
278	20	15	15	15	25	10	88	2604	5.4	1.3	166
279	20	10	25	10	30	5	80	2604	5.3	1.3	141
280	15	15	15	20	5	30	87	2606	7.3	1.3	292
281	20	15	15	35	10	5	84	2606	4.2	1.2	154
282	15	20	5	25	0	35	95	2606	7.5	1.4	304
283	20	20	5	40	5	10	91	2606	4.4	1.2	179
284	20	25	0	5	50	0	88	2608	4.7	1.5	96
285	20	10	20	15	5	30	83	2608	7.3	1.2	271
286	25	15	10	35	5	10	88	2608	4.3	1.1	163
287	15	10	20	0	0	55	85	2608	10.4	1.4	372

288	20	15	10	20	0	35	92	2608	7.4	1.3	282
289	15	15	20	0	40	10	87	2609	6.3	1.5	172
290	15	20	10	5	35	15	93	2609	6.5	1.5	193
291	15	25	0	10	30	20	89	2610	6.6	1.5	210
292	15	20	10	25	20	10	90	2610	5.3	1.4	186
293	15	25	0	30	15	15	95	2611	5.4	1.5	208
294	15	25	0	50	0	10	93	2612	4.2	1.4	200
295	20	15	15	0	35	15	91	2612	6.4	1.4	177
296	20	20	5	5	30	20	91	2613	6.6	1.4	193
297	20	15	15	20	20	10	87	2613	5.2	1.3	170
298	15	10	25	0	20	30	82	2613	8.2	1.4	282
299	20	20	5	25	15	15	95	2614	5.4	1.3	191
300	15	15	15	5	15	35	90	2614	8.3	1.4	293
301	20	15	15	40	5	5	83	2614	4.1	1.2	158
302	20	20	5	45	0	10	90	2614	4.2	1.2	184
303	15	15	15	25	0	30	86	2615	7.2	1.3	299
304	15	20	5	10	10	40	91	2615	8.5	1.5	301
305	25	10	20	15	20	10	83	2616	5.2	1.1	155
306	20	10	20	0	15	35	86	2617	8.3	1.3	272
307	25	15	10	40	0	10	86	2617	4.2	1.1	168
308	20	10	20	20	0	30	82	2618	7.1	1.2	278
309	15	15	20	5	35	10	86	2618	6.2	1.4	177
310	20	25	0	10	45	0	90	2618	4.5	1.5	100
311	20	15	10	5	10	40	92	2618	8.4	1.3	278
312	15	20	10	10	30	15	93	2619	6.3	1.5	199
313	15	20	10	30	15	10	89	2619	5.1	1.4	191
314	15	25	0	15	25	20	91	2620	6.4	1.5	216
315	15	25	0	35	10	15	95	2620	5.2	1.4	213
316	20	10	25	0	35	10	82	2621	6.1	1.3	161
317	10	25	0	0	20	45	82	2621	9.5	1.7	318
318	20	15	15	45	0	5	82	2622	3.9	1.2	162
319	20	15	15	25	15	10	86	2622	5.1	1.3	174
320	20	15	15	5	30	15	90	2622	6.2	1.4	182
321	15	10	25	5	15	30	81	2622	8.0	1.4	288
322	20	20	5	30	10	15	94	2623	5.2	1.3	196
323	20	20	5	10	25	20	93	2623	6.4	1.4	198
324	15	15	15	10	10	35	89	2623	8.2	1.4	301
325	15	20	5	15	5	40	92	2625	8.3	1.4	309
326	25	10	20	20	15	10	82	2625	5.0	1.1	159
327	15	15	20	10	30	10	85	2626	6.0	1.4	181
328	15	20	10	35	10	10	88	2627	4.9	1.4	195
329	10	20	5	0	0	65	84	2627	11.4	1.6	392
330	20	10	20	5	10	35	85	2627	8.1	1.3	279
331	15	20	10	15	25	15	92	2627	6.1	1.5	204
332	20	25	0	15	40	0	92	2628	4.3	1.5	103
333	15	25	0	40	5	15	95	2628	5.0	1.4	218
334	15	25	0	20	20	20	93	2629	6.2	1.5	222
335	20	15	10	10	5	40	93	2629	8.3	1.3	286
336	20	10	25	5	30	10	81	2629	5.9	1.3	166
337	15	25	0	0	35	25	84	2630	7.4	1.6	220
338	20	15	15	30	10	10	85	2630	4.9	1.2	179

339	15	10	25	10	10	30	80	2631	7.8	1.3	295
340	20	15	15	10	25	15	89	2631	6.1	1.3	187
341	15	25	5	0	55	0	91	2632	5.2	1.6	107
342	20	20	5	35	5	15	92	2632	5.0	1.3	201
343	15	15	15	15	5	35	88	2633	8.0	1.4	309
344	20	20	5	15	20	20	94	2634	6.2	1.4	204
345	25	10	20	25	10	10	81	2634	4.8	1.1	163
346	15	20	5	20	0	40	94	2635	8.1	1.4	317
347	15	20	10	20	20	15	91	2636	5.9	1.4	209
348	15	25	0	45	0	15	94	2637	4.9	1.4	224
349	15	20	5	0	15	45	87	2637	9.3	1.5	303
350	20	25	0	20	35	0	94	2637	4.1	1.4	106
351	20	10	20	10	5	35	84	2637	7.9	1.2	287
352	15	20	10	0	35	20	92	2638	7.1	1.5	213
353	15	25	0	25	15	20	94	2638	6.0	1.5	228
354	20	15	15	35	5	10	84	2638	4.7	1.2	183
355	20	25	0	0	50	5	85	2639	5.3	1.5	117
356	20	15	10	15	0	40	93	2640	8.1	1.3	294
357	20	15	15	15	20	15	88	2640	5.9	1.3	192
358	15	25	0	5	30	25	86	2640	7.2	1.6	226
359	15	25	5	5	50	0	93	2641	5.0	1.6	110
360	20	20	5	40	0	15	91	2641	4.8	1.2	206
361	15	15	15	20	0	35	87	2642	7.8	1.4	316
362	20	20	5	20	15	20	95	2643	6.0	1.3	210
363	15	15	20	0	35	15	87	2644	6.8	1.5	199
364	15	15	15	0	15	40	89	2644	9.0	1.5	307
365	15	20	10	25	15	15	90	2644	5.7	1.4	214
366	25	10	20	10	20	15	84	2645	5.8	1.2	176
367	20	20	10	0	50	0	94	2646	5.0	1.5	98
368	25	15	10	35	0	15	88	2646	4.8	1.1	189
369	20	25	0	25	30	0	94	2646	4.0	1.4	109
370	20	20	5	0	30	25	89	2646	7.2	1.4	208
371	20	15	15	40	0	10	82	2646	4.5	1.2	188
372	20	10	20	15	0	35	83	2647	7.7	1.2	294
373	15	20	10	5	30	20	93	2647	6.9	1.5	218
374	15	25	0	30	10	20	95	2647	5.9	1.5	233
375	15	20	5	5	10	45	89	2647	9.1	1.5	311
376	20	15	15	20	15	15	87	2649	5.7	1.3	197
377	20	25	0	5	45	5	88	2649	5.1	1.5	121
378	15	25	5	10	45	0	94	2649	4.9	1.6	114
379	15	10	25	0	15	35	82	2650	8.6	1.4	305
380	15	25	0	10	25	25	89	2650	7.0	1.6	233
381	15	15	20	5	30	15	86	2652	6.6	1.5	205
382	15	20	10	30	10	15	89	2652	5.5	1.4	219
383	20	15	15	0	30	20	91	2652	6.9	1.4	201
384	20	20	5	25	10	20	95	2652	5.8	1.3	215
385	15	15	15	5	10	40	89	2653	8.8	1.4	315
386	25	10	20	15	15	15	83	2654	5.6	1.2	180
387	20	25	0	30	25	0	95	2655	3.8	1.4	112
388	20	20	10	5	45	0	94	2655	4.8	1.4	101
389	15	25	0	35	5	20	95	2655	5.7	1.4	239

390	15	20	10	10	25	20	93	2656	6.7	1.5	224
391	20	20	5	5	25	25	91	2657	7.0	1.4	214
392	15	25	5	15	40	0	95	2657	4.7	1.6	117
393	20	15	15	25	10	15	86	2657	5.5	1.3	202
394	20	10	25	0	30	15	82	2657	6.6	1.3	188
395	15	20	5	10	5	45	90	2658	8.9	1.5	320
396	15	10	25	5	10	35	81	2658	8.5	1.4	313
397	20	25	0	10	40	5	90	2659	5.0	1.5	124
398	15	25	0	15	20	25	90	2660	6.9	1.5	239
399	20	10	20	0	10	40	86	2660	8.7	1.3	292
400	20	20	5	30	5	20	94	2661	5.6	1.3	221
401	20	15	15	5	25	20	90	2662	6.7	1.4	206
402	15	15	15	10	5	40	89	2662	8.6	1.4	323
403	20	25	0	35	20	0	95	2663	3.6	1.4	115
404	20	20	10	10	40	0	93	2663	4.6	1.4	104
405	25	10	20	20	10	15	82	2663	5.5	1.1	185
406	15	25	0	40	0	20	95	2664	5.5	1.4	245
407	15	20	10	15	20	20	92	2664	6.5	1.5	230
408	20	15	10	5	5	45	91	2665	8.9	1.3	296
409	15	25	5	20	35	0	95	2665	4.5	1.5	120
410	20	15	15	30	5	15	85	2665	5.3	1.2	207
411	20	10	25	5	25	15	81	2666	6.4	1.3	193
412	20	20	5	10	20	25	92	2666	6.8	1.4	220
413	15	20	5	15	0	45	92	2667	8.7	1.5	329
414	20	25	0	15	35	5	92	2668	4.8	1.5	128
415	15	25	0	20	15	25	92	2668	6.7	1.5	245
416	25	20	5	30	20	0	93	2669	3.5	1.2	102
417	20	10	20	5	5	40	85	2669	8.6	1.3	300
418	25	15	15	5	40	0	90	2670	4.6	1.3	92
419	20	20	5	35	0	20	93	2670	5.4	1.3	227
420	15	25	5	0	50	5	91	2670	5.7	1.6	134
421	20	15	15	10	20	20	89	2670	6.5	1.3	212
422	20	25	0	40	15	0	94	2671	3.4	1.3	118
423	15	15	15	15	0	40	88	2671	8.4	1.4	331
424	20	20	10	15	35	0	92	2671	4.4	1.4	107
425	25	10	20	25	5	15	81	2672	5.3	1.1	190
426	15	20	10	20	15	20	91	2672	6.3	1.5	235
427	15	25	5	25	30	0	94	2673	4.3	1.5	123
428	20	15	15	35	0	15	83	2673	5.1	1.2	212
429	15	20	15	0	50	0	91	2673	5.3	1.6	112
430	15	25	0	0	30	30	84	2675	7.9	1.6	240
431	20	15	10	10	0	45	92	2675	8.7	1.3	305
432	20	20	5	15	15	25	94	2676	6.6	1.4	226
433	20	25	0	20	30	5	93	2676	4.6	1.4	132
434	15	25	0	25	10	25	94	2677	6.5	1.5	252
435	25	20	5	35	15	0	92	2677	3.4	1.2	105
436	15	20	10	0	30	25	91	2678	7.5	1.5	236
437	25	15	15	10	35	0	89	2678	4.4	1.3	95
438	15	25	5	5	45	5	92	2678	5.5	1.6	137
439	20	25	0	45	10	0	94	2678	3.2	1.3	122
440	20	10	20	10	0	40	84	2679	8.4	1.3	308

441	20	15	15	15	15	20	88	2679	6.3	1.3	217
442	20	20	10	20	30	0	91	2679	4.3	1.4	110
443	15	20	10	25	10	20	90	2680	6.2	1.4	241
444	15	15	20	0	30	20	86	2681	7.2	1.5	226
445	20	25	0	0	45	10	85	2683	5.8	1.5	140
446	15	25	0	5	25	30	86	2684	7.7	1.6	247
447	15	20	5	0	10	50	86	2684	9.7	1.5	320
448	20	25	0	25	25	5	94	2685	4.4	1.4	135
449	20	20	5	20	10	25	95	2685	6.4	1.4	233
450	15	25	0	30	5	25	95	2685	6.3	1.5	258
451	25	20	5	40	10	0	91	2685	3.2	1.2	109
452	20	25	0	50	5	0	93	2686	3.0	1.3	125
453	20	20	10	0	45	5	93	2686	5.4	1.5	124
454	15	25	5	10	40	5	93	2686	5.3	1.6	141
455	25	15	15	15	30	0	88	2686	4.2	1.2	98
456	15	20	10	5	25	25	92	2686	7.3	1.5	242
457	20	20	10	25	25	0	90	2687	4.1	1.4	113
458	25	10	20	10	15	20	84	2687	6.3	1.2	200
459	15	15	15	0	10	45	88	2687	9.4	1.5	327
460	20	15	15	20	10	20	87	2687	6.1	1.3	223
461	20	15	20	0	45	0	87	2688	5.1	1.4	102
462	15	10	25	0	10	40	82	2689	9.1	1.4	329
463	20	25	0	55	0	0	92	2693	2.8	1.3	128
464	20	25	0	30	20	5	95	2693	4.2	1.4	139
465	20	25	0	5	40	10	87	2693	5.6	1.5	144
466	25	20	5	45	5	0	90	2693	3.0	1.2	112
467	15	25	0	35	0	25	95	2693	6.1	1.4	265
468	15	25	0	10	20	30	88	2693	7.5	1.6	254
469	20	20	5	25	5	25	95	2693	6.3	1.3	239
470	20	20	5	0	25	30	88	2694	7.6	1.5	228
471	15	25	5	15	35	5	94	2694	5.1	1.6	145
472	20	20	10	30	20	0	89	2694	3.9	1.3	116
473	20	20	10	5	40	5	94	2694	5.3	1.5	127
474	15	20	5	5	5	50	88	2694	9.5	1.5	329
475	25	15	15	20	25	0	87	2694	4.0	1.2	101
476	15	20	10	10	20	25	92	2694	7.2	1.5	248
477	20	15	15	25	5	20	86	2695	5.9	1.3	228
478	20	15	15	0	25	25	90	2695	7.3	1.4	223
479	25	10	20	15	10	20	83	2695	6.1	1.2	205
480	20	15	20	5	40	0	86	2695	4.9	1.4	105
481	15	15	15	5	5	45	89	2695	9.2	1.4	336
482	20	10	25	0	25	20	82	2696	7.0	1.3	213
483	25	20	5	50	0	0	88	2700	2.8	1.1	115
484	20	25	0	35	15	5	95	2700	4.0	1.4	143
485	20	20	10	35	15	0	88	2701	3.7	1.3	120
486	15	25	5	20	30	5	94	2701	4.9	1.5	149
487	20	25	0	10	35	10	89	2701	5.4	1.5	148
488	20	20	5	30	0	25	94	2702	6.1	1.3	245
489	25	15	15	25	20	0	85	2702	3.8	1.2	104
490	15	25	0	15	15	30	90	2702	7.3	1.5	261
491	20	20	10	10	35	5	93	2702	5.1	1.4	131

492	20	15	15	30	0	20	85	2702	5.7	1.2	234
493	15	20	10	15	15	25	92	2702	7.0	1.5	255
494	20	15	20	10	35	0	84	2702	4.7	1.4	108
495	20	20	5	5	20	30	90	2703	7.4	1.4	234
496	25	10	20	20	5	20	82	2703	5.9	1.1	211
497	15	20	5	10	0	50	89	2703	9.3	1.5	338
498	25	10	25	0	40	0	82	2703	4.9	1.3	93
499	20	15	15	5	20	25	90	2703	7.1	1.4	229
500	20	10	25	5	20	20	81	2704	6.8	1.3	219
501	15	15	15	10	0	45	88	2704	9.0	1.4	344
502	20	15	10	0	5	50	89	2705	9.5	1.4	304
503	20	10	20	0	5	45	86	2705	9.2	1.3	312
504	20	20	10	40	10	0	87	2708	3.5	1.3	123
505	20	25	0	40	10	5	95	2708	3.8	1.4	147
506	25	15	15	30	15	0	84	2709	3.7	1.2	107
507	25	20	5	30	15	5	93	2709	4.0	1.2	129
508	20	15	20	15	30	0	83	2709	4.6	1.3	111
509	20	20	10	15	30	5	92	2710	4.9	1.4	135
510	15	20	10	20	10	25	91	2710	6.8	1.5	261
511	20	25	0	15	30	10	91	2710	5.2	1.5	153
512	15	25	0	20	10	30	91	2710	7.1	1.5	268
513	15	25	5	0	45	10	90	2710	6.1	1.6	159
514	25	10	20	25	0	20	81	2711	5.7	1.1	216
515	25	10	25	5	35	0	81	2711	4.7	1.2	96
516	25	15	15	5	35	5	90	2711	5.0	1.3	118
517	20	15	15	10	15	25	89	2712	6.9	1.3	236
518	20	20	5	10	15	30	92	2712	7.3	1.4	241
519	20	20	10	45	5	0	86	2714	3.3	1.3	126
520	20	10	20	5	0	45	85	2714	9.0	1.3	320
521	20	25	0	45	5	5	94	2715	3.6	1.3	151
522	20	15	10	5	0	50	91	2715	9.3	1.3	313
523	20	15	20	20	25	0	82	2716	4.4	1.3	114
524	25	15	15	35	10	0	83	2716	3.5	1.2	110
525	20	20	10	20	25	5	91	2717	4.7	1.4	138
526	25	20	5	35	10	5	92	2717	3.8	1.2	133
527	15	25	5	5	40	10	92	2718	5.9	1.6	164
528	20	25	0	20	25	10	93	2718	5.0	1.4	157
529	15	25	0	25	5	30	93	2718	6.9	1.5	275
530	25	15	15	10	30	5	89	2719	4.8	1.3	121
531	20	15	15	15	10	25	88	2719	6.7	1.3	242
532	20	20	10	50	0	0	85	2720	3.1	1.2	129
533	15	20	10	0	25	30	91	2720	8.0	1.6	258
534	20	20	5	15	10	30	93	2721	7.1	1.4	248
535	20	25	0	50	0	5	93	2721	3.4	1.3	155
536	15	25	0	0	25	35	83	2722	8.3	1.6	260
537	20	15	20	25	20	0	81	2722	4.2	1.3	117
538	25	15	15	40	5	0	82	2723	3.3	1.1	113
539	20	20	10	25	20	5	90	2724	4.5	1.4	142
540	25	20	5	40	5	5	91	2724	3.6	1.2	136
541	15	25	5	10	35	10	93	2725	5.7	1.6	168
542	15	25	0	30	0	30	94	2725	6.7	1.5	282

543	20	25	0	25	20	10	94	2725	4.8	1.4	161
544	20	15	20	0	40	5	86	2726	5.6	1.4	130
545	20	15	15	20	5	25	87	2727	6.6	1.3	248
546	25	15	15	15	25	5	88	2727	4.7	1.3	125
547	15	20	10	5	20	30	91	2728	7.8	1.5	265
548	20	20	10	0	40	10	93	2728	5.9	1.5	149
549	20	15	20	30	15	0	80	2728	4.0	1.3	121
550	20	20	5	20	5	30	94	2729	6.9	1.4	255
551	25	15	15	45	0	0	81	2729	3.1	1.1	116
552	25	10	20	10	10	25	84	2730	6.7	1.2	223
553	20	20	10	30	15	5	89	2730	4.3	1.3	146
554	15	25	0	5	20	35	85	2731	8.1	1.6	267
555	20	25	0	0	40	15	84	2731	6.2	1.5	162
556	25	20	5	45	0	5	90	2731	3.4	1.2	140
557	15	25	5	15	30	10	94	2732	5.5	1.6	172
558	15	15	15	0	5	50	88	2732	9.8	1.5	346
559	20	25	0	30	15	10	95	2733	4.6	1.4	166
560	20	15	20	5	35	5	85	2733	5.4	1.4	134
561	20	15	15	25	0	25	86	2734	6.4	1.3	254
562	25	15	15	20	20	5	86	2734	4.5	1.2	128
563	15	20	5	0	5	55	85	2735	10.2	1.5	336
564	15	20	10	10	15	30	92	2736	7.6	1.5	272
565	20	20	10	5	35	10	93	2736	5.7	1.5	153
566	20	20	5	25	0	30	94	2737	6.7	1.3	261
567	20	10	25	0	20	25	82	2737	7.4	1.3	238
568	20	20	10	35	10	5	88	2737	4.1	1.3	150
569	25	10	20	15	5	25	83	2738	6.5	1.2	229
570	15	25	0	10	15	35	87	2739	7.9	1.6	275
571	20	25	0	5	35	15	87	2739	6.0	1.5	167
572	20	15	20	10	30	5	84	2740	5.2	1.4	137
573	20	25	0	35	10	10	95	2740	4.4	1.4	170
574	15	15	15	5	0	50	88	2740	9.7	1.5	355
575	20	15	15	0	20	30	90	2740	7.7	1.4	245
576	25	15	15	25	15	5	85	2741	4.3	1.2	132
577	15	20	10	15	10	30	92	2743	7.4	1.5	279
578	20	20	10	10	30	10	93	2743	5.5	1.4	157
579	20	20	10	40	5	5	87	2743	3.9	1.3	154
580	20	10	25	5	15	25	81	2744	7.2	1.3	244
581	15	20	5	5	0	55	87	2744	10.0	1.5	346
582	25	10	25	0	35	5	82	2744	5.3	1.3	120
583	20	20	5	0	20	35	87	2744	8.1	1.5	246
584	25	20	5	25	15	10	94	2745	4.6	1.3	151
585	25	10	20	20	0	25	82	2745	6.3	1.1	235
586	20	15	20	15	25	5	83	2746	5.0	1.4	141
587	20	25	0	40	5	10	95	2747	4.3	1.4	175
588	15	25	0	15	10	35	89	2747	7.7	1.6	282
589	20	25	0	10	30	15	89	2747	5.8	1.5	171
590	25	15	15	30	10	5	84	2748	4.1	1.2	135
591	20	15	15	5	15	30	90	2748	7.6	1.4	252
592	25	15	15	0	35	10	91	2748	5.7	1.3	139
593	20	20	10	45	0	5	86	2749	3.8	1.3	157

594	20	20	10	15	25	10	92	2750	5.3	1.4	161
595	25	10	25	5	30	5	81	2751	5.1	1.2	124
596	25	20	5	30	10	10	93	2752	4.4	1.2	155
597	20	15	20	20	20	5	82	2752	4.8	1.3	145
598	15	25	5	0	40	15	89	2752	6.5	1.7	184
599	20	20	5	5	15	35	89	2753	7.9	1.4	254
600	20	25	0	45	0	10	94	2753	4.1	1.3	179
601	20	10	20	0	0	50	85	2754	9.6	1.3	330
602	25	15	15	35	5	5	83	2754	3.9	1.2	139
603	15	25	0	20	5	35	91	2754	7.5	1.5	290
604	20	25	0	15	25	15	91	2755	5.6	1.5	176
605	20	15	15	10	10	30	89	2755	7.4	1.4	258
606	25	15	15	5	30	10	90	2756	5.5	1.3	143
607	20	20	10	20	20	10	91	2757	5.1	1.4	166
608	20	15	20	25	15	5	81	2758	4.6	1.3	148
609	25	20	5	35	5	10	92	2759	4.2	1.2	159
610	15	25	5	5	35	15	91	2759	6.4	1.6	189
611	20	15	10	0	0	55	89	2760	9.9	1.4	320
612	25	15	15	40	0	5	82	2760	3.7	1.1	143
613	20	20	5	10	10	35	91	2761	7.7	1.4	261
614	15	25	0	25	0	35	92	2761	7.4	1.5	297
615	20	25	0	20	20	15	92	2762	5.4	1.5	181
616	20	15	15	15	5	30	88	2762	7.2	1.3	265
617	20	20	10	25	15	10	90	2763	4.9	1.4	170
618	25	15	15	10	25	10	89	2763	5.3	1.3	147
619	20	15	20	30	10	5	80	2764	4.4	1.3	152
620	25	20	5	40	0	10	91	2765	4.0	1.2	163
621	15	20	10	0	20	35	90	2765	8.4	1.6	280
622	15	25	5	10	30	15	92	2766	6.2	1.6	194
623	20	15	20	0	35	10	86	2767	6.0	1.4	157
624	20	20	5	15	5	35	92	2769	7.5	1.4	268
625	20	25	0	25	15	15	94	2769	5.3	1.4	186
626	20	15	15	20	0	30	87	2769	7.0	1.3	272
627	20	20	10	30	10	10	89	2769	4.8	1.3	174
628	25	15	15	15	20	10	88	2770	5.1	1.3	151
629	25	10	20	5	10	30	85	2770	7.3	1.2	239
630	15	20	10	5	15	35	91	2772	8.2	1.5	287
631	15	25	0	0	20	40	82	2773	8.7	1.6	278
632	20	15	20	5	30	10	85	2773	5.8	1.4	161
633	20	20	10	0	35	15	92	2773	6.3	1.5	173
634	20	20	10	35	5	10	88	2775	4.6	1.3	179
635	20	25	0	30	10	15	95	2775	5.1	1.4	191
636	20	20	5	20	0	35	94	2776	7.3	1.4	276
637	25	15	15	20	15	10	86	2776	4.9	1.2	155
638	25	10	20	10	5	30	84	2777	7.1	1.2	245
639	20	15	20	10	25	10	84	2779	5.6	1.4	165
640	15	20	10	10	10	35	91	2779	8.0	1.5	295
641	20	10	25	0	15	30	81	2780	7.9	1.3	262
642	20	20	10	5	30	15	93	2780	6.1	1.5	177
643	15	15	15	0	0	55	87	2780	10.3	1.5	364
644	15	25	0	5	15	40	84	2780	8.5	1.6	286

645	20	20	10	40	0	10	87	2780	4.4	1.3	183
646	20	25	0	0	35	20	84	2781	6.6	1.6	183
647	20	25	0	35	5	15	95	2781	4.9	1.4	196
648	25	15	15	25	10	10	85	2782	4.7	1.2	159
649	15	30	0	0	55	0	87	2783	5.1	1.7	104
650	25	10	20	15	0	30	83	2784	7.0	1.2	252
651	20	15	20	15	20	10	83	2785	5.4	1.4	170
652	20	10	25	5	10	30	80	2786	7.7	1.3	269
653	20	20	10	10	25	15	93	2786	5.9	1.4	182
654	25	10	25	0	30	10	81	2787	5.8	1.3	146
655	15	25	0	10	10	40	86	2787	8.4	1.6	294
656	20	25	0	40	0	15	95	2787	4.7	1.4	201
657	25	15	15	30	5	10	84	2788	4.5	1.2	163
658	20	15	15	0	15	35	89	2788	8.2	1.4	266
659	20	25	0	5	30	20	86	2789	6.4	1.5	188
660	15	30	0	5	50	0	89	2789	4.9	1.7	107
661	15	20	5	0	0	60	84	2790	10.6	1.5	351
662	20	15	20	20	15	10	82	2790	5.2	1.3	174
663	25	20	5	25	10	15	94	2791	5.0	1.3	175
664	20	20	10	15	20	15	92	2793	5.8	1.4	187
665	25	10	25	5	25	10	80	2793	5.6	1.3	151
666	25	15	15	35	0	10	83	2794	4.3	1.2	167
667	15	25	0	15	5	40	88	2794	8.2	1.6	303
668	20	15	15	5	10	35	89	2795	8.0	1.4	273
669	20	15	20	25	10	10	81	2795	5.1	1.3	178
670	20	25	0	10	25	20	88	2796	6.3	1.5	194
671	25	15	15	0	30	15	91	2796	6.1	1.3	162
672	25	20	5	30	5	15	93	2797	4.9	1.3	180
673	15	25	5	0	35	20	89	2797	7.0	1.7	208
674	20	20	10	20	15	15	91	2798	5.6	1.4	192
675	20	20	5	0	15	40	87	2799	8.5	1.5	264
676	20	15	20	30	5	10	80	2801	4.9	1.3	183
677	15	25	0	20	0	40	90	2801	8.0	1.5	311
678	20	15	15	10	5	35	88	2801	7.8	1.4	281
679	20	25	0	15	20	20	90	2802	6.1	1.5	199
680	25	15	15	5	25	15	90	2803	5.9	1.3	167
681	25	20	5	35	0	15	92	2803	4.7	1.2	185
682	15	25	5	5	30	20	90	2803	6.8	1.6	213
683	20	20	10	25	10	15	90	2804	5.4	1.4	197
684	20	25	5	0	50	0	91	2805	4.9	1.6	95
685	20	20	5	5	10	40	88	2806	8.3	1.5	272
686	20	15	15	15	0	35	88	2808	7.6	1.3	288
687	20	25	0	20	15	20	92	2808	5.9	1.5	205
688	25	15	15	10	20	15	89	2809	5.7	1.3	171
689	20	20	10	30	5	15	89	2809	5.2	1.4	202
690	20	15	20	0	30	15	86	2810	6.4	1.4	183
691	25	25	0	15	35	0	91	2810	4.0	1.4	90
692	20	25	5	5	45	0	92	2810	4.7	1.6	98
693	20	20	5	10	5	40	90	2813	8.1	1.4	280
694	15	20	10	0	15	40	89	2813	8.8	1.6	300
695	20	25	0	25	10	20	93	2814	5.7	1.4	210

696	20	20	10	35	0	15	88	2815	5.0	1.3	207
697	25	15	15	15	15	15	88	2815	5.5	1.3	176
698	20	15	20	5	25	15	85	2815	6.2	1.4	188
699	20	25	5	10	40	0	93	2816	4.5	1.5	101
700	25	25	0	20	30	0	93	2816	3.8	1.4	93
701	15	20	10	5	10	40	90	2819	8.7	1.6	308
702	20	20	5	15	0	40	92	2820	7.9	1.4	288
703	20	25	0	30	5	20	95	2820	5.5	1.4	216
704	25	10	20	5	5	35	85	2820	7.8	1.2	260
705	20	15	20	10	20	15	84	2820	6.1	1.4	193
706	25	15	15	20	10	15	86	2821	5.3	1.2	181
707	20	20	10	0	30	20	91	2821	6.8	1.5	196
708	20	25	5	15	35	0	94	2821	4.3	1.5	104
709	25	25	0	25	25	0	94	2822	3.6	1.4	96
710	20	15	20	15	15	15	83	2825	5.9	1.4	198
711	20	25	0	35	0	20	95	2825	5.3	1.4	221
712	20	10	25	0	10	35	81	2825	8.3	1.4	285
713	25	15	15	25	5	15	85	2826	5.2	1.2	185
714	25	10	20	10	0	35	84	2826	7.6	1.2	267
715	20	25	5	20	30	0	94	2826	4.1	1.5	107
716	15	25	0	0	15	45	81	2827	9.2	1.6	296
717	20	20	10	5	25	20	92	2827	6.6	1.5	201
718	15	30	0	0	50	5	87	2827	5.5	1.8	130
719	25	25	0	30	20	0	94	2827	3.4	1.3	99
720	25	20	10	0	45	0	93	2829	4.7	1.4	86
721	20	15	20	20	10	15	82	2830	5.7	1.3	203
722	20	10	25	5	5	35	80	2831	8.1	1.3	292
723	25	15	15	30	0	15	84	2831	5.0	1.2	190
724	20	25	5	25	25	0	93	2831	3.9	1.5	110
725	20	20	10	10	20	20	92	2832	6.4	1.5	207
726	25	25	0	35	15	0	94	2833	3.2	1.3	102
727	25	10	25	0	25	15	81	2833	6.2	1.3	172
728	15	25	0	5	10	45	84	2833	9.0	1.6	304
729	25	20	5	20	10	20	94	2834	5.7	1.3	193
730	25	20	10	5	40	0	94	2834	4.5	1.4	89
731	20	15	20	25	5	15	81	2835	5.5	1.3	208
732	20	25	0	0	30	25	83	2835	7.1	1.6	203
733	20	25	5	30	20	0	93	2836	3.8	1.5	113
734	25	25	0	40	10	0	94	2838	3.0	1.3	105
735	20	20	10	15	15	20	92	2838	6.2	1.4	212
736	20	20	15	0	45	0	90	2838	5.0	1.5	99
737	25	10	25	5	20	15	80	2838	6.0	1.3	177
738	15	25	0	10	5	45	86	2839	8.8	1.6	313
739	25	20	5	25	5	20	94	2839	5.5	1.3	198
740	20	15	15	0	10	40	88	2839	8.6	1.4	286
741	25	20	10	10	35	0	93	2840	4.3	1.4	91
742	20	25	5	35	15	0	92	2840	3.6	1.4	116
743	20	25	0	5	25	25	86	2841	6.9	1.5	209
744	25	25	0	45	5	0	93	2842	2.9	1.3	108
745	20	20	10	20	10	20	91	2843	6.0	1.4	218
746	20	20	15	5	40	0	89	2843	4.8	1.5	102

747	15	25	5	0	30	25	88	2845	7.4	1.7	230
748	25	20	10	15	30	0	92	2845	4.1	1.4	94
749	15	25	0	15	0	45	88	2845	8.6	1.6	322
750	25	20	5	30	0	20	93	2845	5.3	1.3	204
751	20	25	5	40	10	0	90	2845	3.4	1.4	119
752	20	15	15	5	5	40	89	2845	8.4	1.4	294
753	25	25	0	50	0	0	92	2847	2.7	1.3	111
754	20	20	15	10	35	0	88	2847	4.6	1.5	105
755	20	25	0	10	20	25	88	2847	6.7	1.5	215
756	20	20	10	25	5	20	90	2847	5.8	1.4	223
757	25	15	15	0	25	20	90	2848	6.5	1.3	184
758	20	25	5	45	5	0	89	2849	3.2	1.4	122
759	25	20	10	20	25	0	91	2849	3.9	1.3	97
760	20	15	15	10	0	40	88	2850	8.2	1.4	302
761	20	20	15	15	30	0	87	2851	4.4	1.5	108
762	20	20	10	30	0	20	89	2852	5.6	1.4	229
763	20	25	5	0	45	5	90	2852	5.3	1.6	120
764	20	25	0	15	15	25	90	2853	6.5	1.5	221
765	25	15	15	5	20	20	90	2853	6.3	1.3	190
766	25	20	10	25	20	0	90	2854	3.7	1.3	100
767	20	15	20	0	25	20	86	2855	6.9	1.4	208
768	20	20	15	20	25	0	86	2856	4.3	1.4	111
769	20	25	5	5	40	5	92	2857	5.1	1.6	124
770	20	20	5	0	10	45	86	2857	8.9	1.5	281
771	20	25	0	20	10	25	91	2858	6.3	1.5	227
772	25	15	15	10	15	20	89	2858	6.2	1.3	195
773	25	20	10	30	15	0	88	2858	3.5	1.3	103
774	20	15	20	5	20	20	85	2859	6.7	1.4	214
775	25	25	0	15	30	5	91	2860	4.4	1.4	115
776	20	25	5	10	35	5	93	2861	4.9	1.5	127
777	25	15	20	0	40	0	86	2862	4.8	1.4	90
778	25	20	10	35	10	0	87	2863	3.3	1.3	106
779	20	25	0	25	5	25	93	2863	6.1	1.5	233
780	25	15	15	15	10	20	87	2863	6.0	1.3	200
781	20	20	5	5	5	45	88	2863	8.8	1.5	290
782	20	15	20	10	15	20	84	2864	6.5	1.4	219
783	15	20	10	0	10	45	88	2864	9.3	1.6	320
784	25	25	0	20	25	5	93	2865	4.2	1.4	118
785	20	25	5	15	30	5	94	2866	4.8	1.5	131
786	25	15	20	5	35	0	85	2866	4.6	1.4	92
787	30	20	5	45	0	0	89	2866	2.6	1.1	99
788	25	20	10	40	5	0	86	2867	3.2	1.2	109
789	20	25	0	30	0	25	94	2867	5.9	1.4	240
790	25	15	15	20	5	20	86	2868	5.8	1.3	206
791	20	15	20	15	10	20	83	2868	6.3	1.4	225
792	20	20	5	10	0	45	89	2869	8.6	1.4	298
793	25	10	20	0	5	40	86	2869	8.4	1.3	272
794	25	25	0	25	20	5	94	2870	4.0	1.4	122
795	20	25	5	20	25	5	94	2870	4.6	1.5	134
796	25	15	20	10	30	0	84	2870	4.4	1.3	95
797	25	20	10	45	0	0	85	2871	3.0	1.2	112

798	20	20	10	0	25	25	91	2872	7.2	1.5	218
799	20	15	20	20	5	20	82	2872	6.1	1.4	230
800	25	15	15	25	0	20	85	2872	5.6	1.2	211
801	20	10	25	0	5	40	81	2874	8.7	1.4	307
802	25	10	20	5	0	40	85	2874	8.2	1.2	280
803	20	25	5	25	20	5	93	2874	4.4	1.5	138
804	25	15	20	15	25	0	83	2874	4.2	1.3	98
805	25	25	0	30	15	5	94	2875	3.9	1.4	125
806	20	20	10	5	20	25	91	2876	7.0	1.5	224
807	20	25	5	30	15	5	92	2878	4.2	1.5	142
808	25	15	20	20	20	0	82	2878	4.0	1.3	101
809	25	25	0	35	10	5	94	2879	3.7	1.3	129
810	30	15	15	25	15	0	85	2879	3.5	1.2	91
811	25	20	10	0	40	5	93	2879	5.1	1.4	111
812	20	20	10	10	15	25	92	2881	6.8	1.5	230
813	25	10	25	0	20	20	81	2881	6.6	1.3	197
814	20	25	5	35	10	5	91	2882	4.0	1.4	146
815	25	15	20	25	15	0	81	2882	3.8	1.3	104
816	20	20	15	0	40	5	90	2883	5.4	1.5	126
817	25	25	0	40	5	5	94	2883	3.5	1.3	132
818	30	15	15	30	10	0	84	2883	3.3	1.1	94
819	25	20	10	5	35	5	93	2884	4.9	1.4	114
820	15	25	0	0	10	50	80	2884	9.6	1.6	312
821	20	20	10	15	10	25	91	2885	6.6	1.4	236
822	25	10	25	5	15	20	80	2885	6.5	1.3	202
823	20	25	5	40	5	5	90	2885	3.8	1.4	149
824	20	20	15	5	35	5	89	2886	5.3	1.5	130
825	25	20	5	20	5	25	94	2887	6.1	1.3	215
826	25	25	0	45	0	5	93	2887	3.3	1.3	136
827	30	15	15	35	5	0	83	2887	3.1	1.1	96
828	25	20	10	10	30	5	93	2888	4.7	1.4	117
829	30	10	25	0	35	0	81	2888	4.6	1.2	81
830	20	20	10	20	5	25	91	2889	6.4	1.4	242
831	15	25	0	5	5	50	83	2889	9.4	1.6	322
832	20	20	15	10	30	5	88	2890	5.1	1.5	133
833	30	15	15	40	0	0	81	2891	2.9	1.1	99
834	25	20	5	25	0	25	94	2891	5.9	1.3	221
835	25	20	10	15	25	5	92	2892	4.5	1.4	121
836	30	10	25	5	30	0	80	2892	4.4	1.2	83
837	20	20	10	25	0	25	90	2893	6.3	1.4	249
838	20	25	0	0	25	30	83	2893	7.5	1.6	222
839	20	20	15	15	25	5	87	2894	4.9	1.5	137
840	15	25	0	10	0	50	85	2894	9.2	1.6	331
841	20	15	15	0	5	45	88	2894	9.1	1.4	305
842	25	20	10	20	20	5	91	2896	4.3	1.3	124
843	20	25	0	5	20	30	85	2898	7.3	1.6	229
844	20	15	15	5	0	45	88	2898	8.9	1.4	314
845	25	20	10	25	15	5	89	2900	4.2	1.3	128
846	20	25	5	0	40	10	89	2902	5.8	1.6	145
847	25	15	15	0	20	25	90	2902	7.0	1.4	206
848	20	25	0	10	15	30	87	2902	7.1	1.5	235

849	20	15	20	0	20	25	86	2902	7.3	1.5	233
850	25	20	10	30	10	5	88	2903	4.0	1.3	131
851	20	25	5	5	35	10	91	2906	5.6	1.6	149
852	20	15	20	5	15	25	85	2906	7.1	1.4	239
853	25	15	15	5	15	25	89	2906	6.8	1.3	212
854	20	25	0	15	10	30	89	2906	6.9	1.5	242
855	25	20	10	35	5	5	87	2907	3.8	1.3	135
856	25	15	20	0	35	5	86	2909	5.2	1.4	116
857	20	15	20	10	10	25	84	2909	6.9	1.4	245
858	20	25	5	10	30	10	92	2910	5.4	1.6	153
859	25	20	10	40	0	5	86	2910	3.6	1.3	139
860	25	15	15	10	10	25	88	2910	6.6	1.3	218
861	25	25	0	10	30	10	88	2910	5.0	1.5	134
862	20	25	0	20	5	30	91	2910	6.8	1.5	249
863	20	15	20	15	5	25	83	2913	6.7	1.4	251
864	25	15	20	5	30	5	85	2913	5.0	1.4	120
865	20	25	5	15	25	10	93	2913	5.2	1.5	157
866	25	15	15	15	5	25	87	2914	6.4	1.3	224
867	20	25	0	25	0	30	92	2914	6.6	1.5	256
868	25	25	0	15	25	10	90	2914	4.9	1.4	138
869	25	15	20	10	25	5	84	2916	4.8	1.3	123
870	20	25	5	20	20	10	94	2916	5.0	1.5	161
871	25	15	15	20	0	25	86	2917	6.2	1.3	230
872	25	25	0	20	20	10	92	2918	4.7	1.4	142
873	25	15	20	15	20	5	83	2919	4.7	1.3	127
874	20	25	5	25	15	10	93	2919	4.8	1.5	166
875	20	20	5	0	5	50	85	2920	9.4	1.5	297
876	25	25	0	25	15	10	94	2921	4.5	1.4	147
877	25	15	20	20	15	5	82	2922	4.5	1.3	130
878	20	25	5	30	10	10	92	2922	4.6	1.5	170
879	20	20	5	5	0	50	87	2924	9.2	1.5	306
880	30	15	15	20	15	5	86	2925	4.1	1.2	115
881	20	10	25	0	0	45	80	2925	9.2	1.4	328
882	25	25	0	30	10	10	94	2925	4.3	1.4	151
883	25	15	20	25	10	5	81	2925	4.3	1.3	134
884	20	25	5	35	5	10	91	2925	4.4	1.4	174
885	20	20	10	0	20	30	90	2926	7.6	1.5	239
886	30	15	15	25	10	5	85	2928	3.9	1.2	118
887	25	10	20	0	0	45	85	2928	8.8	1.3	290
888	25	25	0	35	5	10	95	2928	4.1	1.3	155
889	20	20	10	5	15	30	91	2929	7.4	1.5	246
890	20	20	15	0	35	10	90	2930	5.9	1.5	153
891	30	15	15	30	5	5	84	2931	3.7	1.1	121
892	25	25	0	40	0	10	94	2931	3.9	1.3	159
893	25	10	25	0	15	25	81	2932	7.1	1.3	220
894	20	20	10	10	10	30	91	2932	7.3	1.5	253
895	20	20	15	5	30	10	89	2933	5.7	1.5	157
896	25	20	10	0	35	10	92	2933	5.5	1.4	135
897	30	15	15	35	0	5	82	2934	3.6	1.1	125
898	20	20	10	15	5	30	91	2935	7.1	1.5	259
899	20	20	15	10	25	10	88	2935	5.5	1.5	161

900	25	20	10	5	30	10	93	2937	5.3	1.4	139
901	20	20	10	20	0	30	90	2938	6.9	1.4	266
902	30	10	25	0	30	5	81	2939	5.0	1.2	107
903	25	20	10	10	25	10	92	2940	5.2	1.4	143
904	25	20	5	15	5	30	92	2940	6.7	1.3	229
905	25	20	10	15	20	10	92	2942	5.0	1.4	147
906	25	20	5	20	0	30	94	2943	6.5	1.3	236
907	25	20	10	20	15	10	91	2945	4.8	1.4	151
908	25	20	10	25	10	10	89	2948	4.6	1.3	155
909	15	25	0	5	0	55	82	2949	9.9	1.6	338
910	25	20	10	30	5	10	88	2950	4.4	1.3	159
911	20	15	15	0	0	50	87	2952	9.5	1.4	323
912	25	20	10	35	0	10	87	2953	4.2	1.3	163
913	20	15	20	0	15	30	85	2953	7.7	1.5	256
914	20	25	0	0	20	35	82	2955	7.9	1.6	240
915	20	25	5	0	35	15	89	2955	6.2	1.6	168
916	20	15	20	5	10	30	84	2955	7.6	1.4	263
917	20	15	20	10	5	30	83	2958	7.4	1.4	270
918	20	25	5	5	30	15	90	2958	6.0	1.6	173
919	20	25	0	5	15	35	84	2958	7.8	1.6	248
920	25	15	20	0	30	10	86	2960	5.7	1.4	142
921	25	15	15	0	15	30	89	2960	7.4	1.4	227
922	20	25	5	10	25	15	92	2960	5.8	1.6	178
923	20	25	0	10	10	35	86	2961	7.6	1.5	255
924	25	15	20	5	25	10	85	2962	5.5	1.4	146
925	20	25	5	15	20	15	93	2963	5.6	1.5	183
926	25	15	15	5	10	30	89	2963	7.2	1.3	233
927	20	25	0	15	5	35	88	2963	7.4	1.5	262
928	25	15	20	10	20	10	83	2964	5.3	1.3	150
929	20	25	5	20	15	15	93	2965	5.4	1.5	187
930	25	15	15	10	5	30	88	2966	7.0	1.3	240
931	20	25	0	20	0	35	90	2966	7.2	1.5	270
932	25	15	20	15	15	10	82	2967	5.1	1.3	154
933	20	25	5	25	10	15	93	2967	5.3	1.5	192
934	25	15	15	15	0	30	87	2968	6.8	1.3	246
935	25	15	20	20	10	10	81	2969	4.9	1.3	159
936	25	25	0	10	25	15	88	2969	5.5	1.5	156
937	20	25	5	30	5	15	92	2969	5.1	1.5	197
938	25	15	20	25	5	10	80	2971	4.7	1.3	163
939	25	25	0	15	20	15	90	2971	5.3	1.4	161
940	25	25	0	20	15	15	92	2974	5.1	1.4	166
941	25	25	0	25	10	15	93	2976	4.9	1.4	170
942	30	15	15	20	10	10	86	2977	4.6	1.2	140
943	25	25	0	30	5	15	94	2978	4.7	1.4	175
944	20	20	15	0	30	15	89	2979	6.3	1.6	179
945	30	15	15	25	5	10	85	2979	4.4	1.2	144
946	25	25	0	35	0	15	95	2980	4.5	1.4	180
947	20	20	15	5	25	15	89	2981	6.1	1.5	183
948	30	15	15	30	0	10	83	2981	4.2	1.2	148
949	20	20	10	0	15	35	89	2983	8.1	1.5	260
950	20	30	0	0	50	0	87	2983	4.8	1.7	91

951	20	20	10	5	10	35	90	2985	7.9	1.5	267
952	20	30	0	5	45	0	88	2985	4.6	1.7	94
953	25	10	25	0	10	30	81	2986	7.5	1.3	243
954	20	20	10	10	5	35	90	2987	7.7	1.5	274
955	20	30	0	10	40	0	90	2987	4.4	1.7	97
956	20	20	5	0	0	55	84	2988	9.8	1.5	312
957	20	30	0	15	35	0	92	2988	4.2	1.6	100
958	20	20	10	15	0	35	90	2989	7.5	1.5	282
959	20	30	0	20	30	0	93	2990	4.0	1.6	103
960	25	20	10	0	30	15	91	2991	6.0	1.5	158
961	20	30	0	25	25	0	94	2992	3.8	1.6	106
962	25	20	10	5	25	15	92	2992	5.8	1.4	162
963	30	10	25	0	25	10	81	2993	5.4	1.2	132
964	25	20	10	10	20	15	92	2994	5.6	1.4	167
965	25	20	10	15	15	15	91	2996	5.4	1.4	171
966	25	20	10	20	10	15	90	2997	5.2	1.4	176
967	25	20	10	25	5	15	89	2999	5.0	1.3	181
968	25	20	10	30	0	15	88	3000	4.8	1.3	186
969	25	20	5	10	5	35	90	3001	7.3	1.4	242
970	25	20	5	15	0	35	92	3002	7.2	1.4	249
971	20	25	10	0	45	0	91	3005	4.9	1.7	95
972	20	15	20	0	10	35	85	3006	8.2	1.5	279
973	20	15	20	5	5	35	84	3007	8.0	1.5	286
974	20	25	5	0	30	20	88	3012	6.6	1.6	191
975	20	25	5	5	25	20	90	3013	6.4	1.6	196
976	25	15	20	0	25	15	85	3013	6.1	1.4	168
977	20	25	5	10	20	20	91	3014	6.3	1.6	202
978	25	15	20	5	20	15	84	3014	5.9	1.4	172
979	20	25	5	15	15	20	92	3015	6.1	1.6	207
980	25	15	20	10	15	15	83	3015	5.7	1.4	177
981	20	25	5	20	10	20	93	3016	5.9	1.5	213
982	25	15	20	15	10	15	82	3016	5.5	1.3	181
983	20	25	5	25	5	20	93	3017	5.7	1.5	218
984	25	15	20	20	5	15	81	3017	5.3	1.3	186
985	25	15	20	25	0	15	80	3018	5.2	1.3	191
986	25	25	5	0	45	0	90	3019	4.5	1.5	83
987	25	25	5	5	40	0	92	3020	4.4	1.5	85
988	25	25	5	10	35	0	93	3021	4.2	1.5	88
989	20	25	0	0	15	40	81	3021	8.4	1.6	258
990	25	25	5	15	30	0	94	3022	4.0	1.5	91
991	20	25	0	5	10	40	84	3022	8.2	1.6	266
992	25	15	15	0	10	35	88	3022	7.8	1.4	247
993	25	25	5	20	25	0	94	3023	3.8	1.5	94
994	20	25	0	10	5	40	86	3023	8.0	1.5	274
995	25	15	15	5	5	35	88	3023	7.7	1.3	254
996	25	25	5	25	20	0	93	3024	3.6	1.4	97
997	25	15	15	10	0	35	88	3024	7.5	1.3	261
998	20	25	0	15	0	40	88	3024	7.8	1.5	282
999	25	25	5	30	15	0	92	3024	3.4	1.4	99
1000	25	25	5	35	10	0	91	3025	3.2	1.4	102
1001	25	25	5	40	5	0	90	3026	3.0	1.4	105

1002	25	25	5	45	0	0	89	3027	2.9	1.3	108
1003	25	25	0	5	25	20	85	3031	6.1	1.5	172
1004	25	25	0	10	20	20	87	3032	5.9	1.5	178
1005	25	25	0	15	15	20	89	3032	5.7	1.5	183
1006	30	15	15	15	10	15	87	3033	5.2	1.2	161
1007	25	25	0	20	10	20	91	3033	5.5	1.4	188
1008	30	15	15	20	5	15	86	3034	5.0	1.2	165
1009	25	25	0	25	5	20	93	3034	5.4	1.4	194
1010	30	15	15	25	0	15	85	3034	4.8	1.2	170
1011	25	25	0	30	0	20	94	3034	5.2	1.4	199
1012	25	20	15	0	40	0	90	3039	4.7	1.5	86
1013	20	30	0	0	45	5	86	3039	5.2	1.7	116
1014	25	20	15	5	35	0	89	3039	4.5	1.5	89
1015	20	30	0	5	40	5	88	3039	5.0	1.7	120
1016	25	20	15	10	30	0	88	3040	4.3	1.4	92
1017	20	30	0	10	35	5	90	3040	4.8	1.7	123
1018	25	20	15	15	25	0	87	3040	4.1	1.4	94
1019	20	30	0	15	30	5	91	3040	4.6	1.6	127
1020	25	20	15	20	20	0	85	3040	3.9	1.4	97
1021	20	30	0	20	25	5	92	3041	4.5	1.6	131
1022	25	20	15	25	15	0	84	3041	3.7	1.4	100
1023	25	20	15	30	10	0	83	3041	3.5	1.4	103
1024	25	20	15	35	5	0	82	3042	3.3	1.3	106
1025	30	25	0	30	15	0	94	3042	3.1	1.3	87
1026	25	20	15	40	0	0	81	3042	3.2	1.3	109
1027	30	25	0	35	10	0	94	3042	2.9	1.3	89
1028	30	25	0	40	5	0	94	3043	2.7	1.3	92
1029	30	25	0	45	0	0	93	3043	2.5	1.2	95
1030	25	10	25	0	5	35	80	3044	8.0	1.3	265
1031	20	20	10	0	10	40	88	3044	8.5	1.5	280
1032	20	20	10	5	5	40	89	3044	8.3	1.5	287
1033	20	20	10	10	0	40	90	3045	8.1	1.5	295
1034	30	10	25	0	20	15	81	3051	5.9	1.2	157
1035	25	20	10	0	25	20	91	3052	6.4	1.5	180
1036	25	20	10	5	20	20	91	3052	6.2	1.4	185
1037	25	20	10	10	15	20	91	3052	6.0	1.4	190
1038	25	20	10	15	10	20	91	3052	5.8	1.4	195
1039	25	20	10	20	5	20	90	3052	5.7	1.4	201
1040	25	20	10	25	0	20	89	3053	5.5	1.4	206
1041	25	15	25	0	35	0	81	3055	4.8	1.4	89
1042	30	20	10	40	0	0	85	3059	2.8	1.2	96
1043	30	20	10	35	5	0	87	3059	3.0	1.2	93
1044	30	20	10	30	10	0	88	3059	3.2	1.3	90
1045	30	20	10	25	15	0	89	3059	3.4	1.3	88
1046	30	20	10	20	20	0	90	3059	3.6	1.3	85
1047	30	20	10	15	25	0	91	3060	3.8	1.3	82
1048	30	20	10	10	30	0	92	3060	3.9	1.3	80
1049	25	15	20	20	0	20	81	3069	5.8	1.3	213
1050	25	15	20	15	5	20	82	3069	6.0	1.3	208
1051	25	20	5	10	0	40	89	3069	7.8	1.4	260
1052	25	15	20	10	10	20	83	3069	6.2	1.4	202

1053	25	15	20	5	15	20	84	3069	6.3	1.4	197
1054	25	15	20	0	20	20	85	3070	6.5	1.4	192
1055	20	25	5	15	10	25	92	3071	6.5	1.6	231
1056	20	25	5	10	15	25	91	3071	6.7	1.6	225
1057	20	25	5	5	20	25	89	3071	6.9	1.6	219
1058	20	25	5	0	25	25	87	3072	7.1	1.6	213
1059	30	15	20	20	15	0	81	3075	3.7	1.2	88
1060	25	25	5	40	0	5	90	3075	3.5	1.4	135
1061	30	15	20	15	20	0	82	3075	3.9	1.3	85
1062	25	25	5	35	5	5	91	3076	3.7	1.4	131
1063	30	15	20	10	25	0	83	3076	4.1	1.3	83
1064	25	25	5	30	10	5	92	3076	3.9	1.4	128
1065	30	15	20	5	30	0	84	3076	4.2	1.3	80
1066	25	25	5	25	15	5	93	3077	4.0	1.4	124
1067	30	15	20	0	35	0	85	3077	4.4	1.3	78
1068	25	25	5	20	20	5	93	3077	4.2	1.5	121
1069	25	25	5	15	25	5	93	3078	4.4	1.5	117
1070	25	25	5	10	30	5	92	3078	4.6	1.5	114
1071	25	25	5	5	35	5	91	3079	4.8	1.5	110
1072	25	25	5	0	40	5	89	3079	5.0	1.6	107
1073	25	15	15	5	0	40	88	3088	8.1	1.4	273
1074	25	20	15	35	0	5	82	3089	3.8	1.3	137
1075	25	15	15	0	5	40	88	3089	8.3	1.4	266
1076	25	20	15	30	5	5	83	3089	4.0	1.4	133
1077	25	20	15	25	10	5	84	3090	4.2	1.4	130
1078	20	25	0	10	0	45	85	3091	8.4	1.6	292
1079	25	20	15	20	15	5	85	3091	4.3	1.4	126
1080	20	25	0	5	5	45	83	3092	8.6	1.6	283
1081	25	20	15	15	20	5	86	3092	4.5	1.4	123
1082	25	20	15	10	25	5	87	3093	4.7	1.5	119
1083	20	25	0	0	10	45	80	3093	8.8	1.6	275
1084	30	15	15	20	0	20	86	3093	5.4	1.2	189
1085	25	20	15	5	30	5	88	3093	4.9	1.5	116
1086	30	15	15	15	5	20	87	3094	5.6	1.2	184
1087	25	20	15	0	35	5	89	3094	5.1	1.5	113
1088	30	15	15	10	10	20	88	3095	5.8	1.3	179
1089	25	25	0	25	0	25	92	3095	5.8	1.4	216
1090	20	30	0	10	30	10	89	3096	5.3	1.7	149
1091	25	25	0	20	5	25	91	3097	6.0	1.4	210
1092	20	30	0	5	35	10	87	3097	5.5	1.7	145
1093	20	30	0	0	40	10	86	3098	5.6	1.7	141
1094	25	25	0	15	10	25	89	3098	6.2	1.5	204
1095	25	25	0	10	15	25	87	3099	6.4	1.5	198
1096	30	25	0	40	0	5	94	3100	3.1	1.3	119
1097	25	25	0	5	20	25	85	3100	6.5	1.5	192
1098	30	25	0	35	5	5	94	3101	3.3	1.3	115
1099	25	25	0	0	25	25	82	3102	6.7	1.5	186
1100	30	25	0	30	10	5	94	3102	3.5	1.3	112
1101	25	15	25	0	30	5	81	3107	5.2	1.4	118
1102	20	20	10	5	0	45	88	3107	8.8	1.5	307
1103	20	20	10	0	5	45	88	3109	8.9	1.5	298

1104	25	20	10	20	0	25	90	3111	6.1	1.4	224
1105	25	20	10	15	5	25	91	3112	6.3	1.4	219
1106	30	10	25	0	15	20	80	3112	6.3	1.3	181
1107	30	20	10	35	0	5	86	3114	3.4	1.2	121
1108	25	20	10	10	10	25	91	3114	6.5	1.4	213
1109	30	20	10	30	5	5	88	3115	3.6	1.3	118
1110	25	20	10	5	15	25	91	3115	6.7	1.5	207
1111	30	20	10	25	10	5	89	3116	3.8	1.3	114
1112	25	20	10	0	20	25	90	3117	6.8	1.5	201
1113	30	20	10	20	15	5	90	3118	4.0	1.3	111
1114	30	20	10	15	20	5	91	3120	4.2	1.3	108
1115	30	20	10	10	25	5	92	3121	4.4	1.4	105
1116	30	20	10	5	30	5	92	3123	4.6	1.4	101
1117	25	15	20	15	0	25	82	3124	6.4	1.4	233
1118	25	15	20	10	5	25	83	3126	6.6	1.4	227
1119	25	15	20	5	10	25	84	3128	6.8	1.4	221
1120	25	25	5	35	0	10	91	3129	4.1	1.4	159
1121	30	15	20	20	10	5	81	3129	4.1	1.3	116
1122	25	15	20	0	15	25	85	3130	7.0	1.4	215
1123	25	25	5	30	5	10	92	3131	4.3	1.4	155
1124	30	15	20	15	15	5	82	3131	4.3	1.3	113
1125	20	25	5	10	10	30	90	3131	7.1	1.6	247
1126	25	25	5	25	10	10	92	3132	4.5	1.5	151
1127	30	15	20	10	20	5	83	3133	4.5	1.3	110
1128	20	25	5	5	15	30	88	3133	7.3	1.6	240
1129	25	25	5	20	15	10	93	3134	4.7	1.5	147
1130	30	15	20	5	25	5	84	3135	4.7	1.3	107
1131	20	25	5	0	20	30	87	3135	7.5	1.6	234
1132	25	25	5	15	20	10	93	3136	4.9	1.5	143
1133	30	15	20	0	30	5	85	3137	4.9	1.3	103
1134	25	25	5	10	25	10	92	3139	5.0	1.5	139
1135	25	25	5	5	30	10	90	3141	5.2	1.5	135
1136	25	20	15	25	5	10	84	3142	4.6	1.4	158
1137	25	25	5	0	35	10	89	3143	5.4	1.6	131
1138	25	20	15	20	10	10	85	3144	4.8	1.4	154
1139	25	20	5	5	0	45	87	3146	8.4	1.4	269
1140	25	20	15	15	15	10	86	3146	5.0	1.4	150
1141	25	20	15	10	20	10	87	3148	5.2	1.5	146
1142	25	20	15	5	25	10	88	3151	5.3	1.5	142
1143	25	20	15	0	30	10	89	3153	5.5	1.5	138
1144	20	30	0	5	30	15	87	3157	5.9	1.7	169
1145	30	15	15	15	0	25	87	3159	6.1	1.2	206
1146	20	30	0	0	35	15	85	3160	6.1	1.7	164
1147	25	15	15	0	0	45	87	3160	8.7	1.4	284
1148	25	15	25	0	25	10	80	3161	5.6	1.5	146
1149	30	15	15	10	5	25	88	3162	6.2	1.3	201
1150	30	25	0	35	0	10	94	3163	3.8	1.3	140
1151	25	25	0	20	0	30	90	3164	6.4	1.4	230
1152	20	25	0	5	0	50	82	3166	9.1	1.6	299
1153	30	25	0	30	5	10	94	3166	3.9	1.3	136
1154	25	25	0	15	5	30	88	3167	6.6	1.5	224

1155	30	25	0	25	10	10	93	3169	4.1	1.4	133
1156	25	25	0	10	10	30	86	3171	6.8	1.5	217
1157	30	20	10	30	0	10	87	3174	4.1	1.3	144
1158	25	25	0	5	15	30	84	3175	7.0	1.5	211
1159	25	20	10	15	0	30	90	3176	6.7	1.4	241
1160	30	20	10	25	5	10	89	3177	4.3	1.3	140
1161	20	20	10	0	0	50	87	3178	9.4	1.6	316
1162	25	25	0	0	20	30	81	3179	7.2	1.5	205
1163	25	20	10	10	5	30	90	3179	6.9	1.4	234
1164	30	20	10	20	10	10	90	3180	4.4	1.3	136
1165	25	20	10	5	10	30	90	3183	7.1	1.5	228
1166	30	20	10	15	15	10	91	3183	4.6	1.3	133
1167	25	15	20	10	0	30	82	3186	7.0	1.4	251
1168	30	15	20	20	5	10	80	3186	4.6	1.3	144
1169	25	20	10	0	15	30	89	3187	7.3	1.5	221
1170	30	20	10	10	20	10	92	3187	4.8	1.4	129
1171	25	25	5	30	0	15	91	3188	4.7	1.4	181
1172	25	15	20	5	5	30	83	3190	7.2	1.4	244
1173	30	15	20	15	10	10	81	3190	4.7	1.3	140
1174	30	20	10	5	25	10	92	3191	5.0	1.4	125
1175	25	25	5	25	5	15	92	3191	4.9	1.5	176
1176	30	15	20	10	15	10	83	3193	4.9	1.3	136
1177	25	15	20	0	10	30	84	3193	7.4	1.4	238
1178	30	20	10	0	30	10	91	3195	5.2	1.4	121
1179	25	25	5	20	10	15	93	3195	5.1	1.5	172
1180	30	15	20	5	20	10	84	3197	5.1	1.3	132
1181	25	25	5	15	15	15	92	3199	5.3	1.5	167
1182	20	25	5	5	10	35	88	3199	7.8	1.6	261
1183	25	20	15	20	5	15	85	3200	5.2	1.4	182
1184	30	15	20	0	25	10	85	3201	5.3	1.4	128
1185	25	30	0	40	5	0	92	3201	2.9	1.5	102
1186	25	25	5	10	20	15	91	3203	5.5	1.5	162
1187	20	25	5	0	15	35	86	3203	7.9	1.6	254
1188	25	20	15	15	10	15	86	3204	5.4	1.5	177
1189	25	30	0	35	10	0	93	3205	3.1	1.5	99
1190	25	25	5	5	25	15	90	3207	5.7	1.6	158
1191	25	20	15	10	15	15	87	3207	5.6	1.5	172
1192	25	30	0	30	15	0	94	3208	3.3	1.5	96
1193	25	20	15	5	20	15	88	3211	5.8	1.5	168
1194	25	25	5	0	30	15	88	3211	5.9	1.6	153
1195	25	30	0	25	20	0	94	3212	3.5	1.6	93
1196	25	20	15	0	25	15	88	3215	6.0	1.5	163
1197	25	30	0	20	25	0	93	3216	3.7	1.6	90
1198	25	30	0	15	30	0	91	3220	3.9	1.6	88
1199	25	25	10	15	25	0	90	3223	4.0	1.5	91
1200	25	30	0	10	35	0	90	3225	4.0	1.6	85
1201	25	25	10	10	30	0	90	3227	4.2	1.6	88
1202	25	30	0	5	40	0	88	3229	4.2	1.6	82
1203	25	25	10	5	35	0	91	3232	4.3	1.6	86
1204	30	25	0	30	0	15	94	3234	4.4	1.3	160
1205	30	15	15	10	0	30	87	3234	6.7	1.3	222

1206	25	30	0	0	45	0	86	3234	4.4	1.7	80
1207	25	20	5	0	0	50	84	3234	9.0	1.5	276
1208	25	25	10	0	40	0	91	3236	4.5	1.6	83
1209	30	25	0	25	5	15	93	3239	4.6	1.4	155
1210	30	15	15	5	5	30	88	3240	6.9	1.3	215
1211	30	20	10	25	0	15	88	3241	4.7	1.3	165
1212	25	25	0	15	0	35	88	3242	7.0	1.5	243
1213	30	25	0	20	10	15	91	3245	4.8	1.4	151
1214	30	20	10	20	5	15	89	3246	4.9	1.3	161
1215	30	25	5	40	0	0	89	3246	2.7	1.3	92
1216	25	25	0	10	5	35	86	3248	7.2	1.5	236
1217	25	20	10	10	0	35	89	3249	7.3	1.4	255
1218	30	25	5	35	5	0	90	3251	2.9	1.4	90
1219	30	20	15	35	0	0	81	3251	3.0	1.3	93
1220	30	20	10	15	10	15	91	3251	5.1	1.3	156
1221	30	15	20	15	5	15	81	3252	5.2	1.3	166
1222	25	25	5	25	0	20	92	3254	5.4	1.5	201
1223	25	25	0	5	10	35	83	3255	7.4	1.5	229
1224	25	20	10	5	5	35	89	3255	7.5	1.5	248
1225	25	15	20	5	0	35	83	3255	7.6	1.4	266
1226	30	25	5	30	10	0	91	3256	3.1	1.4	87
1227	30	20	15	30	5	0	82	3256	3.2	1.3	90
1228	30	15	20	10	10	15	82	3257	5.4	1.3	161
1229	30	20	10	10	15	15	91	3257	5.3	1.4	152
1230	25	25	5	20	5	20	92	3259	5.5	1.5	196
1231	30	20	15	25	10	0	83	3261	3.4	1.3	87
1232	25	15	20	0	5	35	84	3261	7.8	1.4	259
1233	30	25	5	25	15	0	92	3261	3.3	1.4	84
1234	25	20	10	0	10	35	88	3261	7.7	1.5	241
1235	25	25	0	0	15	35	81	3262	7.6	1.5	222
1236	30	15	20	5	15	15	83	3263	5.6	1.3	157
1237	30	20	10	5	20	15	91	3263	5.4	1.4	148
1238	25	25	5	15	10	20	92	3265	5.7	1.5	191
1239	30	20	15	20	15	0	84	3266	3.6	1.4	85
1240	30	25	5	20	20	0	93	3267	3.4	1.4	82
1241	25	30	0	30	10	5	94	3268	3.7	1.5	124
1242	30	15	20	0	20	15	84	3268	5.7	1.4	153
1243	25	20	15	10	10	20	86	3269	6.0	1.5	197
1244	30	20	10	0	25	15	91	3270	5.6	1.4	143
1245	25	25	5	10	15	20	91	3271	5.9	1.5	185
1246	30	20	15	15	20	0	86	3271	3.7	1.4	82
1247	30	25	5	15	25	0	93	3272	3.6	1.4	79
1248	25	30	0	25	15	5	93	3273	3.9	1.6	120
1249	25	20	15	5	15	20	87	3275	6.2	1.5	192
1250	30	20	15	10	25	0	87	3277	3.9	1.4	79
1251	25	25	5	5	20	20	89	3277	6.1	1.6	180
1252	30	25	5	10	30	0	92	3279	3.8	1.5	77
1253	25	30	0	20	20	5	92	3279	4.1	1.6	117
1254	25	20	15	0	20	20	87	3281	6.4	1.5	187
1255	30	20	15	5	30	0	88	3282	4.1	1.4	77
1256	25	25	5	0	25	20	88	3284	6.3	1.6	175

1257	25	30	0	15	25	5	91	3285	4.3	1.6	114
1258	30	25	5	5	35	0	91	3285	4.0	1.5	74
1259	30	20	15	0	35	0	89	3289	4.3	1.5	74
1260	25	30	0	10	30	5	89	3291	4.5	1.6	110
1261	30	25	5	0	40	0	89	3292	4.2	1.5	72
1262	25	25	10	5	30	5	90	3294	4.8	1.6	112
1263	25	30	0	5	35	5	87	3298	4.7	1.7	107
1264	25	25	10	0	35	5	90	3300	5.0	1.6	109
1265	35	20	10	35	0	0	86	3302	2.7	1.2	81
1266	25	30	0	0	40	5	86	3305	4.9	1.7	104
1267	35	20	10	30	5	0	87	3309	2.8	1.2	78
1268	30	25	5	35	0	5	90	3313	3.3	1.4	117
1269	30	25	0	25	0	20	92	3314	5.0	1.4	178
1270	30	20	15	30	0	5	82	3315	3.6	1.3	119
1271	30	20	10	20	0	20	89	3316	5.3	1.3	184
1272	35	20	10	25	10	0	88	3316	3.0	1.2	76
1273	30	15	20	15	0	20	81	3317	5.6	1.3	191
1274	30	15	15	5	0	35	87	3319	7.3	1.3	235
1275	30	25	5	30	5	5	91	3320	3.5	1.4	114
1276	30	20	15	25	5	5	83	3321	3.8	1.4	116
1277	30	25	0	20	5	20	91	3322	5.2	1.4	172
1278	30	20	10	15	5	20	90	3324	5.5	1.4	179
1279	35	20	10	20	15	0	89	3324	3.2	1.3	73
1280	30	15	20	10	5	20	82	3325	5.8	1.3	186
1281	35	15	20	15	15	0	81	3325	3.5	1.2	73
1282	25	25	5	20	0	25	92	3327	6.0	1.5	219
1283	30	25	5	25	10	5	92	3327	3.7	1.4	111
1284	30	20	15	20	10	5	84	3328	4.0	1.4	113
1285	30	15	15	0	5	35	87	3328	7.5	1.3	228
1286	30	25	0	15	10	20	89	3331	5.4	1.4	167
1287	25	25	0	10	0	40	85	3331	7.7	1.5	254
1288	30	20	10	10	10	20	91	3332	5.7	1.4	174
1289	25	20	10	5	0	40	88	3332	8.0	1.5	267
1290	35	15	20	10	20	0	82	3332	3.7	1.3	71
1291	30	15	20	5	10	20	83	3332	6.0	1.3	181
1292	25	15	20	0	0	40	83	3332	8.3	1.4	280
1293	30	25	5	20	15	5	93	3335	3.9	1.4	107
1294	25	25	5	15	5	25	91	3335	6.2	1.5	213
1295	30	20	15	15	15	5	85	3335	4.2	1.4	109
1296	25	30	0	25	10	10	93	3337	4.4	1.6	147
1297	35	15	20	5	25	0	83	3340	3.9	1.3	69
1298	30	15	20	0	15	20	84	3340	6.2	1.4	176
1299	30	20	10	5	15	20	90	3341	5.9	1.4	169
1300	25	20	10	0	5	40	87	3341	8.2	1.5	260
1301	25	25	0	5	5	40	83	3341	7.9	1.5	246
1302	30	20	15	10	20	5	86	3343	4.4	1.4	106
1303	30	25	5	15	20	5	93	3343	4.1	1.5	104
1304	25	20	15	5	10	25	87	3343	6.7	1.5	216
1305	25	25	5	10	10	25	90	3343	6.4	1.5	208
1306	25	30	0	20	15	10	92	3345	4.5	1.6	143
1307	35	15	20	0	30	0	84	3348	4.1	1.3	66

1308	30	20	10	0	20	20	90	3350	6.1	1.4	164
1309	30	20	15	5	25	5	87	3350	4.6	1.4	103
1310	25	20	15	0	15	25	87	3351	6.8	1.5	210
1311	30	25	5	10	25	5	92	3351	4.3	1.5	101
1312	25	25	0	0	10	40	80	3352	8.0	1.6	238
1313	25	25	5	5	15	25	89	3352	6.5	1.6	202
1314	25	30	0	15	20	10	90	3353	4.7	1.6	139
1315	30	20	15	0	30	5	88	3359	4.7	1.5	100
1316	30	25	5	5	30	5	90	3360	4.4	1.5	98
1317	25	25	5	0	20	25	87	3361	6.7	1.6	196
1318	25	30	0	10	25	10	89	3362	4.9	1.6	135
1319	30	25	5	0	35	5	89	3370	4.6	1.5	95
1320	25	30	0	5	30	10	87	3371	5.1	1.7	131
1321	35	20	10	30	0	5	87	3379	3.3	1.2	105
1322	25	30	0	0	35	10	85	3380	5.3	1.7	127
1323	30	20	15	25	0	10	83	3385	4.2	1.4	143
1324	30	25	5	30	0	10	91	3388	3.9	1.4	140
1325	35	20	10	25	5	5	88	3389	3.5	1.2	101
1326	30	20	15	20	5	10	84	3394	4.4	1.4	140
1327	35	15	20	15	10	5	81	3394	4.0	1.2	100
1328	30	15	20	10	0	25	81	3396	6.2	1.3	210
1329	30	25	5	25	5	10	92	3397	4.1	1.4	136
1330	35	20	10	20	10	5	89	3399	3.7	1.3	98
1331	30	20	10	15	0	25	90	3401	5.9	1.4	201
1332	30	20	15	15	10	10	85	3403	4.6	1.4	136
1333	35	15	20	10	15	5	82	3404	4.2	1.3	97
1334	30	25	0	20	0	25	90	3406	5.6	1.4	193
1335	30	15	20	5	5	25	82	3406	6.4	1.4	204
1336	30	25	5	20	10	10	92	3407	4.3	1.4	132
1337	35	20	10	15	15	5	90	3409	3.8	1.3	95
1338	25	25	5	15	0	30	90	3409	6.6	1.5	235
1339	30	20	10	10	5	25	90	3411	6.1	1.4	196
1340	30	20	15	10	15	10	86	3412	4.8	1.4	132
1341	35	15	20	5	20	5	83	3415	4.3	1.3	94
1342	30	15	15	0	0	40	86	3417	7.9	1.3	246
1343	30	15	20	0	10	25	83	3417	6.6	1.4	198
1344	30	25	0	15	5	25	88	3418	5.8	1.4	187
1345	30	25	5	15	15	10	92	3418	4.5	1.5	129
1346	25	25	5	10	5	30	89	3420	6.8	1.6	229
1347	30	20	15	5	20	10	87	3422	5.0	1.5	128
1348	30	20	10	5	10	25	90	3423	6.3	1.4	190
1349	35	15	20	0	25	5	84	3425	4.5	1.3	91
1350	25	30	0	15	15	15	90	3425	5.2	1.6	163
1351	25	20	10	0	0	45	87	3426	8.6	1.5	277
1352	30	25	5	10	20	10	91	3429	4.7	1.5	125
1353	30	25	0	10	10	25	86	3431	6.0	1.4	182
1354	25	25	5	5	10	30	88	3432	7.0	1.6	222
1355	30	20	15	0	25	10	88	3433	5.2	1.5	125
1356	25	25	0	5	0	45	82	3434	8.3	1.5	262
1357	30	20	10	0	15	25	89	3436	6.5	1.4	185
1358	25	30	0	10	20	15	88	3436	5.4	1.6	158

1359	30	25	5	5	25	10	90	3440	4.9	1.5	121
1360	25	25	5	0	15	30	86	3444	7.2	1.6	216
1361	25	30	0	5	25	15	86	3448	5.5	1.7	154
1362	30	30	0	40	0	0	91	3452	2.6	1.4	89
1363	30	25	5	0	30	10	88	3453	5.1	1.5	117
1364	25	30	0	0	30	15	84	3460	5.7	1.7	149
1365	30	30	0	35	5	0	92	3463	2.8	1.5	86
1366	30	20	15	20	0	15	83	3463	4.9	1.4	166
1367	35	20	10	25	0	10	88	3465	3.9	1.3	126
1368	35	15	20	15	5	10	80	3468	4.4	1.2	126
1369	30	25	5	25	0	15	91	3472	4.6	1.4	161
1370	30	30	0	30	10	0	93	3474	3.0	1.5	84
1371	30	20	15	15	5	15	84	3474	5.1	1.4	161
1372	30	25	10	20	15	0	87	3476	3.4	1.5	81
1373	35	20	10	20	5	10	89	3478	4.1	1.3	123
1374	35	15	20	10	10	10	81	3481	4.6	1.3	122
1375	30	25	5	20	5	15	92	3484	4.8	1.4	157
1376	30	15	20	5	0	30	82	3485	6.9	1.4	226
1377	30	30	0	25	15	0	93	3485	3.1	1.5	81
1378	30	20	15	10	10	15	85	3486	5.2	1.4	157
1379	30	25	10	15	20	0	88	3487	3.6	1.5	79
1380	35	20	10	15	10	10	90	3492	4.3	1.3	119
1381	35	15	20	5	15	10	82	3494	4.8	1.3	119
1382	30	20	10	10	0	30	89	3497	6.6	1.4	216
1383	30	25	5	15	10	15	92	3497	4.9	1.5	152
1384	30	30	0	20	20	0	92	3498	3.3	1.5	78
1385	30	15	20	0	5	30	83	3498	7.1	1.4	220
1386	30	20	15	5	15	15	86	3499	5.4	1.5	153
1387	30	25	10	10	25	0	89	3499	3.8	1.5	76
1388	25	25	5	10	0	35	89	3502	7.2	1.6	249
1389	35	20	10	10	15	10	91	3506	4.5	1.3	116
1390	35	15	20	0	20	10	84	3507	5.0	1.3	115
1391	30	25	0	15	0	30	88	3510	6.3	1.4	206
1392	30	30	0	15	25	0	91	3511	3.5	1.6	76
1393	30	25	5	10	15	15	91	3511	5.1	1.5	148
1394	30	20	10	5	5	30	89	3512	6.8	1.4	210
1395	30	25	10	5	30	0	90	3512	4.0	1.6	74
1396	30	20	15	0	20	15	87	3512	5.6	1.5	148
1397	25	25	5	5	5	35	87	3517	7.4	1.6	242
1398	35	20	15	30	0	0	81	3518	2.8	1.3	77
1399	30	30	0	10	30	0	89	3525	3.7	1.6	73
1400	30	25	10	0	35	0	90	3525	4.2	1.6	71
1401	30	25	5	5	20	15	89	3526	5.3	1.5	143
1402	30	25	0	10	5	30	85	3527	6.4	1.5	200
1403	30	20	10	0	10	30	88	3528	6.9	1.4	204
1404	25	30	0	5	20	20	86	3530	6.0	1.7	176
1405	35	25	5	35	0	0	89	3531	2.5	1.3	77
1406	35	20	15	25	5	0	82	3531	3.0	1.3	75
1407	25	25	5	0	10	35	86	3532	7.6	1.6	235
1408	30	30	0	35	0	5	92	3534	3.2	1.5	114
1409	30	30	0	5	35	0	88	3539	3.9	1.6	71

1410	30	25	5	0	25	15	88	3542	5.5	1.5	139
1411	35	20	15	20	10	0	83	3544	3.2	1.3	73
1412	35	25	5	30	5	0	90	3544	2.7	1.3	75
1413	30	25	0	5	10	30	83	3546	6.6	1.5	194
1414	25	30	0	0	25	20	84	3546	6.2	1.7	171
1415	30	30	0	30	5	5	93	3547	3.4	1.5	110
1416	30	20	15	15	0	20	84	3550	5.5	1.4	186
1417	30	30	0	0	40	0	86	3555	4.1	1.6	69
1418	35	20	15	15	15	0	84	3558	3.4	1.3	70
1419	35	25	5	25	10	0	91	3559	2.9	1.4	73
1420	30	25	10	15	15	5	88	3561	4.1	1.5	106
1421	30	30	0	25	10	5	93	3562	3.6	1.5	107
1422	35	15	20	10	5	15	81	3562	5.0	1.3	147
1423	35	20	10	20	0	15	88	3563	4.5	1.3	146
1424	30	20	15	10	5	20	85	3564	5.7	1.4	181
1425	30	25	5	20	0	20	91	3566	5.2	1.5	180
1426	35	20	15	10	20	0	85	3573	3.6	1.4	68
1427	35	25	5	20	15	0	92	3575	3.1	1.4	70
1428	30	25	10	10	20	5	89	3575	4.3	1.5	103
1429	30	30	0	20	15	5	92	3577	3.8	1.5	104
1430	35	15	20	5	10	15	82	3578	5.2	1.3	143
1431	30	20	15	5	10	20	86	3580	5.9	1.5	176
1432	35	20	10	15	5	15	89	3580	4.7	1.3	142
1433	30	25	5	15	5	20	91	3582	5.4	1.5	175
1434	30	15	20	0	0	35	82	3585	7.5	1.4	241
1435	35	20	15	5	25	0	86	3589	3.8	1.4	66
1436	30	25	10	5	25	5	89	3590	4.4	1.6	100
1437	35	25	5	15	20	0	93	3591	3.3	1.4	68
1438	30	30	0	15	20	5	90	3592	4.0	1.6	101
1439	35	15	20	0	15	15	83	3595	5.4	1.3	138
1440	30	20	15	0	15	20	86	3596	6.1	1.5	171
1441	35	20	10	10	10	15	90	3598	4.9	1.3	138
1442	30	25	5	10	10	20	90	3599	5.6	1.5	170
1443	35	20	15	0	30	0	87	3606	4.0	1.4	63
1444	35	20	15	25	0	5	82	3606	3.5	1.3	103
1445	30	25	10	0	30	5	89	3606	4.6	1.6	97
1446	30	20	10	5	0	35	88	3606	7.2	1.4	229
1447	25	25	5	5	0	40	87	3607	7.9	1.6	261
1448	35	25	5	10	25	0	92	3609	3.5	1.4	65
1449	30	30	0	10	25	5	89	3609	4.1	1.6	98
1450	35	20	10	5	15	15	90	3617	5.1	1.4	134
1451	30	25	5	5	15	20	89	3617	5.8	1.5	165
1452	35	20	15	20	5	5	83	3622	3.7	1.3	100
1453	30	30	0	30	0	10	92	3625	3.8	1.5	136
1454	35	25	5	30	0	5	90	3626	3.2	1.3	101
1455	40	20	10	30	0	0	86	3626	2.5	1.2	67
1456	25	25	5	0	5	40	85	3627	8.0	1.6	253
1457	30	20	10	0	5	35	87	3627	7.4	1.5	223
1458	30	30	0	5	30	5	87	3627	4.3	1.6	95
1459	35	25	5	5	30	0	91	3628	3.7	1.4	63
1460	30	25	0	10	0	35	85	3632	6.9	1.5	218

1461	30	25	5	0	20	20	87	3637	5.9	1.5	160
1462	35	20	15	15	10	5	84	3639	3.8	1.4	97
1463	30	30	0	25	5	10	92	3642	4.0	1.5	132
1464	35	25	5	25	5	5	91	3643	3.4	1.4	98
1465	40	20	10	25	5	0	87	3644	2.7	1.2	64
1466	30	30	0	0	35	5	85	3647	4.5	1.6	92
1467	30	20	15	10	0	25	84	3647	6.1	1.5	205
1468	35	25	5	0	35	0	89	3648	3.9	1.5	61
1469	35	15	20	10	0	20	80	3648	5.5	1.3	170
1470	30	25	0	5	5	35	83	3655	7.1	1.5	211
1471	35	20	15	10	15	5	85	3656	4.0	1.4	94
1472	40	15	20	10	15	0	81	3658	3.4	1.2	60
1473	30	30	0	20	10	10	91	3660	4.2	1.6	129
1474	35	25	5	20	10	5	92	3662	3.5	1.4	95
1475	30	20	15	5	5	25	85	3666	6.3	1.5	199
1476	35	15	20	5	5	20	81	3668	5.6	1.3	165
1477	30	25	5	15	0	25	90	3672	5.8	1.5	196
1478	30	25	10	5	20	10	89	3673	4.9	1.6	125
1479	35	20	10	15	0	20	89	3674	5.2	1.3	164
1480	35	20	15	5	20	5	86	3675	4.2	1.4	91
1481	40	15	20	5	20	0	82	3678	3.6	1.2	58
1482	30	30	0	15	15	10	90	3679	4.4	1.6	125
1483	35	25	5	15	15	5	92	3682	3.7	1.4	92
1484	30	20	15	0	10	25	85	3685	6.5	1.5	193
1485	35	15	20	0	10	20	82	3688	5.8	1.3	161
1486	30	25	10	0	25	10	88	3692	5.1	1.6	121
1487	30	25	5	10	5	25	89	3693	6.0	1.5	191
1488	35	20	15	0	25	5	87	3695	4.4	1.4	88
1489	35	20	10	10	5	20	89	3696	5.3	1.3	159
1490	40	15	20	0	25	0	83	3699	3.7	1.3	56
1491	30	30	0	10	20	10	88	3700	4.6	1.6	121
1492	35	25	5	10	20	5	91	3703	3.9	1.4	89
1493	35	20	15	20	0	10	82	3704	4.1	1.3	126
1494	30	25	5	5	10	25	88	3715	6.2	1.5	185
1495	35	20	10	5	10	20	89	3720	5.5	1.4	154
1496	30	30	0	5	25	10	87	3721	4.8	1.6	117
1497	35	20	15	15	5	10	83	3724	4.3	1.4	122
1498	35	25	5	5	25	5	90	3726	4.1	1.5	86
1499	35	25	5	25	0	10	90	3732	3.8	1.4	123
1500	30	20	10	0	0	40	86	3733	7.8	1.5	240
1501	40	20	10	25	0	5	87	3737	3.1	1.2	89
1502	30	25	5	0	15	25	86	3739	6.4	1.6	180
1503	30	30	0	0	30	10	85	3744	5.0	1.6	114
1504	35	20	15	10	10	10	84	3745	4.5	1.4	119
1505	35	20	10	0	15	20	89	3745	5.7	1.4	150
1506	30	30	0	20	5	15	91	3749	4.6	1.6	152
1507	40	15	20	10	10	5	80	3750	3.8	1.2	85
1508	35	25	5	0	30	5	88	3751	4.3	1.5	83
1509	35	25	5	20	5	10	91	3755	4.0	1.4	119
1510	40	20	10	20	5	5	88	3761	3.3	1.2	86
1511	35	15	20	5	0	25	81	3763	6.1	1.3	187

1512	35	20	15	5	15	10	85	3767	4.7	1.4	115
1513	30	30	0	15	10	15	90	3771	4.8	1.6	148
1514	35	25	10	25	5	0	85	3773	2.9	1.4	72
1515	30	25	0	5	0	40	82	3773	7.5	1.5	227
1516	40	15	20	5	15	5	81	3774	4.0	1.2	82
1517	35	25	5	15	10	10	91	3778	4.2	1.4	115
1518	30	20	15	0	5	30	85	3780	6.9	1.5	215
1519	35	30	0	35	0	0	91	3783	2.4	1.4	74
1520	35	15	20	0	5	25	82	3788	6.3	1.3	182
1521	35	20	15	0	20	10	86	3791	4.8	1.4	112
1522	30	25	5	10	0	30	89	3792	6.4	1.5	211
1523	35	25	10	20	10	0	86	3794	3.1	1.4	70
1524	30	30	0	10	15	15	88	3796	5.0	1.6	144
1525	40	15	20	0	20	5	83	3799	4.2	1.3	80
1526	35	20	10	10	0	25	89	3801	5.8	1.4	180
1527	35	25	5	10	15	10	91	3804	4.4	1.4	112
1528	35	30	0	30	5	0	92	3805	2.6	1.5	72
1529	35	20	15	15	0	15	83	3814	4.7	1.4	147
1530	35	25	10	15	15	0	87	3816	3.3	1.5	67
1531	30	25	5	5	5	30	87	3819	6.6	1.5	205
1532	30	30	0	5	20	15	86	3821	5.2	1.6	139
1533	35	20	20	0	25	0	81	3827	4.0	1.5	62
1534	35	30	0	25	10	0	92	3829	2.8	1.5	70
1535	35	20	10	5	5	25	88	3830	6.0	1.4	174
1536	35	25	5	5	20	10	89	3831	4.5	1.5	108
1537	35	20	15	10	5	15	84	3839	4.9	1.4	143
1538	35	25	10	10	20	0	88	3840	3.5	1.5	65
1539	35	25	0	15	0	25	88	3847	5.5	1.4	171
1540	30	25	5	0	10	30	86	3848	6.8	1.6	199
1541	30	30	0	0	25	15	84	3849	5.4	1.7	135
1542	35	25	5	20	0	15	91	3853	4.4	1.4	142
1543	35	30	0	20	15	0	92	3854	3.0	1.5	67
1544	35	20	10	0	10	25	88	3860	6.2	1.4	169
1545	35	25	5	0	25	10	88	3861	4.7	1.5	105
1546	40	20	10	20	0	10	87	3865	3.8	1.2	110
1547	35	20	15	5	10	15	85	3865	5.1	1.4	139
1548	35	25	10	5	25	0	89	3865	3.7	1.5	63
1549	40	20	15	25	0	0	80	3868	2.7	1.3	64
1550	40	15	20	5	10	10	81	3877	4.4	1.3	106
1551	35	30	0	15	20	0	91	3881	3.2	1.5	65
1552	35	25	5	15	5	15	91	3881	4.6	1.4	138
1553	35	25	10	0	30	0	89	3892	3.8	1.5	61
1554	35	20	15	0	15	15	85	3893	5.3	1.4	134
1555	40	20	15	20	5	0	81	3894	2.9	1.3	61
1556	35	15	20	0	0	30	81	3894	6.7	1.4	203
1557	40	20	10	15	5	10	89	3895	3.9	1.3	106
1558	30	30	0	10	10	20	87	3898	5.4	1.6	165
1559	35	30	0	30	0	5	92	3898	3.0	1.5	98
1560	40	15	20	0	15	10	82	3907	4.6	1.3	103
1561	35	25	10	15	10	5	86	3908	3.7	1.5	93
1562	35	30	0	10	25	0	89	3910	3.4	1.5	63

1563	40	25	5	30	0	0	89	3911	2.4	1.3	64
1564	35	25	5	10	10	15	90	3912	4.8	1.5	134
1565	40	20	15	15	10	0	83	3921	3.1	1.3	59
1566	35	30	0	25	5	5	92	3925	3.2	1.5	95
1567	30	30	0	5	15	20	86	3928	5.6	1.6	160
1568	30	25	5	5	0	35	87	3931	7.1	1.5	224
1569	35	25	10	10	15	5	87	3935	3.9	1.5	90
1570	35	20	15	10	0	20	83	3938	5.3	1.4	166
1571	40	25	5	25	5	0	90	3940	2.6	1.3	62
1572	35	30	0	5	30	0	87	3941	3.5	1.6	60
1573	35	25	5	5	15	15	89	3944	5.0	1.5	130
1574	35	20	10	5	0	30	88	3948	6.4	1.4	193
1575	40	20	15	10	15	0	84	3950	3.2	1.3	57
1576	35	30	0	20	10	5	91	3955	3.4	1.5	92
1577	30	30	0	0	20	20	84	3960	5.8	1.7	156
1578	35	25	10	5	20	5	88	3965	4.1	1.5	88
1579	30	25	5	0	5	35	85	3965	7.3	1.6	217
1580	35	20	15	5	5	20	84	3969	5.5	1.4	161
1581	40	25	5	20	10	0	91	3971	2.8	1.3	59
1582	35	30	0	0	35	0	85	3974	3.7	1.6	58
1583	35	25	5	0	20	15	87	3979	5.2	1.5	126
1584	40	20	15	5	20	0	85	3981	3.4	1.4	55
1585	35	20	10	0	5	30	87	3985	6.6	1.4	187
1586	35	30	0	15	15	5	90	3986	3.6	1.5	89
1587	40	15	20	5	5	15	80	3986	4.9	1.3	129
1588	35	25	5	15	0	20	90	3991	5.0	1.4	160
1589	40	20	15	20	0	5	81	3992	3.3	1.3	87
1590	35	25	10	0	25	5	88	3996	4.3	1.5	85
1591	35	20	15	0	10	20	85	4001	5.7	1.5	156
1592	40	25	5	15	15	0	91	4005	2.9	1.4	57
1593	40	20	10	15	0	15	88	4011	4.4	1.3	128
1594	35	25	0	10	0	30	85	4013	6.1	1.4	183
1595	40	20	15	0	25	0	86	4015	3.6	1.4	53
1596	35	30	0	10	20	5	89	4019	3.8	1.6	86
1597	40	15	20	0	10	15	81	4021	5.1	1.3	125
1598	40	20	15	15	5	5	82	4023	3.5	1.3	85
1599	35	25	5	10	5	20	89	4027	5.2	1.5	155
1600	35	30	0	25	0	10	91	4028	3.7	1.5	119
1601	40	25	5	10	20	0	91	4041	3.1	1.4	55
1602	40	25	5	25	0	5	89	4048	3.0	1.3	86
1603	40	20	10	10	5	15	89	4049	4.6	1.3	124
1604	35	30	0	5	25	5	87	4055	4.0	1.6	83
1605	40	20	15	10	10	5	83	4057	3.7	1.3	82
1606	35	30	0	20	5	10	91	4062	3.9	1.5	115
1607	35	25	5	5	10	20	88	4065	5.4	1.5	150
1608	35	20	15	5	0	25	83	4079	6.0	1.4	183
1609	40	25	5	5	25	0	90	4080	3.3	1.4	53
1610	40	25	5	20	5	5	90	4084	3.2	1.4	83
1611	30	25	5	0	0	40	85	4090	7.7	1.6	234
1612	40	20	10	5	10	15	89	4091	4.8	1.3	120
1613	40	20	15	5	15	5	84	4093	3.9	1.4	79

1614	35	30	0	0	30	5	85	4094	4.2	1.6	80
1615	35	30	0	15	10	10	90	4098	4.0	1.5	112
1616	35	25	5	0	15	20	87	4106	5.6	1.5	145
1617	35	25	10	0	20	10	87	4106	4.7	1.6	108
1618	35	20	15	0	5	25	84	4117	6.2	1.5	177
1619	45	15	20	5	15	0	80	4118	3.2	1.2	48
1620	35	20	10	0	0	35	86	4118	7.0	1.4	205
1621	40	25	5	0	30	0	89	4122	3.5	1.4	51
1622	40	25	5	15	10	5	91	4123	3.4	1.4	81
1623	40	20	15	0	20	5	85	4131	4.1	1.4	77
1624	40	20	15	15	0	10	81	4132	3.9	1.3	109
1625	35	30	0	10	15	10	88	4136	4.2	1.6	108
1626	40	15	20	0	5	20	80	4144	5.5	1.3	146
1627	35	25	5	10	0	25	88	4149	5.7	1.5	175
1628	40	25	10	25	0	0	83	4156	2.6	1.4	61
1629	40	25	5	10	15	5	91	4165	3.6	1.4	78
1630	40	20	15	10	5	10	82	4170	4.1	1.4	106
1631	35	30	0	5	20	10	87	4178	4.4	1.6	105
1632	40	20	10	10	0	20	88	4180	5.0	1.3	145
1633	40	25	10	20	5	0	84	4192	2.8	1.4	58
1634	35	25	5	5	5	25	88	4194	5.9	1.5	170
1635	40	25	5	20	0	10	90	4205	3.6	1.4	106
1636	35	25	0	5	0	35	82	4210	6.7	1.4	193
1637	40	25	5	5	20	5	90	4211	3.8	1.4	75
1638	40	20	15	5	10	10	83	4212	4.3	1.4	103
1639	35	30	0	15	5	15	89	4217	4.5	1.5	134
1640	35	30	0	0	25	10	85	4223	4.6	1.6	101
1641	40	30	0	30	0	0	90	4225	2.3	1.4	61
1642	40	20	10	5	5	20	88	4229	5.2	1.3	140
1643	40	25	10	15	10	0	85	4231	2.9	1.4	56
1644	45	20	10	20	0	5	86	4238	3.0	1.2	75
1645	35	25	5	0	10	25	86	4242	6.0	1.5	164
1646	40	25	5	15	5	10	90	4250	3.8	1.4	103
1647	40	20	15	0	15	10	84	4256	4.5	1.4	99
1648	40	25	5	0	25	5	88	4260	3.9	1.4	73
1649	35	30	0	10	10	15	88	4261	4.7	1.6	130
1650	40	30	0	25	5	0	91	4267	2.4	1.4	59
1651	40	25	10	10	15	0	86	4272	3.1	1.5	54
1652	40	20	10	0	10	20	87	4282	5.4	1.3	136
1653	40	20	15	10	0	15	81	4291	4.6	1.4	129
1654	45	15	20	0	15	5	80	4293	3.8	1.2	69
1655	40	25	5	10	10	10	90	4298	4.0	1.4	100
1656	35	30	0	5	15	15	86	4309	4.9	1.6	126
1657	40	30	0	20	10	0	91	4312	2.6	1.5	57
1658	40	25	10	5	20	0	87	4317	3.3	1.5	52
1659	35	25	5	5	0	30	87	4332	6.3	1.5	188
1660	40	20	15	5	5	15	82	4338	4.7	1.4	125
1661	40	25	5	5	15	10	89	4351	4.2	1.4	96
1662	40	30	0	15	15	0	91	4360	2.8	1.5	55
1663	35	30	0	0	20	15	84	4361	5.0	1.6	122
1664	40	25	10	0	25	0	87	4364	3.5	1.5	50

1665	40	20	10	5	0	25	87	4378	5.6	1.3	159
1666	40	25	5	15	0	15	89	4385	4.3	1.4	124
1667	45	20	15	15	5	0	80	4386	2.7	1.3	49
1668	35	25	5	0	5	30	85	4388	6.5	1.5	182
1669	40	20	15	0	10	15	83	4389	4.9	1.4	121
1670	40	30	0	25	0	5	91	4391	2.9	1.4	83
1671	40	25	5	0	20	10	88	4408	4.4	1.5	93
1672	40	30	0	10	20	0	89	4412	3.0	1.5	53
1673	45	20	10	15	0	10	87	4432	3.6	1.2	94
1674	45	25	5	25	0	0	88	4434	2.2	1.3	51
1675	45	20	15	10	10	0	81	4437	2.9	1.3	47
1676	40	20	10	0	5	25	86	4440	5.8	1.4	154
1677	40	25	5	10	5	15	89	4441	4.4	1.4	121
1678	40	30	0	20	5	5	91	4442	3.1	1.5	80
1679	40	25	10	5	15	5	86	4444	3.8	1.5	76
1680	40	30	0	5	25	0	87	4469	3.2	1.5	51
1681	40	20	15	5	0	20	81	4473	5.2	1.4	146
1682	45	25	5	20	5	0	89	4490	2.4	1.3	49
1683	45	20	15	5	15	0	83	4492	3.1	1.3	45
1684	45	20	10	10	5	10	88	4494	3.8	1.2	91
1685	40	30	0	15	10	5	90	4497	3.3	1.5	78
1686	40	25	10	0	20	5	86	4499	3.9	1.5	74
1687	40	25	5	5	10	15	88	4502	4.6	1.4	117
1688	35	30	0	0	15	20	84	4509	5.5	1.6	141
1689	40	30	0	0	30	0	86	4530	3.4	1.6	49
1690	40	20	15	0	5	20	82	4531	5.4	1.4	142
1691	35	25	5	0	0	35	85	4545	6.9	1.5	200
1692	45	25	5	15	10	0	90	4550	2.6	1.3	47
1693	45	20	15	0	20	0	84	4551	3.3	1.3	43
1694	40	30	0	10	15	5	89	4556	3.4	1.5	75
1695	40	25	5	0	15	15	87	4568	4.8	1.5	113
1696	45	20	15	10	5	5	81	4575	3.3	1.3	71
1697	40	30	0	20	0	10	90	4580	3.5	1.5	103
1698	40	25	5	10	0	20	88	4594	4.9	1.4	141
1699	40	20	10	0	0	30	85	4610	6.3	1.4	171
1700	45	25	5	10	15	0	90	4616	2.8	1.3	46
1701	40	30	0	5	20	5	87	4621	3.6	1.5	72
1702	45	20	15	5	10	5	82	4637	3.5	1.3	68
1703	45	25	5	20	0	5	88	4638	2.8	1.3	72
1704	40	30	0	15	5	10	90	4642	3.7	1.5	100
1705	45	20	10	10	0	15	87	4659	4.2	1.3	111
1706	40	25	5	5	5	20	87	4663	5.1	1.4	136
1707	45	25	5	5	20	0	90	4687	3.0	1.4	44
1708	40	30	0	0	25	5	85	4691	3.8	1.6	70
1709	50	20	10	20	0	0	85	4704	2.2	1.1	42
1710	45	20	15	0	15	5	83	4705	3.7	1.3	66
1711	45	25	5	15	5	5	89	4707	3.0	1.3	70
1712	40	30	0	10	10	10	88	4710	3.9	1.5	96
1713	45	20	10	5	5	15	87	4737	4.4	1.3	108
1714	40	25	5	0	10	20	86	4740	5.3	1.5	132
1715	45	25	5	0	25	0	88	4766	3.2	1.4	42

1716	40	25	0	5	0	30	82	4782	5.9	1.4	162
1717	45	25	5	10	10	5	89	4782	3.2	1.4	67
1718	40	30	0	5	15	10	87	4783	4.1	1.5	93
1719	45	20	15	5	5	10	81	4793	4.0	1.3	91
1720	45	20	10	0	10	15	87	4823	4.6	1.3	104
1721	45	30	0	25	0	0	89	4833	2.1	1.4	49
1722	40	25	5	5	0	25	86	4837	5.5	1.5	155
1723	40	30	0	0	20	10	85	4863	4.3	1.6	90
1724	45	25	5	5	15	5	89	4864	3.4	1.4	65
1725	45	20	15	0	10	10	82	4869	4.2	1.4	88
1726	45	25	5	15	0	10	88	4875	3.5	1.3	91
1727	45	25	10	5	15	0	84	4902	3.0	1.4	43
1728	45	30	0	20	5	0	90	4909	2.3	1.4	47
1729	40	25	5	0	5	25	85	4924	5.7	1.5	149
1730	45	20	10	5	0	20	86	4927	4.8	1.3	127
1731	45	25	5	0	20	5	88	4954	3.6	1.4	62
1732	45	25	5	10	5	10	88	4961	3.7	1.4	88
1733	50	20	10	15	0	5	85	4964	2.8	1.2	62
1734	45	25	10	0	20	0	85	4982	3.2	1.5	41
1735	45	30	0	15	10	0	90	4990	2.5	1.4	45
1736	45	20	15	0	5	15	80	5045	4.6	1.4	108
1737	40	30	0	0	15	15	84	5049	4.7	1.6	109
1738	40	30	0	10	0	20	87	5050	4.8	1.5	136
1739	45	25	5	5	10	10	88	5054	3.9	1.4	85
1740	45	25	10	5	10	5	83	5068	3.4	1.4	65
1741	45	30	0	20	0	5	89	5078	2.7	1.4	69
1742	45	30	0	10	15	0	89	5079	2.7	1.5	43
1743	40	25	5	0	0	30	84	5124	6.1	1.5	167
1744	40	30	0	5	5	20	85	5144	4.9	1.6	132
1745	45	25	5	10	0	15	87	5152	4.1	1.4	108
1746	45	25	5	0	15	10	87	5157	4.0	1.4	82
1747	45	25	10	0	15	5	84	5157	3.6	1.5	63
1748	45	30	0	15	5	5	89	5170	2.9	1.5	67
1749	45	30	0	5	20	0	87	5176	2.9	1.5	41
1750	50	25	5	20	0	0	86	5178	2.1	1.3	40
1751	45	20	10	0	0	25	84	5246	5.5	1.3	140
1752	40	30	0	0	10	20	84	5248	5.1	1.6	128
1753	45	25	5	5	5	15	87	5259	4.3	1.4	104
1754	50	20	15	0	15	0	81	5265	2.9	1.3	34
1755	45	30	0	10	10	5	88	5270	3.1	1.5	64
1756	50	25	5	15	5	0	87	5281	2.3	1.3	38
1757	45	30	0	0	25	0	85	5282	3.0	1.5	40
1758	45	25	10	0	10	10	82	5345	4.0	1.5	84
1759	45	30	0	15	0	10	88	5362	3.4	1.5	88
1760	45	25	5	0	10	15	86	5377	4.5	1.4	101
1761	45	30	0	5	15	5	87	5380	3.3	1.5	62
1762	50	25	5	10	10	0	88	5394	2.4	1.3	37
1763	45	30	0	10	5	10	87	5475	3.5	1.5	85
1764	45	25	5	5	0	20	86	5479	4.7	1.4	123
1765	50	25	5	15	0	5	86	5492	2.7	1.3	60
1766	45	30	0	0	20	5	85	5500	3.5	1.5	60

1767	50	25	5	5	15	0	88	5519	2.6	1.3	35
1768	45	30	0	5	10	10	86	5599	3.7	1.5	82
1769	45	25	5	0	5	20	85	5614	4.9	1.4	118
1770	50	25	5	10	5	5	87	5621	2.9	1.3	57
1771	50	20	10	5	0	15	85	5637	4.1	1.2	96
1772	50	25	5	0	20	0	87	5658	2.8	1.4	33
1773	50	25	10	5	10	0	81	5673	2.6	1.4	34
1774	50	30	0	20	0	0	87	5698	1.9	1.4	38
1775	45	30	0	0	15	10	85	5736	3.9	1.5	79
1776	50	25	5	5	10	5	87	5763	3.1	1.3	55
1777	50	20	10	0	5	15	85	5793	4.3	1.3	92
1778	50	25	10	0	15	0	82	5802	2.8	1.4	32
1779	50	30	0	15	5	0	88	5832	2.1	1.4	36
1780	50	25	5	10	0	10	86	5865	3.3	1.3	77
1781	45	25	5	0	0	25	84	5871	5.3	1.4	135
1782	50	25	5	0	15	5	86	5920	3.3	1.4	53
1783	50	30	0	10	10	0	88	5979	2.3	1.4	34
1784	50	25	5	5	5	10	86	6026	3.5	1.4	74
1785	55	20	10	10	0	5	83	6064	2.7	1.2	51
1786	50	30	0	15	0	5	86	6074	2.6	1.4	57
1787	50	20	10	0	0	20	83	6082	4.7	1.3	110
1788	50	30	0	5	15	0	87	6141	2.5	1.5	33
1789	50	25	5	0	10	10	85	6206	3.7	1.4	71
1790	50	30	0	10	5	5	86	6240	2.8	1.4	55
1791	55	25	5	15	0	0	84	6282	1.9	1.3	30
1792	50	25	5	5	0	15	84	6312	3.9	1.4	93
1793	50	30	0	0	20	0	86	6322	2.7	1.5	31
1794	50	30	0	5	10	5	86	6424	2.9	1.5	53
1795	55	25	5	10	5	0	85	6474	2.1	1.3	28
1796	50	25	5	0	5	15	84	6517	4.1	1.4	89
1797	55	20	10	5	0	10	82	6576	3.3	1.2	67
1798	50	25	0	5	0	20	84	6580	4.4	1.3	104
1799	50	30	0	0	15	5	85	6629	3.1	1.5	50
1800	55	25	5	5	10	0	85	6689	2.3	1.3	27
1801	55	25	5	10	0	5	83	6793	2.5	1.3	48
1802	55	20	10	0	5	10	83	6819	3.5	1.2	64
1803	50	25	5	0	0	20	82	6859	4.6	1.4	106
1804	55	25	5	0	15	0	85	6932	2.5	1.3	26
1805	55	25	5	5	5	5	84	7038	2.7	1.3	46
1806	55	25	0	10	0	10	87	7191	3.0	1.2	64
1807	55	20	10	0	0	15	81	7212	3.9	1.2	81
1808	50	25	0	0	0	25	81	7306	5.0	1.3	114
1809	55	25	5	0	10	5	84	7316	2.9	1.3	44
1810	60	20	10	5	5	0	81	7411	2.1	1.1	21
1811	55	25	5	5	0	10	82	7422	3.2	1.3	64
1812	55	25	0	5	5	10	85	7531	3.2	1.2	62
1813	55	25	5	0	5	10	82	7742	3.3	1.3	62
1814	60	20	10	0	10	0	82	7747	2.3	1.2	20
1815	60	25	0	15	0	0	88	7871	1.6	1.1	24
1816	55	25	0	0	10	10	83	7928	3.4	1.3	59
1817	55	25	0	5	0	15	85	8051	3.6	1.3	77

1818	60	25	0	10	5	0	88	8288	1.8	1.2	22
1819	60	25	5	5	5	0	80	8429	1.9	1.3	20
1820	55	25	0	0	5	15	83	8523	3.8	1.3	74
1821	60	25	0	5	10	0	86	8781	1.9	1.2	21

Bibliography

[1] International Energy Agency. Technical report, International Energy Agency, (2006).

[2] Achermann, M., Petruska, M. a., Kos, S., Smith, D. L., Koleske, D. D., and Klimov, V. I. *Nature* **429**(6992), 642–6 June (2004).

[3] Klimov, V. *Nanocrystal Quantum Dots*. 2nd editio edition, (2012).

[4] Narayanaswamy, A., A. Meijerink, L. F. F., and P J Van Der Zaag. *ACSNano* **3**(9), 2539–2546 (2009).

[5] Nizamoglu, S. and Demir, H. V. *Journal of Optics A: Pure and Applied Optics* **9**(9), S419–S424 September (2007).

[6] Smith, A. M. and Nie, S. *Accounts of chemical research* **43**(2), 190–200 February (2010).

[7] Reiss, P., Protière, M., and Li, L. *Small (Weinheim an der Bergstrasse, Germany)* **5**(2), 154–68 February (2009).

[8] Yin, Y. and Alivisatos, A. P. *Nature* **437**, 664–670 (2005).

[9] Xu, S., Ziegler, J., and Nann, T. *Journal of Materials Chemistry* **18**(23), 2653–2656 (2008).

[10] Li, L. and Reiss, P. *J. Am. Chem. Soc.* **130**(35), 11588–11589 (2008).

[11] Xie, R., Battaglia, D., and Peng, X. *Journal of the American Chemical Society* **129**(50), 15432–3 December (2007).

[12] Www.NN-Labs.com.

[13] Achermann, M., Petruska, M. a., Koleske, D. D., Crawford, M. H., and Klimov, V. I. *Nano letters* **6**(7), 1396–400 July (2006).

[14] de Mello Donega, C., Hickey, S. G., Wuister, S. F., Vanmaekelbergh, D., and Meijerink, A. *ChemInform* **34**(12), 489–496 March (2003).

[15] Wehrenberg, B. L., Wang, C., and Guyot-Sionnest, P. *The Journal of Physical Chemistry B* **106**(41), 10634–10640 October (2002).

[16] Rosner, S. J., Carr, E. C., Ludowise, M. J., Girolami, G., and Erikson, H. I. *Applied Physics Letters* **70**(4), 420 (1997).

[17] Pophristic, M., Long, F. H., Tran, C., Karlicek, R. F., Feng, Z. C., and Ferguson, I. T. *Applied Physics Letters* **73**(6), 815 (1998).

[18] Chen, F., Kirkey, W., Furis, M., Cheung, M., and Cartwright, A. *Solid State Communications* **125**(11-12), 617–622 March (2003).

[19] Chichibu, S., Wada, K., and Nakamura, S. *Applied Physics Letters* **71**(16), 2346 (1997).

[20] Gardner, N. F., Muller, G. O., Shen, Y. C., Chen, G., Watanabe, S., Gotz, W., and Krames, M. R. *Applied Physics Letters* **91**(24), 243506 (2007).

[21] Swathi, R. S. and Sebastian, K. L. *Journal of Chemical Sciences* **121**(5), 777–787 November (2009).

[22] Chanyawadee, S., Lagoudakis, P. G., Harley, R. T., Charlton, M. D. B., Talapin, D. V., Huang, H. W., and Lin, C.-H. *Advanced materials (Deerfield Beach, Fla.)* **22**(5), 602–6 February (2010).

[23] Nizamoglu, S., Zengin, G., and Demir, H. V. *Applied Physics Letters* **92**(3), 031102 (2008).

[24] CIE. *International Lighting Vocabulary, CIE 17.4-1987*. 4th edition, (1987).

[25] Narukawa, Y., Ichikawa, M., Sanga, D., Sano, M., and Mukai, T. *Journal of Physics D: Applied Physics* **43**(35), 354002 September (2010).

[26] Günter Wyszecki, W. S. *Color Science - Concepts and Methods, Quantitative Data and Formulae (2nd ed.)*. Wiley-Interscience, (2000).

[27] V. Lampret, J. Peternelj, A. K. *Solar Energy Materials and Solar Cells* **73**(5), 319–329 (2002).

[28] Www.Osram.com.

[29] Zheludev, N. **1**(April), 189–192 (2007).

[30] Schubert, E. F. *Light-Emitting Diodes*. Cambridge University Press, 2nd edition, (2006).

[31] Li, Y.-L., Gessmann, T., Schubert, E. F., and Sheu, J. K. *Journal of Applied Physics* **94**(4), 2167 (2003).

[32] Chhajed, S., Xi, Y., Li, Y.-L., Gessmann, T., and Schubert, E. F. *Journal of Applied Physics* **97**(5), 054506 (2005).

[33] Nakamura, S., Mukai, T., and Senoh, M. *Applied Physics Letters* **64**(13), 1687 (1994).

[34] Kanji Bando, Kensho Sakano, Yasunobu Noguchi, Y. S. In *Lux Pacifica 3rd Pacific Basin Lighting Congress*, (1997).

[35] Lin, C. C. and Liu, R.-S. *The Journal of Physical Chemistry Letters* **2**(11), 1268–1277 June (2011).

[36] Itskos, G., Belton, C. R., Heliotis, G., Watson, I. M., Dawson, M. D., Murray, R., and Bradley, D. D. C. *Nanotechnology* **20**(27), 275207 July (2009).

[37] Eaton, D. F. *Pure & Appl. Chem.,* **60**(7), 1107–1114 (1988).

[38] Shirazi, R., Kopylov, O., Kovacs, A., and Kardynał, B. E. *Applied Physics Letters* **101**(9), 091910 (2012).

[39] Jiang, Z.-j. and Kelley, D. F. *Nano Letters* **11**, 4067–4073 (2011).

[40] Lo, S. S., Khan, Y., Jones, M., and Scholes, G. D. *The Journal of chemical physics* **131**(8), 084714 August (2009).

[41] Knowles, K. E., Mcarthur, E. A., and Weiss, E. A. *ACS Nano* **5**(3), 2026–2035 (2011).

[42] Jones, M. and Scholes, G. D. *Journal of Materials Chemistry* **20**(18), 3533 (2010).

[43] Micic, O. I., Cheong, H. M., Fu, H., Zunger, A., Sprague, J. R., Mascarenhas, A., and Nozik, A. J. **5647**(97), 4904–4912 (1997).

[44] Pijpers, J., Hendry, E., Milder, M., Fanciulli, R., Savolainen, J., Herek, J., Vanmaekelbergh, D., Ruhman, S., Mocatta, D., Oron, D., Aharoni, a., Banin, U., and Bonn, M. *Journal of Physical Chemistry C* **111**(11), 4146–4152 March (2007).

[45] van Driel, a., Nikolaev, I., Vergeer, P., Lodahl, P., Vanmaekelbergh, D., and Vos, W. *Physical Review B* **75**(3), 1–8 January (2007).

[46] Nikolaev, I., Lodahl, P., van Driel, a., Koenderink, a., and Vos, W. *Physical Review B* **75**(11), 115302 March (2007).

[47] Fisher, B. R., Stott, N. E., and Bawendi, M. G. *Journal of Physical Chemistry B* **118**(1), 143–148 (2004).

[48] Tang, J. and Marcus, R. a. *The Journal of chemical physics* **123**(20), 204511 November (2005).

[49] van Driel, a., Allan, G., Delerue, C., Lodahl, P., Vos, W., and Vanmaekelbergh, D. *Physical Review Letters* **95**(23), 1–4 December (2005).

[50] Thuy, U. T. D., Thuy, P. T., Liem, N. Q., Li, L., and Reiss, P. *Applied Physics Letters* **96**(7), 073102 (2010).

[51] Kim, M. R., Chung, J. H., Lee, M., Lee, S., and Jang, D.-J. *Journal of colloid and interface science* **350**(1), 5–9 October (2010).

[52] Li, C., Ando, M., Enomoto, H., and Murase, N. *The Journal of Physical Chemistry C* **112**(51), 20190–20199 December (2008).

[53] Wolters, R. H., Heath, J. R., and Introduction, I. **105**(18), 7957–7963 (1996).

[54] Jones, M. and Scholes, G. D. *Journal of Materials Chemistry* **20**(18), 3533 (2010).

[55] Yang, X., Zhao, D., Leck, K. S., Tan, S. T., Tang, Y. X., Zhao, J., Demir, H. V., and Sun, X. W. *Advanced materials (Deerfield Beach, Fla.)* **24**(30), 4180–5 August (2012).

[56] Hines, M. a. and Guyot-Sionnest, P. *The Journal of Physical Chemistry* **100**(2), 468–471 January (1996).

[57] van Dijken, a., Makkinje, J., and Meijerink, A. *Journal of Luminescence* **92**(4), 323–328 April (2001).

[58] Luo, J., Franceschetti, a., and Zunger, a. *Physical Review B* **79**(20), 201301 May (2009).

[59] Crooker, S. a., Barrick, T., Hollingsworth, J. a., and Klimov, V. I. *Applied Physics Letters* **82**(17), 2793 (2003).

[60] Bawendi, M. G., Carroll, P. J., Wilson, W. L., and Brus, L. E. *The Journal of Chemical Physics* **96**(2), 946 (1992).

[61] Franceschetti, a., Fu, H., Wang, L., and Zunger, a. *Physical Review B* **60**(3), 1819–1829 July (1999).

[62] Wuister, S. F., de Mello Donega, C., and Meijerink, A. *The Journal of chemical physics* **121**(9), 4310–5 September (2004).

[63] Cichos, F., Vonborczyskowski, C., and Orrit, M. *Current Opinion in Colloid & Interface Science* **12**(6), 272–284 December (2007).

[64] Zan, F., Dong, C., Liu, H., and Ren, J. *The Journal of Physical Chemistry C* **116**(6), 3944–3950 February (2012).

[65] Sugisaki, M., Ren, H.-W., Nishi, K., and Masumoto, Y. *Physical Review Letters* **86**(21), 4883–4886 May (2001).

[66] Yao, J., Larson, D. R., Vishwasrao, H. D., Zipfel, W. R., and Webb, W. W. *Proceedings of the National Academy of Sciences of the United States of America* **102**(40), 14284–9 October (2005).

[67] Talapin, D. V., Rogach, A. L., Shevchenko, E. V., Kornowski, A., Haase, M., and Weller, H. *Journal of the American Chemical Society* **124**(20), 5782–90 May (2002).

[68] Kamat, P. V. *Journal of Physical Chemistry C* **112**(48), 18737–18753 October (2008).

[69] Page, L. E., Zhang, X., Jawaid, A. M., and Snee, P. T. *Chemical communications (Cambridge, England)* **47**(27), 7773–5 July (2011).

[70] Eisler, H.-J., Sundar, V. C., Bawendi, M. G., Walsh, M., Smith, H. I., and Klimov, V. *Applied Physics Letters* **80**(24), 4614 (2002).

[71] Drexhage, K. H. and Jose, S. *Journal of Luminescence* **2**, 693–701 (1970).

[72] Walters, R., Kalkman, J., Polman, A., Atwater, H., and de Dood, M. *Physical Review B* **73**(13), 132302 April (2006).

[73] Johansen, J., Stobbe, S. r., Nikolaev, I., Lund-Hansen, T., Kristensen, P., Hvam, J. r., Vos, W., and Lodahl, P. *Physical Review B* **77**(7), 073303 February (2008).

[74] Brokmann, X., Coolen, L., Dahan, M., and Hermier, J. *Physical Review Letters* **93**(10), 1–4 September (2004).

[75] R. R. Chance, A. Prock and Silbey, R. In *Advances In Chemical Physics*, volume 37. Wiley, New York (1978).

[76] Jones, M., Lo, S. S., and Scholes, G. D. *Journal of Physical Chemistry Chysical Chemistry* **113**, 18632–18642 (2009).

[77] Chen, Y., Vela, J., Schaller, R. D., Hollingsworth, J. A., and Klimov, V. I. *Nano letters* **9**(10), 3482–3488 (2009).

[78] K. P. O'Donnell, X. C. *Applied Physics Letters* **58**(26), 2924–2926 (1991).

[79] Kang, J., Chen, Y., and Wang, Z. In *8th International Conference on Electronic Materials*, number June, 10–14, (2002).

[80] Pham, T. T., Chi Tran, T. K., and Nguyen, Q. L. *Advances in Natural Sciences: Nanoscience and Nanotechnology* **2**(2), 025001 April (2011).

[81] Moreels, I., Lambert, K., De Muynck, D., Vanhaecke, F., Poelman, D., Martins, J. C., Allan, G., and Hens, Z. *Chemistry of Materials* **19**(25), 6101–6106 December (2007).

[82] Kim, S.-H., Wolters, R. H., and Heath, J. R. *The Journal of Chemical Physics* **105**(18), 7957 (1996).

[83] Fu, H. and Zunger, A. *Physical Review B* **56**(3), 1496–1508 July (1997).

[84] Thuy, P. T., Thuy, U. T. D., Chi, T. T. K., Phuong, L. Q., Liem, N. Q., Li, L., and Reiss, P. *Journal of Physics: Conference Series* **187**, 012014 September (2009).

[85] McGuire, J. a., Joo, J., Pietryga, J. M., Schaller, R. D., and Klimov, V. I. *Accounts of chemical research* **41**(12), 1810–9 December (2008).

[86] Brovelli, S., Schaller, R. D., Crooker, S. a., García-Santamaría, F., Chen, Y., Viswanatha, R., Hollingsworth, J. a., Htoon, H., and Klimov, V. I. *Nature communications* **2**, 280 January (2011).

[87] Seth Coe, Wing-Keung Woo, Moungi Bawendi, V. B. *Letters to nature* **420**(19/26), 800–803 (2002).

[88] Mueller, A. H., Petruska, M. a., Achermann, M., Werder, D. J., Akhadov, E. a., Koleske, D. D., Hoffbauer, M. a., and Klimov, V. I. *Nano letters* **5**(6), 1039–44 June (2005).

[89] Achermann, M., Petruska, M. a., Koleske, D. D., Crawford, M. H., and Klimov, V. I. *Nano letters* **6**(7), 1396–400 July (2006).

[90] Kos, v., Achermann, M., Klimov, V., and Smith, D. *Physical Review B* **71**(20), 205309 May (2005).

[91] D. Ricard, M. Ghanassi, M. S.-K. *Optics Communications* **108**(4-6), 311–318 (1994).

[92] SOPRA. , N & K database.

[93] Leatherdale, C. A., Mikulec, F. V., and Bawendi, M. G. **02139**, 7619–7622 (2002).

[94] Koole, R. , 6511–6520 (2009).

[95] Basko, D., Rocca, G. C. L., Bassani, F., and Agranovich, V. M. **362**, 353–362 (1999).

[96] Rindermann, J., Pozina, G., Monemar, B., Hultman, L., Amano, H., and Lagoudakis, P. *Physical Review Letters* **107**(23), 236805 November (2011).

[97] Főrster, T. *Naturwissenschaften* **33**(166) (1946).

[98] Pophristic, M. and Long, F. H. *Applied Physics Letters* **73**(6), 815–817 (1998).

[99] O. Ambacher, D. Brunner, R. Dimitrov, M. Stutzmann, A. Sohmer and Scholtz, F. *Jpn. J. Appl. Phys.* **37**, 745–752 (1998).

[100] CIE13.31995. .

[101] Ohno, Y. In *Fourth International Conference on Solid State Lighting,* Ferguson, I. T., Narendran, N., DenBaars, S. P., and Carrano, J. C., editors, volume 5530, 88–98, October (2004).